INVESTIGATIONS AND SEPARATION OF VARIOUS CONTRIBUTIONS TO DIELECTRIC RESPONSE OF ADVANCED CERAMIC AND POLYMERIC MATERIALS

Andreja Eršte

Doctoral Dissertation
Jožef Stefan International Postgraduate School
Ljubljana, Slovenia, December 2012

Evaluation Board:

Prof. Dr. Zdravko Kutnjak, Chairman, Jožef Stefan Institute and Jožef Stefan International Postgraduate School, Jamova cesta 39, 1000 Ljubljana, Slovenia

Prof. Dr. Boštjan Zalar, Member, Jožef Stefan Institute and Jožef Stefan International Postgraduate School, Jamova cesta 39, 1000 Ljubljana, Slovenia

Prof. Dr. Qiming Zhang, Member, The Pennsylvania State University, N-219 Millennium Science Complex, University Park, PA 16802, USA

MEDNARODNA PODIPLOMSKA ŠOLA JOŽEFA STEFANA
JOŽEF STEFAN INTERNATIONAL POSTGRADUATE SCHOOL

Andreja Eršte

INVESTIGATIONS AND SEPARATION OF VARIOUS CONTRIBUTIONS TO DIELECTRIC RESPONSE OF ADVANCED CERAMIC AND POLYMERIC MATERIALS

Doctoral Dissertation

RAZISKAVE IN SEPARACIJA RAZLIČNIH PRISPEVKOV K DIELEKTRIČNEMU ODZIVU NAPREDNIH KERAMIČNIH IN POLIMERNIH MATERIALOV

Doktorska disertacija

Supervisor: Asst. Prof. Dr. Vid Bobnar

Ljubljana, Slovenia, December 2012

Stop. Breathe. Allow yourself the luxury of doing nothing for a moment, or an hour, or even a day. It is in emptiness that inspiration will appear.

C. Katchen

Index

Abstract

Dielectric materials, used to control and store charges and electric energy, play a key role in modern electronics and electric power systems. Dielectric spectroscopy is a versatile method, well-suited for detection, separation and characterization of various contributions to dielectric response of advanced ceramic and polymeric materials, as it enables understanding of the behaviour of interfaces at the boundary of two different materials or material phases and accurate control of material properties. This doctoral dissertation presents the recent studies conducted in advanced ceramic and polymeric systems by means of dielectric spectroscopy.

In the beginning, a brief overview of theoretical background, analysis and used experimental techniques of dielectric spectroscopy is presented. Then, the first main focus of the dissertation is set on $CaCu_3Ti_4O_{12}$ ceramic thin films. First, the dielectric response of core-shell structured ceramic material is modelled in terms of an equivalent electric circuit with elements that describe distinctive contributions of grains and grain boundaries. Then, the results of investigations of the influence of preparation conditions on dielectric properties of $CaCu_3Ti_4O_{12}$ thin films are presented: It is shown that by proper post-annealing process a high dielectric constant of $\sim$ 3000 can be obtained in films with thickness below 600 nm. Afterwards, the main focus of the dissertation shifts towards advanced polymeric materials. Firstly, the results of studies of dielectric properties of distinctive dynamic processes in a new class of relaxor polymers, the relaxor reduced poly(vinylidene fluoride-trifluoroethylene) copolymer system, are presented and are then used in studies of changes in dynamic processes of organic and inorganic relaxors due to a dc bias electric field. Secondly, the structural, caloric, and dielectric properties in blends of relaxor poly(vinylidene fluoride-trifluoroethylene-chlorofluoroethylene) terpolymer with a small amount of poly(vinylidene fluoride-chlorotrifluoroethylene) copolymer, developed on aluminum foil, are presented. In the end, the dielectric response of relaxor polymer systems, in which two different dynamic processes take place and superimpose in the detected dielectric response, is modelled.

Scientific work, presented in this dissertation, was conducted at the Dielectric Spectroscopy Laboratory of the Condensed Matter Physics Department of the Jožef Stefan Institute. The work on $CaCu_3Ti_4O_{12}$ ceramic thin films has been done in collaboration between the Condensed Matter Physics Department, F5, and the Electronic Ceramics Department, K5, of the Jožef Stefan Institute. Investigations of the reduced P(VDF-TrFE) copolymer and the terpolymer-copolymer blends have been done in collaboration with the groups of Prof. Dr. Qun-Dong Shen from the Nanjing University in China and of Prof. Dr. Horst Beige from the Martin Luther University in Halle, Germany.

This doctoral dissertation, scientific accomplishments of which have been published in eight articles in peer-reviewed scientific journals, presents the dielectric spectroscopy as a powerful tool for investigations of both basic and applicatory-oriented properties of various organic and inorganic materials. This is anticipated to result in their optimization or even in the synthesis of new materials for advanced applications.

Keywords: dielectric spectroscopy, $CaCu_3Ti_4O_{12}$ ceramic thin film, equivalent circuit, film on surface, polymer blend, relaxor, reduced P(VDF-TrFE) copolymer

PACS (2010): 77.22.Ch, 77.22.Gm, 77.80.Jk, 77.84.Jd, 77.84.Bw

Povzetek

Dielektrični materiali igrajo ključno vlogo v sodobni elektroniki in električnih sistemih, saj se uporabljajo za nadzor in shranjevanje električnega naboja in električne energije. Dielektrična spektroskopija je vsestranska metoda, ki je zelo primerna za detekcijo, separacijo in karakterizacijo različnih prispevkov k dielektričnemu odzivu naprednih keramičnih in polimernih materialov, saj omogoča razumevanje odziva na meji med dvema različnima materialoma ali materialnima fazama ter natančen nadzor nad lastnostmi samega materiala. V tej doktorski disertaciji so predstavljeni rezultati študij naprednih keramičnih in polimernih materialov z metodami dielektrične spektroskopije.

Najprej je predstavljen krajši pregled teoretičnega ozadja ter analitičnih in merskih metod, uporabljenih pri raziskavah. Potem se disertacija osredotoči na $CaCu_3Ti_4O_{12}$ keramične tanke plasti, kjer je najprej predstavljeno modeliranje dielektričnega odziva keramičnih materialov s strukturo jedro-lupina z uporabo ekvivalentnih krogov, katerih posamezni elementi opisujejo ločene prispevke zrn ter mej med zrni. Zatem so predstavljeni rezultati raziskav vpliva pogojev priprave na dielektrične lastnosti $CaCu_3Ti_4O_{12}$ tankih plasti: s primerno termično obdelavo je možno doseči visoke vrednosti dielektrične konstante, ki znaša približno 3000 v filmih tanjših od 600 nm. Zatem se disertacija osredotoči na napredne polimerne materiale: najprej so predstavljeni rezultati študij dielektričnih lastnosti razločljivih dinamičnih procesov v novem razredu relaksorskih polimerov, relaksorskem reduciranem poli(vinilden fluorid-trifluoroetilen) kopolimeru, ki se v nadaljevanju navezujejo na raziskave sprememb v dinamičnih procesih organskih ter anorganskih relaksorjev v velikih zunanjih električnih poljih. Nato so predstavljeni rezultati strukturnih, kaloričnih in dielektričnih lastnosti mešanic relaksorskega poli(vinilden fluorid-trifluoroetilen-klorofluoroetilen) terpolimera z manjšimi količinami poli(vinilden fluorid-klorotrifluoroetilen) kopolimera, razvitih na aluminijevi podlagi. Na koncu so predstavljeni rezultati modeliranja dielektričnega odziva relaksorskih polimernih sistemov, kjer potekata dva različna dinamična procesa, ki se prekrivata v zaznanem dielektričnem odzivu.

Raziskovalno delo, predstavljeno v tej disertaciji, je bilo opravljeno v Laboratoriju za dielektrično spektroskopijo na Odseku za fiziko trdne snovi Instituta "Jožef Stefan". Raziskave $CaCu_3Ti_4O_{12}$ keramičnih tankih plasti so bile opravljene v sodelovanju med Odsekom za fiziko trdne snovi, F5, ter Odsekom za elektronsko keramiko, K5. Študije na reduciranem poli(vinilden fluorid-trifluoroetilen) kopolimeru ter na mešanicah terpolimer-kopolimer so bile opravljene v sodelovanju s skupinama prof. dr. Qun-Dong Shena z Univerze v Nanjingu na Kitajskem in prof. dr. Horsta Beigeja z Univerze Martin Luther v Halleju v Nemčiji.

Ta doktorska disertacija predstavlja dielektrično spektroskopijo kot močno raziskovalno orodje za študije tako bazičnih kot aplikativno naravnanih lastnosti različnih organskih ter anorganskih materialov, in lahko posledično vpliva na njihovo optimizacijo ter sintezo novih materialov za napredne aplikacije. Predstavljeni znanstveni dosežki so zajeti v osmih člankih, ki so objavljeni v različnih mednarodnih znanstvenih revijah.

Ključne besede: dielektrična spektroskopija, $CaCu_3Ti_4O_{12}$ keramična tanka plast, ekvivalentni krog, plast na podlagi, polimerna mešanica, relaksor, reduciran P(VDF-TrFE) kopolimer

Abbreviations

1+X-layer films	=	CCTO films with a nucleation layer
1D	=	one-dimensional
2D	=	two-dimensional
3D	=	three-dimensional
9/65/35 PLZT	=	$Pb_{1-x}La_x(Zr_yTi_{1-y})_{1-x/4}O_3$ ($x = 0.09$, $y = 0.65$)
AC	=	alternating current
CCTO	=	$CaCu_3Ti_4O_{12}$
CFE	=	chlorofluoroethylene
CTFE	=	chlorotrifluoroethylene
DC	=	direct current
DG	=	dipolar glass
DSC	=	differential scanning calorimetry
FE-SEM	=	field emission scanning electron microscopy
FT-IR	=	fourier transform infrared spectroscopy
FE	=	ferroelectric
H–H	=	head-to-head
H–T	=	head-to-tail
P(VDF)	=	poly(vinylidene fluoride)
P(VDF-CTFE)	=	poly(vinylidene fluoride-chlorotrifluoroethylene)
P(VDF-TrFE)	=	poly(vinylidene fluoride-trifluoroethylene)
P(VDF-TrFE-CFE)	=	poly(vinylidene fluoride-trifluoroethylene-chlorofluoroethylene)
PNRs	=	polar nanoregions
RTA	=	rapid thermal annealing
SG	=	spin glass
T–T	=	tail-to-tail
TrFE	=	trifluoroethylene
UDR	=	universal dielectric response
VDF	=	vinylidene fluoride
V-F	=	Vogel-Fulcher
VRH	=	variable range hopping
XRD	=	X-ray diffraction

1 Introduction

Dielectric materials, which are used to control and store charges and electric energy, play a key role in modern electronics and electric power systems. As commercial, consumer and military requirements for compact and low cost electronic and electrical power systems as well as for highly energy capacitive storage systems are growing substantially, the development of high dielectric constant and high electric energy density materials is becoming one of the major scientific and technological issues. For instance, high energy density dielectric capacitors are urgently needed in hybrid electric vehicles to markedly reduce the volume, weight and cost of the electric power system. Thus, not only the understanding of the behaviour of interfaces at the boundary of two different materials or material phases and accurate control of material properties, but also the separation and characterization of various contributions in novel organic and inorganic materials with high dielectric response has become increasingly important in the development of dielectric materials. Dielectric investigations are also of utmost importance in the development of basic science: e.g., the Vogel-Fulcher behaviour, which is typical for all relaxor systems, has experimentally been observed in a variety of systems (organic and inorganic), however, its derivation at the mesoscopic level has just recently been proposed.

Over the last decade, $CaCu_3Ti_4O_{12}$ (CCTO) has been intensively studied due to very high values of the dielectric constant that reveal immense potential for the use of this material in various modern electronic and electromechanical applications. The origin of such high values, which are almost constant in a broad frequency and temperature range, has at first been attributed to either (i) intrinsic effect, due to the perovskite-like crystal structure of CCTO, or (ii) extrinsic effect, i.e., the insulating grain boundaries and semiconducting grains that form an effective circuit of parallel capacitors. In initial research, an intrinsic mechanism was proposed for CCTO single crystal. However, it was later shown that in fact a non-intrinsic mechanism governs its dielectric properties. In further studies, dielectric spectroscopy turned out to be a powerful tool for revealing this extrinsic effect, i.e., electrical heterogeneities in the microstructure, as the origin of large values of the dielectric permittivity in CCTO in general and recent reports indicate that dielectric behaviour of CCTO ceramics and thin films can be influenced by the preparation conditions.

The increase of the dielectric constant does not represent a major challenge only in inorganic systems, but also in the development of organic materials for electromechanical applications. The input electric energy that can be converted into strain energy during an electromechanical application is directly proportional to the dielectric constant of the electroactive material. It has been shown that relaxor polymers, such as poly(vinylidene fluoride-trifluoroethylene) [P(VDF-TrFE)] copolymer, irradiated with high-energy electrons, and VDF-TrFE-based terpolymers, exhibit a giant electrostrictive response. Their dielectric response is almost identical as in classical inorganic relaxors: a broad frequency dispersion in linear and nonlinear dielectric constants, a typical temperature dependence of the dielectric nonlinearity and an asymmetric temperature evolution of the relaxation spectrum as the longest relaxation time diverges at a finite freezing temperature, while the bulk of relaxation times remain active even below this temperature. The dielectric analysis of relaxor polymers has, however, been incomplete until now. Data interpretation and understanding

were complicated by the fact that two similar dynamic processes are taking part in the same temperature range, i.e., the relaxor dynamic maximum was not far enough in temperature from the glass transition occurring in the amorphous matrix. Relaxor P(VDF-TrFE) copolymer, synthesized via reductive dechlorination from the poly (vinylidene fluoride-chlorotrifluoroethylene) [P(VDF-CTFE)], represents a new class of relaxor polymers: in this system, the dynamic relaxor peaks take place at much higher temperatures than that of previous reported relaxor polymers (where they remained in the temperature region of a previous ferroelectric phase transition) and thus also much higher than is the temperature of the glass transition in the amorphous matrix, which makes this system compelling to further studies from aspects of both, material development and basic science. Recent reports also indicate much higher values of polarization in terpolymer-copolymer blends than in VDF-TrFE-based terpolymers, which could lead to a breakthrough in applicatory properties of relaxor polymers.

Dielectric spectroscopy is a versatile method, well-suited for detection and separation of various contributions to dielectric response of advanced ceramic and polymeric materials. This doctoral dissertation presents an overview of the experimental and analytical work, carried out during the past three and a half years at the Dielectric Spectroscopy Laboratory of the Condensed Matter Physics Department of the Jožef Stefan Institute. The main focus of the work was investigations and separation of various contributions to dielectric response of novel ceramic and polymeric materials with a special emphasis on modelling the dielectric response of the investigated systems. The work on CCTO ceramic thin films has been done in collaboration between the Condensed Matter Physics Department, F5, and the Electronic Ceramics Department, K5, of the Jožef Stefan Institute. Investigations of the reduced P(VDF-TrFE) copolymer and the terpolymer-copolymer blends have been done in collaboration with the groups of Prof. Dr. Qun-Dong Shen from the Nanjing University in China and of Prof. Dr. Horst Beige from the Martin Luther University in Halle, Germany.

Chapter 2 serves as an overview of the fundamental and theoretical background of dielectric spectroscopy. The basics of dielectric spectroscopy, together with functions and models used for describing, analysing and modelling the detected dielectric response are extrapolated. Although chapter 3 is entitled “Experimental techniques and methods”, it is not intended to be a complex overview of the topic, but rather a collection of techniques, used to obtain the dielectric data. It briefly describes the lock-in bridge technique used to stabilize the temperature of the samples and the constant wave impedance measurement methods used for obtaining the data, together with the system used for simultaneous measurements of the linear and the nonlinear dielectric constant.

The actual results are presented in chapters 4, 5 and 6. The chapter about the studies of the $CaCu_3Ti_4O_{12}$ ceramic thin films begins with a brief historic overview of the scientific interest in the CCTO systems and then continues with modelling the temperature- and frequency-dependent dielectric response of core-shell structures in terms of the equivalent circuit [1]. The rest of the chapter focuses on the presentation of the experimental data and the results of the analysis and modelling of the dielectric response. The influence of preparation conditions on the dielectric properties of CCTO ceramic thin films was studied by detailed dielectric investigations in broad temperature and frequency ranges [2]. Analysis in terms of the equivalent circuit was used in order to study the extrinsic effect and investigate how the preparation conditions govern the distinctive contributions of insulating grain boundaries and semiconducting grains in different temperature and frequency ranges. In addition, the electrical conductivity, obtained from the analysis in terms of the equivalent circuit, was modelled in order to determine the charge transport behaviour in CCTO thin films.

Chapters 5 and 6 are focused primarily on studies of novel relaxor polymer systems. In chapter 5, the contributions of distinctive dynamic processes to the dielectric response of reduced P(VDF-TrFE) copolymer system were intensively studied by investigations of

the linear and nonlinear dielectric response, influence of DC bias electrical field and the electromechanic response [3,4]. In the reduced P(VDF-TrFE) copolymer and the inorganic relaxor lanthanum-modified lead zirconate titanate ceramics $Pb_{1-x}La_x(Zr_yTi_{1-y})_{1-x/4}O_3$ ($x = 0.09$, $y = 0.65$, denoted as 9/65/35 PLZT) the influence of DC bias electrical field on the Vogel-Fulcher dynamics were extensively investigated and the results of the analysis were compared to the newly derived mesoscopic model from reference 5 [4]. Chapter 6 is organized according to the types of experiments that were conducted on poly(vinylidene fluoride-trifluoroethylene-chlorofluoroethylene) [P(VDF-TrFE-CFE)] (66.3/26.4/7.3 mol%) terpolymer and poly(vinylidene fluoride-chlorotrifluoroethylene) [P(VDF-CTFE)] (91/9 mol%) copolymer blends on aluminium foil: X-ray diffraction spectroscopy, differential scanning calorimetry and high resolution linear dielectric spectroscopy in broad temperature and frequency ranges. In this system, the case, in which two different contributions superimpose in the detected dielectric response of a relaxor, was investigated and modelled in order to reveal how this phenomena influences on the characteristic relaxation times and, concomitantly, on the Vogel-Fulcher behaviour [6].

2 Dielectric spectroscopy

Over the last few decades, dielectric spectroscopy turned out to be a powerful tool for detection and separation of various contributions to the electric response of advanced ceramic and polymeric materials. This chapter serves as an overview of the fundamentals of dielectric spectroscopy, together with functions and models used for describing, analysing and modelling the detected dielectric response.

2.1 Fundamentals of dielectric spectroscopy

A dielectric material, i.e., a dielectric, is a material that supports charge without conducting it to a significant degree. In dielectrics, a linear relation between the electric displacement field, $\vec{D}$, and the applied electric field, $\vec{E}$, is satisfied by definition:

$$\vec{D} = \varepsilon\varepsilon_0\vec{E}, \tag{1}$$

where ε is the dielectric constant (a 2^{nd}-order tensor) of the material. External electric field orients the electric dipoles in a dielectric, inducing electric polarization, $\vec{P}$ (defined as dipole moment per unit volume), thus increasing the value of $\vec{D}$:

$$\vec{D} = \varepsilon_0\vec{E} + \vec{P}, \tag{2}$$

where ε_0 is the permittivity of free space ($\varepsilon_0 = 8.854 \times 10^{-12}$ F m^{-1}). Following from Equations 1 and 2, polarization is:

$$\vec{P} = \big(\varepsilon - 1\big)\varepsilon_0\vec{E} = \chi\varepsilon_0\vec{E}, \tag{3}$$

where ε is the dielectric constant, which describes the dielectric displacement that originates from the response of a material to an applied external electric field only, and $\chi = \varepsilon - 1$ is the dielectric susceptibility [7].

Polarization defined in Equation 3 is a linear function of dielectric susceptibility and the external electric field. This linear approximation is inadequate for higher external field strengths, in which nonlinear effects may take place. In this general case, the polarization is described by function [8]:

$$\vec{P} = \varepsilon_0\chi_1\vec{E} + \varepsilon_0\chi_3E^2\vec{E} + \varepsilon_0\chi_5E^4\vec{E} + \ldots = \varepsilon_0\sum_{j=1,\ldots}\chi_jE^{j+1}\vec{E}\ , \tag{4}$$

in which $\chi_j = \varepsilon_j - 1$ (χ_1 is the linear case, coefficients $\chi_{j,\ j>1}$ are called hyperpolarizabilities). Often, due to the symmetry that usually occurs in observed systems ($\vec{P}(\vec{E}) = \vec{P}(-\vec{E})$) and thermodynamic reasons, only odd powers contribute to that series development.

From here on, the tensor character of ε and vector characters of $\vec{D}$, $\vec{E}$ and $\vec{P}$ will be disregarded and all quantities will be treated as scalars due to simplicity. If the dielectric has been exposed to an external electric field, $E(u)$, during a time between u and $u + du$ the resulting electric displacement is:

$$D(t) = \varepsilon_\infty\varepsilon_0E(t),\ u > t > u + du, \tag{5}$$

and

$$dD(t) = \varepsilon_0 E(u)\alpha(t-u)du,\ t > u + du, \tag{6}$$

where ε_∞ is the high frequency dielectric constant and $\alpha(t-u)$ is a decay function. If there are several field pulses at different times, then the resulting displacements superimpose linearly. In cases, where there exists a continuously varying field $E(u)$ initiated at time $u = 0$, total displacement is a sum of displacements:

$$D(t) = \varepsilon_\infty \varepsilon_0 E(t) + \varepsilon_0 \int_0^\infty E(u)\alpha(t-u)du, \tag{7}$$

where $\alpha(t-u)$ is a decay function, which describes the gradual decrease of D in the dielectric after the external electric field has been removed, so that $\alpha(t-u) \to 0$ if $t \to \infty$ [7, 9].

2.1.1 Complex dielectric constant

In the case of periodic electric fields, $E(t) = E_0 \cos(\omega t)$, where the periodic electric field has persisted for a time longer than the characteristic decay time at which the decay function vanished, the integration over x in Equation 7 can be extended to infinity by changing the variable u to $x = t - u$. Here, the characteristic decay time is the time needed for a specific dipole moment to return to its initial position after E has been removed. Concomitantly, electric displacement field, D, is also periodic in time, however, it is not necessarily in phase with E, i.e.,

$$D(t) = D_0 \cos(\omega t - \delta). \tag{8}$$

In order to better describe this situation, two different, frequency-dependent dielectric constants, ε' and ε'', can be introduced, so that [7]:

$$D(t) = E_0 \varepsilon_0 \big(\varepsilon' \cos(\omega t) + \varepsilon'' \sin(\omega t)\big), \tag{9}$$

in which ε' represents the part that follows the time varying electric field, ε'' represents the part that is shifted for $\frac{\pi}{2}$ and

$$\tan(\delta) = \frac{\varepsilon''}{\varepsilon'}. \tag{10}$$

By comparing Equation 9 to Equation 7, which can be rewritten as:

$$D(t) = \varepsilon_0 E_0 \cos(\omega t)\left(\varepsilon_\infty + \int_0^\infty \alpha(x)\cos(\omega x)dx\right) + \varepsilon_0 E_0 \sin(\omega t)\int_0^\infty \sin(\omega x)dx, \tag{11}$$

ε' and ε'' can be expressed as:

$$\varepsilon'(\omega) = \varepsilon_\infty + \int_0^\infty \alpha(x)\cos(\omega x)dx \tag{12}$$

and

$$\varepsilon''(\omega) = \int_0^\infty \sin(\omega x)dx. \tag{13}$$

By introducing a complex dielectric constant [7]:

$$\varepsilon^* = \varepsilon' - i\varepsilon'', \tag{14}$$

relations in Equations 12 and 13 can be expressed in a more condensed form:

$$\varepsilon^*(\omega) = \varepsilon'(\omega) - i\varepsilon''(\omega) = \varepsilon_\infty + \int_0^\infty \alpha(x)\exp\left[-i\omega x\right]dx. \tag{15}$$

The frequency-dependence of the complex dielectric constant, ε^*, which measures the response of a dielectric material to a time varying electric field, is thus completely determined by the decay function $\alpha(x)$ [7, 10].

Following from Equation 15, ε' and ε'' can both be derived from the same decay function $\alpha(x)$ and, concomitantly, they cannot be independent of each other, i.e., the dynamic response of ε' is influenced by the dynamic response of ε'' (and vice versa), resulting in a dispersion in the detected dielectric response. By performing the Fourier transformation on Equation 15, the decay function can be extrapolated as [7]:

$$\alpha(x) = \frac{2}{\pi} \int_0^\infty \left(\varepsilon'(\omega') - \varepsilon_\infty\right) \cos(\omega' x) d\omega' \tag{16}$$

and

$$\alpha(x) = \frac{2}{\pi} \int_0^\infty \varepsilon''(\omega') \sin(\omega' x) d\omega', \tag{17}$$

in which ω' is an integration variable.

2.1.2 Electric polarization

Electric polarization (i.e., polarization density or polarization) is a vector field, which expresses the density of permanent or induced electric dipole moments in a dielectric material, and is defined as dipole moment per unit volume. In other words, polarization is the response of a charge in a dielectric to an applied electric field. In a dielectric material, the applied external electric field, E causes a displacement of charge and affects the polarization, thus causing occurrence of several polarization mechanisms.

2.1.2.1 Polarization mechanisms

Figure 1 illustrates four basic polarization mechanisms: electronic, atomic and orientation polarization, which can exist in homogeneous materials, and space-charge polarization that is often detected in electrically heterogeneous materials. Several more polarization mechanisms can occur due to other factors, e.g., the presence of various phases and defects in the material [8, 11].

Instantaneous polarization [11] is a term that describes two polarization mechanisms, which form completely in a time much shorter than the time needed to apply the electric field and are found in all materials: electronic and atomic polarization. Electronic polarization neutralizes a part of the applied electric field and arises from a displacement caused by a shift of the centre of mass of the negative electron charge cloud, which surrounds the positive atomic nucleus, under applied field. The applied field also causes the equilibrium positions of the atoms to change and, due to the relative motion of the atoms, atomic polarization occurs.

Upon formation of molecules, the rearrangement of electrons can cause a dipole moment in a molecule. In the absence of an external electric field, dipole moments of molecules are oriented randomly and no net charge is present in the material. Orientation polarization mechanism originates from the reorientation of dipole moments of the molecules under applied electric field and (similar to electronic polarization) nullifies a part of that field. [11].

Space-charge or interfacial polarization arises due to charges, which build up at interfaces and can be polarized in an applied electric field. This mechanism often depends on the conductivities of present phases, i.e., the motion of charge carriers may occur more easily through one phase and is then constricted at phase boundaries [11].

2.1.2.2 Frequency effects and total polarization

Polarization mechanisms are characterized by a step-like decrease of the real, ε', and a peak in the imaginary, ε'', part of the complex dielectric constant from Equation 15, i.e., each mechanism has its own specific features in the frequency (and temperature) dependence of the complex dielectric constant [8]. This arises from the fact that dielectrics are not ideal

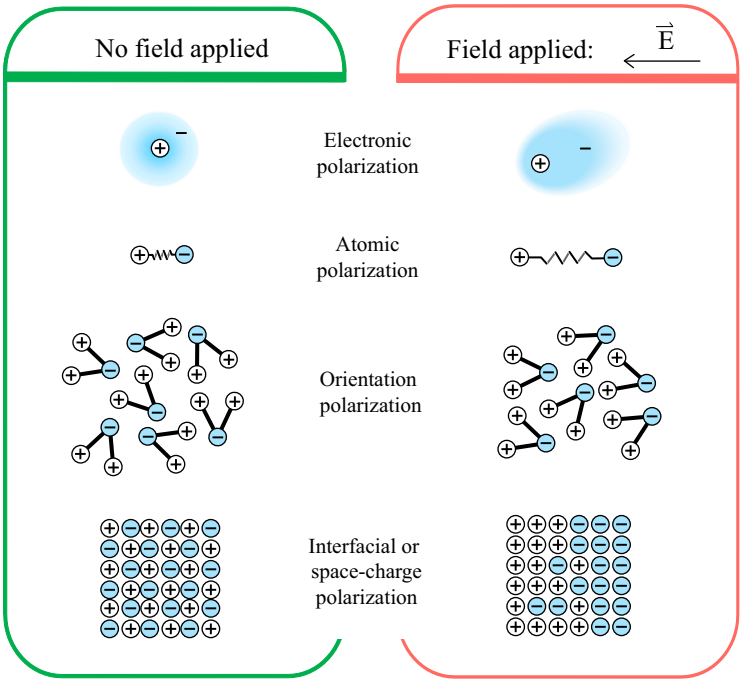

Figure 1: *Polarization mechanisms.* Illustration of different polarization mechanisms that occur in dielectric materials after an external electric field has been applied.

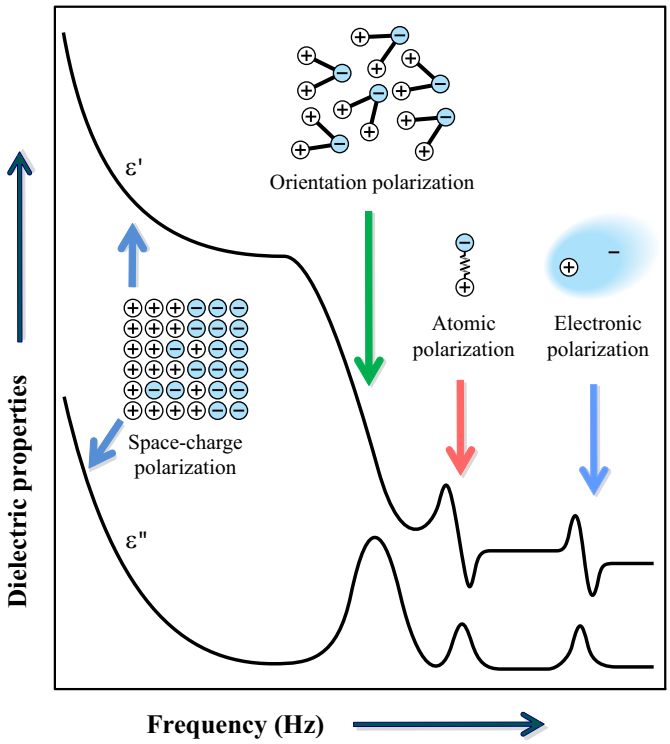

Figure 2: *Polarization mechanisms in a dielectric material.* Contribution of the different polarization mechanisms to the frequency dependence of the complex dielectric constant. The applied external electric field causes displacement of charge, thus affecting the value of the complex dielectric constant [11].

materials and, thus, a finite time is required for each polarization mechanism to take effect: after an electric field is applied, an inertia-to-charge phenomena occurs, in which charge transport or dipole rearrangement takes place over a relaxation time τ. In the case of an alternating electric field, τ defines a relaxation frequency $\omega = 1/\tau$, which in term varies upon polarization mechanisms [11, 12].

Total polarization field of a dielectric is the sum of the polarization resulting from each mechanism [11]:

$$P_{total}(t) = P_{orientation}(t) + P_{atomic}(t) + P_{electronic}(t) + P_{interfacial}(t). \tag{18}$$

Using Equations 2, 3, 8 and 9, total polarization can be separated to a sum of two parts:

$$P_{total}(t) = P_1(t) + P_2(t) \ , \tag{19}$$

where

$$P_1(t) = \big(\varepsilon'(\omega) - 1\big)\varepsilon_0 E_0 \cos(\omega t) \tag{20}$$

represents the part that follows the changes in the electric field and

$$P_2(t) = \varepsilon''(\omega)\varepsilon_0 E_0 \sin(\omega t) \tag{21}$$

the part shifted for $\frac{\pi}{2}$ and $\varepsilon'(\omega)$ and $\varepsilon''(\omega)$ are the parts of frequency dependent dielectric constant, which in term measures the response of a material to a time varying electric field, as shown in Figure 2.

2.1.3 Heat losses

In a dielectric, absorption of energy arises due to the lag between polarization and the applied electric field. Any change in the polarization leads to displacement current of density, $i = dP/dt$, and Joule heating

$$Q = Ei = E\frac{dP}{dt} \tag{22}$$

per unit volume. By averaging the expression in Equation 22 over a complete cycle of the electric field, the net rate of Joule heat is [9]:

$$Q_{average} = \frac{\varepsilon_0 \omega E_0^2}{8\pi}\varepsilon'' \ , \tag{23}$$

where ε'' is the imaginary part of the frequency dependent complex dielectric constant, ε_0 is the dielectric constant of free space and E_0 is the amplitude of the applied electric field. Following from Equation 23, ε'' controls the rate at which electrical energy is converted into heat in the medium and is thus sometimes called the dielectric loss factor in literature.

Absolute released heat is more important than heat losses per unit volume in practical applications. In order to depict dielectric losses, the loss tangent $\tan\delta = \varepsilon''/\varepsilon'$ (Equation 10), is used, where ε' defines the volume of a practical device (higher ε', smaller device) and ε'' represents heat losses per unit volume.

2.2 Dynamic response

Dielectric relaxation processes are usually analysed using model functions. This section serves as a brief overview of the basic theoretical and empirical functions used to describe dispersive dielectric behaviour detected in dielectric materials. Functions that describe symmetric broadening of the complex dielectric constant are extrapolated in more detail, as they will be encountered in the analysis and modelling of the dielectric response in later chapters of this dissertation.

2.2.1 Kramers-Kronig dispersion relations

By inserting Equations 16 and 17 in Equation 15, we obtain the Kramers-Kronig dispersion relations:

$$\varepsilon'(\omega) - \varepsilon_\infty = \frac{2}{\pi}\int_0^\infty \varepsilon''(\omega')\frac{\omega'}{\omega'^2 - \omega^2}d\omega' \tag{24}$$

and

$$\varepsilon''(\omega) = \frac{2}{\pi}\int_0^\infty \big(\varepsilon'(\omega') - \varepsilon_\infty\big)\frac{\omega'}{\omega'^2 - \omega^2}d\omega', \tag{25}$$

where the integrals are principal values. These results are completely general, since no assumptions have been made regarding the nature of the decay function so far.

Kramers-Kronig dispersion relations can be used to establish a connection between the static and the dynamic response of dielectric systems [7, 8]. For example, a resonance type dielectric and absorption response is obtained, if the decay function is assumed to be in the form of a dampened harmonic oscillator [7]:

$$\alpha(t) = \gamma \exp\left[-\frac{t}{\tau}\right]\cos(\omega_0 t + \psi), \tag{26}$$

in which γ and ψ are constants that can be temperature dependent.

2.2.2 Debye relaxational dispersion

Theoretically well founded Debye expression is used to describe the case of an ideal, noninteracting population of dipoles, to an alternating external electric field. Assuming a simple exponential form of the decay function [7],

$$\alpha(t) = \frac{\varepsilon_s - \varepsilon_\infty}{\tau}\exp\left[-\frac{t}{\tau}\right], \tag{27}$$

and inserting it into Equation 15, the Debye equation can be expressed as:

$$\varepsilon^*(\omega) = \varepsilon_\infty + \frac{\Delta\varepsilon}{1 + i\omega\tau}, \tag{28}$$

which in term describes a relaxational dispersion of the frequency-dependent complex dielectric constant with a characteristic relaxation time τ and a dielectric intensity

$$\Delta\varepsilon = \varepsilon_s - \varepsilon_\infty, \tag{29}$$

where ε_s is the static and ε_∞ is the high-frequency dielectric constant and $\varepsilon_s > \varepsilon_\infty$. Following from Equation 28,

$$\varepsilon'(\omega) = \varepsilon_\infty + \frac{\Delta\varepsilon}{1 + \big(\omega\tau\big)^2}, \tag{30}$$

is the real and

$$\varepsilon''(\omega) = \frac{\Delta\varepsilon\omega\tau}{1 + \big(\omega\tau\big)^2}, \tag{31}$$

is the imaginary part of the frequency-dependent complex dielectric constant. In literature, the dielectric intensity, $\Delta\varepsilon$, is often referred to as the dielectric relaxation strength [9].

Figure 3 depicts the real, ε', and the imaginary, ε'', parts of the complex dielectric constant vs. frequency, obtained from Equations 30 and 31, respectively. The two black curves reveal the Debye relaxational dispersion, which is characterized by a drop in the value of ε', accompanied by an increase in the value of ε'' that occurs at the characteristic relaxation frequency $\omega_0 = 1/\tau$ (dashed blue line). At that frequency, the value of ε'' is maximal and the value of ε' is $\varepsilon_\infty + \frac{\Delta\varepsilon}{2}$. [9].

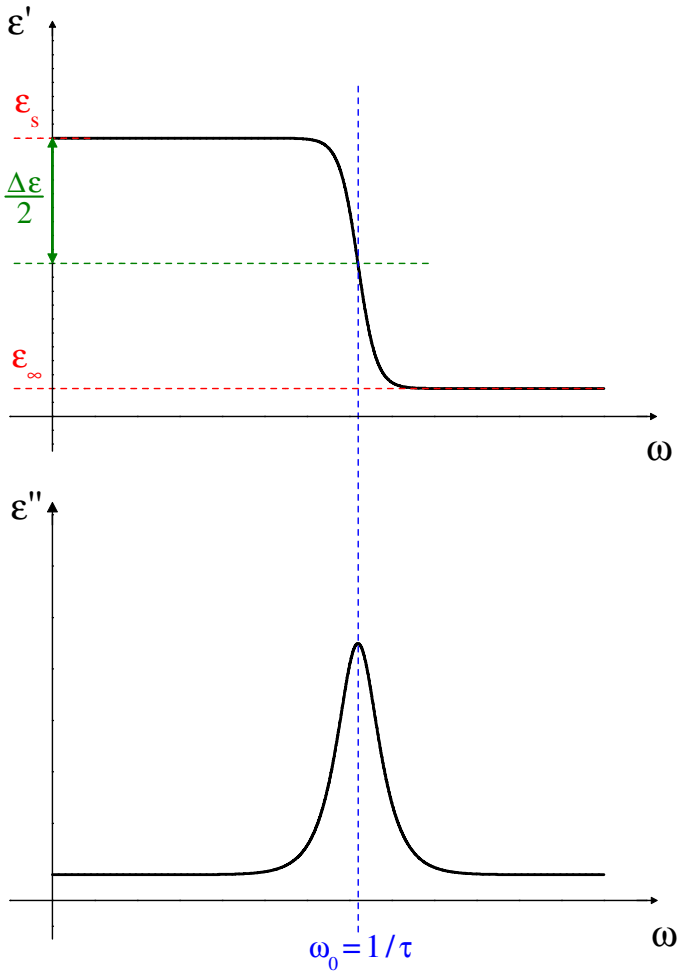

Figure 3: *Debye relaxational dispersion.* Debye relaxational dispersion of both parts of the frequency-dependent complex dielectric constant from Equations 30 (upper frame) and 31 (lower frame). Red dashed lines indicate the values of the static, ε_s, and the high-frequency, ε_∞, dielectric constant and blue dashed line emphasizes the characteristic relaxation frequency, $\omega_0 = 1/\tau$. Green arrow depicts the length $\Delta\varepsilon/2$, which corresponds to the radius of the Debye semicircle.

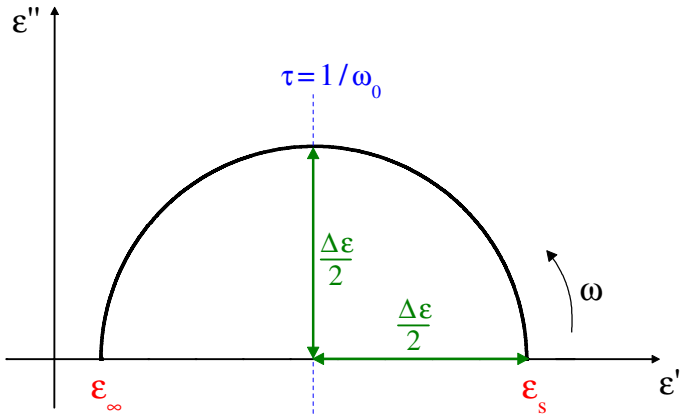

Figure 4: *Debye semicircle.* Debye semicircle in the complex ε', ε'' plane. The centre of the circle lies on the abscissa axis at $\varepsilon_\infty + \Delta\varepsilon/2$ and its radius corresponds to the value of one half of the dielectric intensity. The black arrow indicates the direction of the increasing frequency.

The Debye expressions in Equations 30 and 31 are the parametric equations of a circle in the ε'', ε' plane [13], i.e., eliminating the parameter $\omega\tau$ and rearranging the two equations yields the ansatz:

$$\left(\varepsilon' - \left(\varepsilon_\infty + \frac{\Delta\varepsilon}{2}\right)\right)^2 + \varepsilon''^2 = \left(\frac{\Delta\varepsilon}{2}\right)^2, \tag{32}$$

which is in fact the equation of a circle with its centre at $(\frac{\Delta\varepsilon}{2} + \varepsilon_\infty, 0)$ and radius $\frac{\Delta\varepsilon}{2}$ in the ε', ε'' plane [9, 13]. However, only the semicircle over which ε'' is positive has physical significance, as shown in Figure 4. The diameter of the semicircle equals the value of the dielectric intensity and the top point of the semicircle matches to the characteristic relaxation time $\tau = 1/\omega_0$. In literature, this semicircle is often referred to as the Debye semicircle.

2.2.3 Empiric model functions

In real systems, several relaxation times can exist, which in term results in a relaxation spectra, i.e., a distribution of relaxation times $g(\tau)$, that is detected in the measured dielectric response. In such cases, Equations 30 and 31 transform into [9]:

$$\varepsilon'(\omega) = \varepsilon_\infty + \Delta\varepsilon \int_0^\infty \frac{g(\tau)d\tau}{1 + \left(\omega\tau\right)^2} \tag{33}$$

and

$$\varepsilon''(\omega) = \Delta\varepsilon \int_0^\infty \frac{g(\tau)\omega\tau d\tau}{1 + \left(\omega\tau\right)^2}. \tag{34}$$

The Debye expression is sufficient to describe only an ideal case, in which the relaxation time is related to the position of the maximal loss via relation $\omega_0 = 2\pi\nu_0 = 1/\tau_{Debye}$ [8]. In a general case, however, even the simplest forms of $g(\tau)$ (e.g., a Gaussian distribution) result in solutions for ε' and ε'', which are often too complicated to use for analysis of the experimental data. Therefore, the following empiric models, described further in this section, are used: (i) the Cole-Cole empiric expression, which arises from a symmetrical distribution of relaxation times, (ii) the Cole-Davidson empiric expression, which can be used to describe a series of relaxation mechanisms of decreasing importance extending to the high-frequency side of the main dispersion and (iii) the Havriliak-Negami empiric expression, which describes any general distribution of characteristic relaxation times [9].

It should also be noted that the results of frequency-dependent permittivity measurements are sometimes displayed by plotting ε'' versus ε'. Although information regarding the independent variable (i.e., the frequency) can not be explicitly shown, such plots can also provide information regarding the broadening of the complex dielectric constant: the broadening of the complex dielectric constant is symmetric, if the locus in the ε', ε'' is symmetrical about a line through its centre [8], e.g. the Debye relaxation model describes symmetrical broadening of the complex dielectric constant for the case, in which the locus in the ε', ε'' plane is a semicircle with its centre on the abscissa axis.

2.2.3.1 Cole-Cole empiric expression

In many materials, such as particularly long-chain molecules and polymers, a broader dispersion curve and lower maximum loss is detected than would be expected from the Debye dispersive relaxation. This broadening of the dielectric function is symmetric (its locus in the ε', ε'' plane is an arc) and can be described by an empirical equation [9]:

$$\varepsilon^*(\omega) = \varepsilon_\infty + \frac{\Delta\varepsilon}{1 + (i\omega\tau)^{1-h}}\ , \tag{35}$$

where $\Delta\varepsilon = \varepsilon_s - \varepsilon_\infty$ is the dielectric relaxation strength, τ is the characteristic relaxation time and h is the parameter describing the distribution of relaxation times, $0 \leq h < 1$.

Equation 35 is commonly referred to as the Cole-Cole ansatz or the Cole-Cole empirical expression in literature.

Figure 5 shows a comparison between the Debye dispersive relaxation and the $\varepsilon'(\omega)$ and $\varepsilon''(\omega)$ curves obtained from the Cole-Cole ansatz for the case, in which the characteristic relaxation time τ and the high-frequency and static dielectric constants have the same values. Both relaxations are characterized by a drop in the value of ε', accompanied by an increase in the value of ε'' at the characteristic relaxation frequency, $\omega_0 = 1/\tau$. In the case of the Cole-Cole curves, the $\varepsilon'(\omega)$ relaxation curve is broader and the accompanying ε'' maximum is lower and broader.

Rationalizing the Cole-Cole ansatz (Equation 35) and using the relation [13]

$$i^{1-h} = \exp\left[\frac{i\pi}{2}(1-h)\right], \tag{36}$$

reveals the real,

$$\varepsilon'(\omega) = \varepsilon_\infty + \frac{\Delta\varepsilon\big(1 + \big(\omega\tau\big)^{1-h}\sin(\frac{\pi h}{2})\big)}{1 + \big(\omega\tau\big)^{2(1-h)} + 2\big(\omega\tau\big)^{1-h}\sin(\frac{\pi h}{2})}, \tag{37}$$

and the imaginary,

$$\varepsilon''(\omega) = \frac{\Delta\varepsilon\big(\omega\tau\big)^{1-h}\cos(\frac{\pi h}{2})}{1 + \big(\omega\tau\big)^{2(1-h)} + 2\big(\omega\tau\big)^{1-h}\sin(\frac{\pi h}{2})}, \tag{38}$$

part of the frequency-dependent complex dielectric constant. Similar as in the case of the Debye expression, Equations 37 and 38 are also parametric equations of a locus in the complex ε'', ε' plane – eliminating the parameter $\omega\tau$ and rearranging results in expression [9, 13]:

$$\left(\varepsilon' - \big(\varepsilon_\infty + \frac{\Delta\varepsilon}{2}\big)\right)^2 + \left(\varepsilon'' + \frac{\Delta\varepsilon}{2}\tan(\frac{\pi h}{2})\right)^2 = \left(\frac{\Delta\varepsilon}{2}\sec(\frac{\pi h}{2})\right)^2, \tag{39}$$

which is the equation of a circle with its centre at $(\varepsilon_\infty + \frac{\Delta\varepsilon}{2}, -\frac{\Delta\varepsilon}{2}\tan(\frac{\pi h}{2}))$ and radius $\frac{\Delta\varepsilon}{2}\sec(\frac{\pi h}{2})$. As shown in Figure 6, only the arc over which ε'' is positive has physical value (solid black line) and is referred to as the Cole-Cole arc in literature. The top point of the Cole-Cole arc corresponds to the characteristic relaxation time τ, which can be determined from the relation [9]:

$$\omega\tau = \left(\frac{\big(\varepsilon' - (\varepsilon_\infty + \Delta\varepsilon)\big)^2 + \varepsilon''^2}{\big(\varepsilon' - \varepsilon_\infty\big)^2 + \varepsilon''^2}\right)^{\frac{1-h}{2}}. \tag{40}$$

In the limit $h = 0$, the Cole-Cole ansatz becomes the Debye expression and describes the case of monodispersive relaxation (solid grey line in Figure 6).

2.2.3.2 Cole-Davidson empiric expression

In the cases of, e.g., liquids and proton glasses, experimental results reveal (i) a skewed arc in the complex ε', ε'' plane (see Fig. 1.17 in Reference 9) and (ii) that the characteristic relaxation time does not coincide with the relaxation time, which is related to the position of maximal loss (see Fig. 3.3.b in Reference 8). This kind of asymmetric broadening of the complex dielectric function can be described by the Cole-Davidson empiric expression:

$$\varepsilon^*(\omega) = \varepsilon_\infty + \frac{\Delta\varepsilon}{\big(1 + i\omega\tau\big)^\alpha}, \tag{41}$$

where α is a parameter that describes an asymmetric broadening of the relaxation function for frequencies $\omega > 1/\tau$, $0 < \alpha \leq 1$, and τ is the characteristic relaxation time. The relation

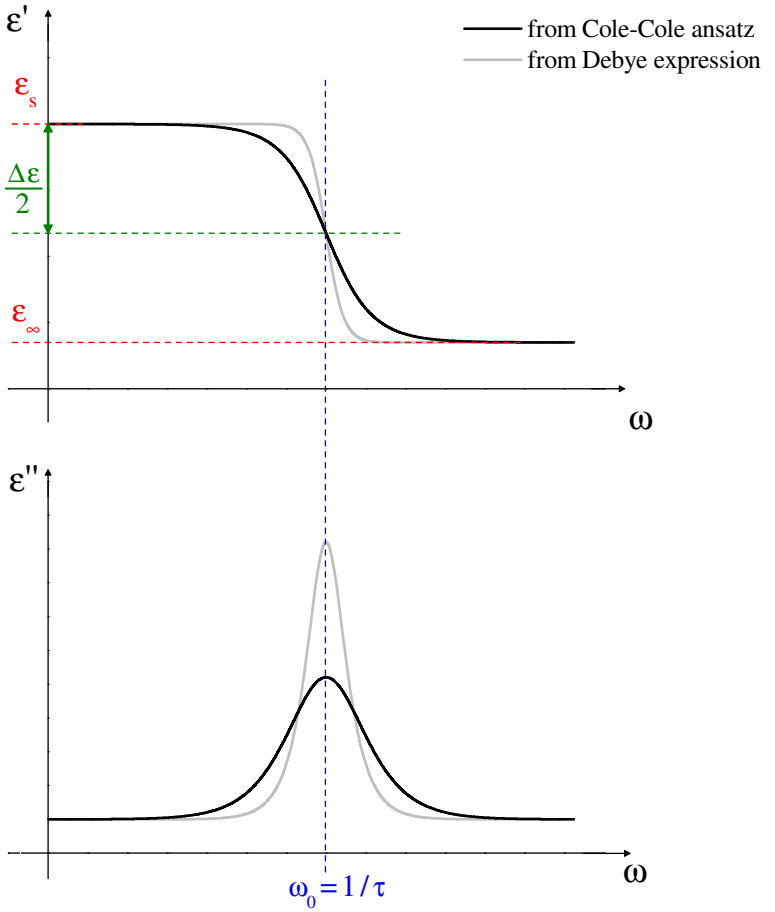

Figure 5: *Cole-Cole empirical model.* Frequency-dependent complex dielectric constant calculated from the Cole-Cole empirical expression in Equations 37 and 38. For comparison, Debye relaxation with the same values of τ, ε_s and ε_∞ is plotted.

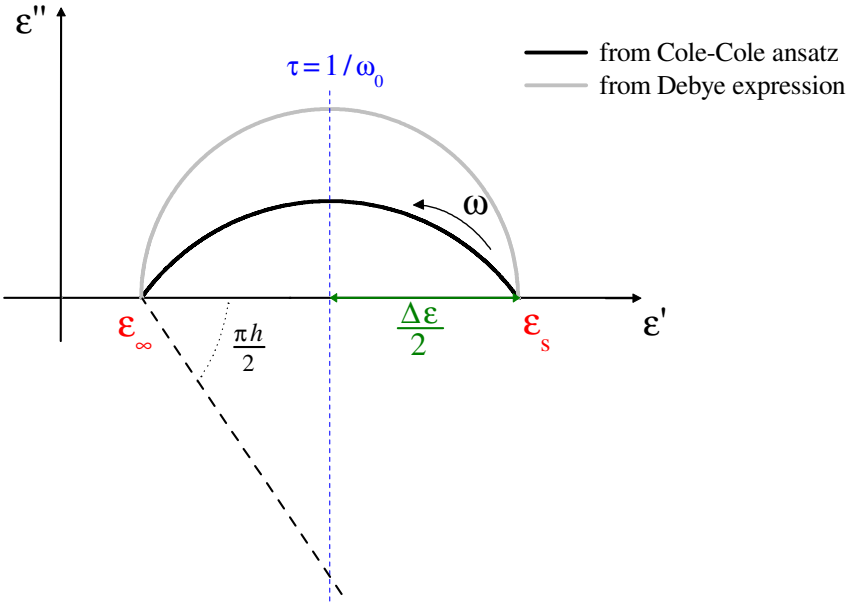

Figure 6: *Cole-Cole arc.* The Cole-Cole arc in the complex ε', ε'' plane (black). The centre of the circle lies below the abscissa and is indicated by the cross-section of the blue dashed line that indicates the top of the arc and the black dashed line, which closes the $\frac{\pi h}{2}$ angle. For comparison, the Debye semicircle is plotted (grey).

between the characteristic relaxation time, τ, and the characteristic relaxation frequency, ω_0 depends on the shape parameter, α:

$$\omega_0 = \frac{1}{\tau}\tan\left(\frac{\pi}{2\gamma+2}\right). \tag{42}$$

In the limit $\alpha = 1$, the Cole-Davidsion expression describes monodispersive relaxation, i.e., if $\alpha = 1$, the Debye expression can be recovered from the Equation 41 [8,9].

2.2.3.3 Havriliak-Negami empiric expression

In order to account for the asymmetry and broadness of the dielectric dispersion curve in general, a combination of the Cole-Cole and the Cole-Davidson ansatzes, i.e., the Havriliak-Negami empiric expression, is used [8,9]:

$$\varepsilon^* = \varepsilon_\infty + \frac{\Delta\varepsilon}{\left(1+(i\omega\tau)^\beta\right)^\gamma}, \tag{43}$$

in which the fractional shape parameters β and γ describe the symmetric and the asymmetric broadening of the complex dielectric constant, respectively, and $0 < \beta$, $\beta\gamma \leq 1$. The characteristic relaxation frequency depends on both shape parameters [8]:

$$\omega_0 = \frac{1}{\tau}\left(\sin\left(\frac{\beta\pi}{2+2\gamma}\right)\sin\left(\frac{\beta\gamma\pi}{2+2\gamma}\right)\right)^{\frac{-1}{\beta}}. \tag{44}$$

If $\beta = 1$ and $\gamma = 1$, the Havriliak-Negami expression is reduced to the Debye expression.

2.3 Equivalent circuit models

When dealing with extrinsic effects that influence the dielectric behaviour of a dielectric material, a straightforward approach to understanding the dielectric behaviour is analysis in terms of the equivalent circuit with elements that describe distinctive contributions to the dielectric response [1,8,14,15]. In this section, representation of the dielectric material as a leaky capacitor are elaborated, together with the model that takes into account the parasitic resistance and inductance of the measuring setup. Basic equivalent circuits commonly used for modelling the extrinsic effect are shown.

2.3.1 Bulk sample and the leaky capacitor

In an ideal case, an ideal capacitor would be used to describe the impedance of dielectric material in circuits. Since the real dielectric material conducts electricity, in impedance spectroscopy, the intrinsic effect of the bulk sample is usually presented by a leaky capacitor [8], depicted in Figure 7.

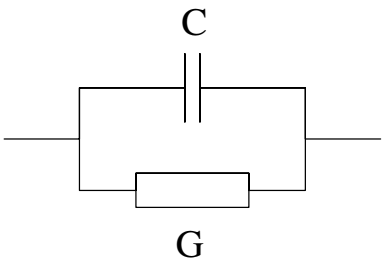

Figure 7: *Leaky capacitor.* The schematic representation of a leaky capacitor. C is the capacitance and G the conductance of the dielectric material.

The reciprocal value of the impedance of a leaky capacitor from Figure 7 and, concomitantly, of a dielectric material, is:

$$\frac{1}{Z} = \frac{1}{R} + i\omega C = G + i\omega C, \tag{45}$$

where $\omega = 2\pi\nu$ is the angular frequency, C is the capacitance, $G = 1/R$ is the conductance and RC is equal to τ, the circuit characteristic time. The resistance, R, takes into account the overall loss due to various extrinsic and intrinsic polarizations and dipole relaxations and the capacitance substantiates the overall ability of the dielectric to store the electric field (via polarization mechanisms) [8].

Equation 45 can be rewritten as:

$$\frac{1}{Z} = i\omega C_0 \varepsilon^* = i\omega C_0(\varepsilon' - i\varepsilon''), \tag{46}$$

where C_0 is the capacitance of the empty capacitor:

$$C_0 = \varepsilon_0 \frac{S}{d}, \tag{47}$$

in which S is the area of overlap and d the separation between two plates of the capacitor. Following from Equations 45 and 46:

$$\varepsilon' = \frac{C}{C_0} \tag{48}$$

is the real and

$$\varepsilon'' = \frac{1}{\omega C_0 R} = \frac{G}{\omega C_0} \tag{49}$$

is the imaginary part of the complex dielectric constant (Equation 14), in which C and G are measured capacitance and conductance of the material. And since [8]:

$$G = \sigma' \frac{S}{d}, \tag{50}$$

Equation 49 also relates the real part of the complex electrical conductivity with the imaginary part of the complex dielectric constant via relation:

$$\sigma' = \omega \varepsilon_0 \varepsilon''. \tag{51}$$

2.3.2 Resistance, inductance and resonance of the measuring setup

Experimentally detected dielectric data could be compromised due to the parasitic inductance or resistance of the measuring setup. Both, inductance and resistance of the measuring setup can be taken into account by performing analysis in terms of the equivalent circuit [8] composed of a resistor and/or an inductor connected in series to a leaky capacitor, which represents the sample.

Figure 8 shows the equivalent circuit for a case, in which both resistance and inductance of the measuring setup influence detected dielectric response. Reciprocal value of the complex impedance of such an equivalent circuit is:

$$\frac{1}{Z} = \left(\frac{1}{G + i\omega C} + R + i\omega L \right)^{-1}. \tag{52}$$

Equation 52 can be rewritten to form [1]:

$$\frac{1}{Z} = G_{MEAS} + i\omega C_{MEAS} = i\omega C_0 \varepsilon^*, \tag{53}$$

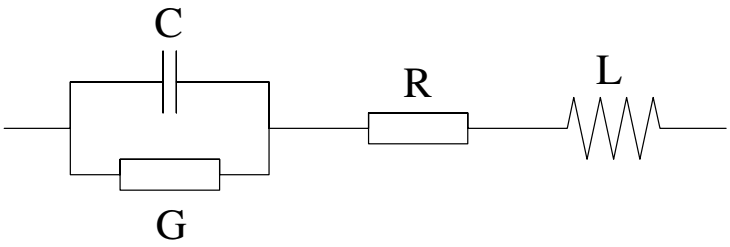

Figure 8: *Equivalent circuit: resistance and inductance of the measuring setup.* A schematic representation of an equivalent circuit composed of a leaky capacitor (sample), a resistor (resistance of the measuring setup) and an inductor (inductance of the measuring setup) connected in series.

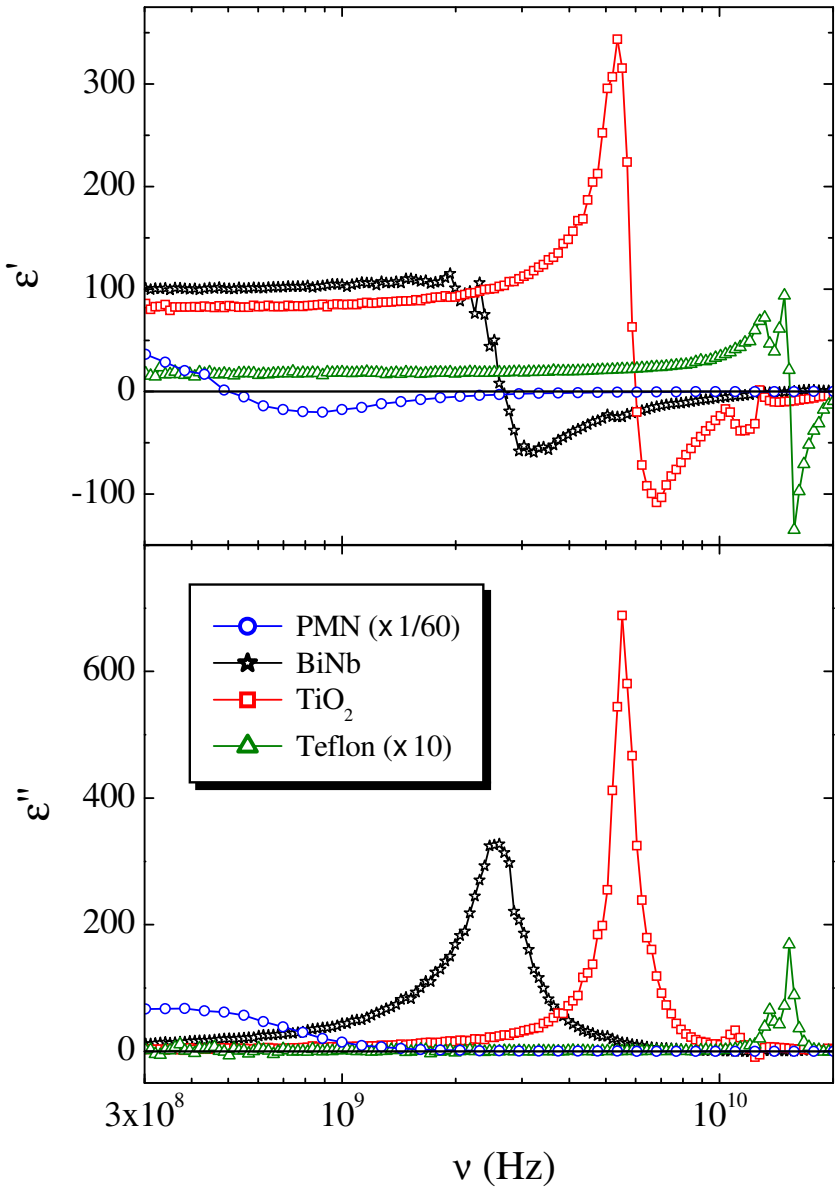

Figure 9: *Resonance.* Resonance due to the measuring setup in various samples, measured with the 8720C Network Analyzer.

where C_{MEAS} and $G_{MEAS} = 1/R_{MEAS}$ are the two quantities that are usually measured by impedance analysers in Cp-Gp mode, ε^* is the complex frequency-dependent dielectric constant and C_0 is the capacitance of an empty capacitor from Equation 47. In this particular case [1]:

$$G_{MEAS} = \frac{G + R\left(G^2 + \omega^2 C^2\right)}{\left(1 - \omega^2 LC + GR\right)^2 + \left(\omega LG + \omega CR\right)^2} \tag{54}$$

and

$$C_{MEAS} = \frac{C - L\left(G^2 + \omega^2 C^2\right)}{\left(1 - \omega^2 LC + GR\right)^2 + \left(\omega LG + \omega CR\right)^2}. \tag{55}$$

At $\omega^2 LC = 1$ resonance occurs due to the inductance of the measuring setup. This can clearly be seen in Figure 9, which depicts resonance due to the measuring setup for several samples at room temperature. Note that the frequency of the resonance, $\omega = 1/\sqrt{LC}$, depends on the material used for measurements – the higher is the dielectric constant (and thus C), the lower is the frequency.

If measurements are performed in a frequency range that is low enough to avoid resonance due to the measuring setup, then $L = 0$ can be assumed. In this case:

$$G_{MEAS} = \frac{G + R\left(G^2 + \omega^2 C^2\right)}{\left(1 + GR\right)^2 + \left(\omega CR\right)^2} \tag{56}$$

and

$$C_{MEAS} = \frac{C}{\left(1 + GR\right)^2 + \left(\omega CR\right)^2} \tag{57}$$

Concomitantly, even a small resistance of the measuring setup (a few Ohm – in this case the term GR in the denominator of Equations 56 and 57 can be neglected) results in an artificial Debye-like relaxation with a frequency of $\omega \simeq \sqrt{2}/CR$ in the detected dielectric response. Although this relaxation frequency, above which the response is incorrect, is usually very high ($C = 50$ pF and $R = 3\ \Omega$ give $\nu = \omega/2\pi \simeq 1.5$ GHz), it can decrease into the measuring frequency window when samples with high capacitance are investigated [1].

2.3.3 Extrinsic effects

Extrinsic effects that influence the dielectric behaviour of a dielectric material, are often detected as an artificial Debye-like relaxation in the dielectric response. In cases like this, analysis in terms of an equivalent circuit enables separation and characterization of distinctive contributions to the dielectric response [1, 14].

Figure 10a shows a simplified equivalent circuit, composed of two leaky capacitors connected in series. Each leaky capacitor describes one contribution to the dielectric response of the material, e.g., in the case of $CaCu_3Ti_4O_{12}$ single crystal one leaky capacitor describes the contributions of the bulk and the other one the contributions of surface layers [16]. In order to account for the semiconduction of bulk material or influence of grain boundaries, the equivalent circuit can be modified by introducing new elements. Figure 10b shows a model for the case in which three distinctive contributions govern the dielectric response: grains, grain boundaries, and surface layers [17] while Figure 10c depicts the case of core-shell structured material, which is composed of semiconducting grains and insulating grain boundaries. As usual in semiconductors [18], intrinsic effect of the bulk sample is given as a sum of (i) frequency dependent AC conductivity, for which the universal dielectric response (UDR) is used with the ansatz $\sigma_{AC} = \sigma_0 \omega^s$, $s < 1$, (ii) DC conductivity, and (iii) high-frequency dielectric constant. The intrinsic complex conductivity ($\sigma^* = \sigma' + i\sigma''$) is given as [1]:

$$\begin{aligned} \sigma' &= \sigma_{DC} + \sigma_0 \omega^s \\ \sigma'' &= \omega \varepsilon_0 \varepsilon' = \tan\frac{s\pi}{2} \sigma_0 \omega^s + \omega \varepsilon_0 \varepsilon_\infty. \end{aligned} \tag{58}$$

Similarly, several extrinsic effects within one material could be described using a customized equivalent circuit, composed of several RC and UDR elements connected in series or parallel. For analysis, the function of the complex dielectric constant is obtained simply by determining the reciprocal value of the impedance of the chosen equivalent circuit and rearranging it to form from Equation 53 [1]. However, the more constituents the model has, the more difficult it is to use it in analysis [2].

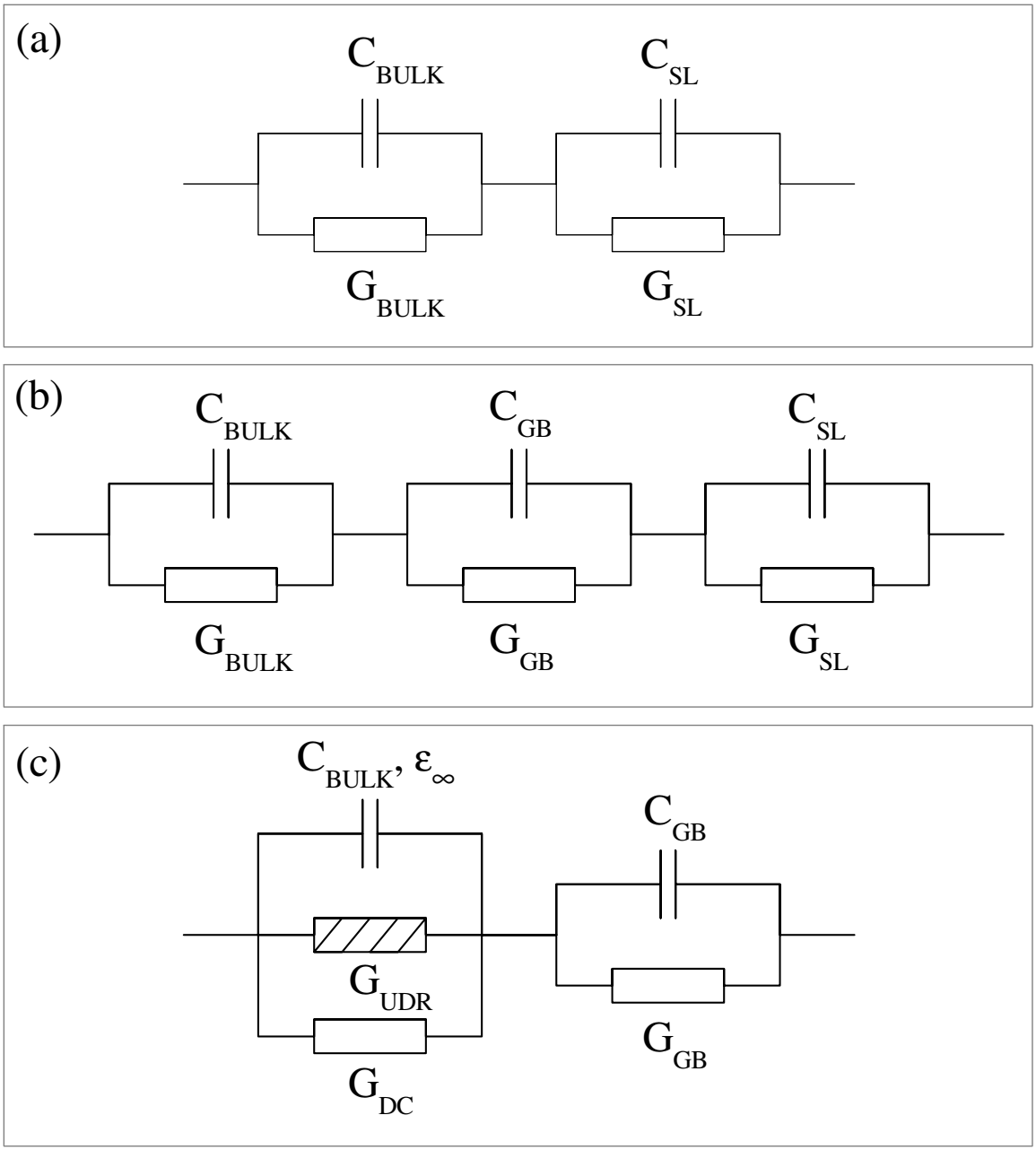

Figure 10: *Equivalent circuits: heterogeneous materials.* Equivalent circuits used for modelling and analysis of the dielectric response of heterogeneous materials. Elements describe distinctive contributions of bulk material ($G_{BULK}C_{BULK}$), surface layers ($G_{SL}C_{SL}$), insulating grain boundaries ($G_{GB}C_{GB}$) or semiconducting grains ($G_{DC}G_{UDR}\varepsilon_{\infty}$) to the dielectric response.

2.4 Arrhenius, Vogel-Fulcher and variable range hopping dynamics

In analysis of the dielectric response of materials, investigated in this dissertation, expressions that describe Arrhenius, Vogel-Fulcher and variable charge hopping dynamics are used. Arrhenius expression is a simple exponential function that can be used to model the temperature-variance of diffusion coefficients, population of crystal vacancies, creep rates, and many thermally-induced processes or reactions. The basic form of the expression is:

$$k = A \exp\left[-\frac{E_a}{RT}\right], \tag{59}$$

in which k is the rate constant of a reaction, T is the absolute temperature and E_a is the activation energy. The pre-exponential factor A and E_a are assumed to be temperature-independent [19].

The Vogel-Fulcher (V-F) relation is used for the analysis of characteristic relaxation times of, e.g., relaxor polymer systems, and reads:

$$\nu = \nu_0 \exp\left[-\frac{E}{k} \cdot \frac{1}{T - T_0}\right], \tag{60}$$

where ν_0 is the inverse attempt frequency, E/k is the activation energy (k is the Boltzmann constant), and T_0 is the Vogel-Fulcher freezing temperature of the characteristic (mean) relaxation time. Although this empirical law has experimentally been observed in a variety of systems, its derivation at the mesoscopic level has just recently been proposed [21].

Variable range hopping (VRH) is a model that describes low temperature conduction in strongly disordered systems with localized states, where $\sigma_{DC} \propto T^{-\frac{1}{1+d}}$ and d is the number of dimensions. It has a characteristic temperature dependence:

$$\sigma = \sigma_0 \exp\left[-\frac{T_0}{T}\right]^{-\frac{1}{1+d}}, \tag{61}$$

in which $d = 0, 1, 2, 3$ is the dimensionality ($d = 0$ describes the Arrhenius dynamics) [20].

3 Experimental techniques and methods

So far, no universal method for measuring the complex dielectric constant in any given frequency range exists. Therefore, measurement methods differ on measurement requirements and conditions (frequency coverage, measurement range, measurement accuracy and ease of operation) and each have their own advantages and disadvantages. This chapter serves as an overview of the measurement techniques that were used for obtaining the experimental data. Constant wave impedance measurement methods and the system used for simultaneous measurements of the linear and the nonlinear dielectric constant are sketched. The lock-in bridge technique used to stabilize the temperature of the samples is described. For a more detailed review, several excellent textbooks exist, written by prominent authors. Among them are references 22–25.

3.1 Impedance measurement techniques

For impedance measurements in the range between mHz and MHz, constant wave methods are used. This section serves as an overview of the methods used by the Novocontrol Alpha High Resolution Dielectric Analyzer and the Hewlett Packard 4284*A* precision LCR-meter, which have been used for measuring the complex dielectric constant.

3.1.1 Wheatstone bridge method

The Wheatstone bridge, depicted in Figure 11, enables high measurement accuracy and wide frequency coverage (DC to 300 MHz, by using different types of bridges); however, a single bridge needs to be manually balanced and covers only a narrow frequency range [22]. The Wheatstone bridge is balanced when there is no current flowing through the detector, D. The unknown impedance, Z_4, which represents the sample, is determined by correlation:

$$Z_4 = \frac{Z_1 Z_3}{Z_2}. \tag{62}$$

By writing out the reciprocal term for Z_4,

$$\frac{1}{Z_4} = \frac{Z_2}{Z_1 Z_3}, \tag{63}$$

and combining it with Equation 53, the complex dielectric constant of the sample is obtained.

This technique is used by the Novocontrol Alpha High Resolution Dielectric Analyzer. With frequency range of 1 μHz to 10 MHz it is useful for low frequency measurements. However, all measurements must be done with an external electrical field that is low enough to maintain a linear dependence between dielectric polarization density and the electric field.

3.1.2 Auto-balancing bridge method

Figure 13 shows a simplified schematic of the auto-balancing bridge, which has a broad frequency coverage (20 Hz to 110 MHz) with a high accuracy over a wide impedance measurement range and enables grounded device measurement. In other words, the method

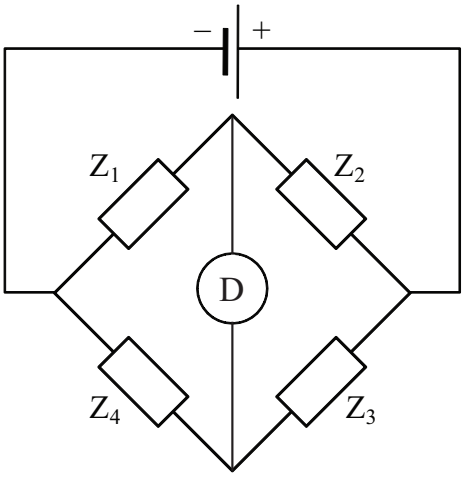

Figure 11: *Wheatstone bridge.* The sample in the circuit is represented by the Z_4 element. In order to balance the Wheatstone bridge, there must be no current flowing through the detector D.

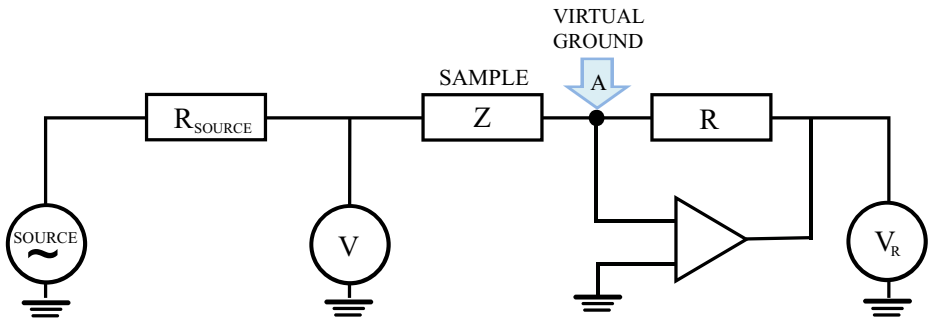

Figure 12: *Simplified schematic of the auto-balancing bridge.* By creating a virtual ground at point A, the value of current through the sample Z is the same to the one through R, $I_Z = I_R = U_R/R$.

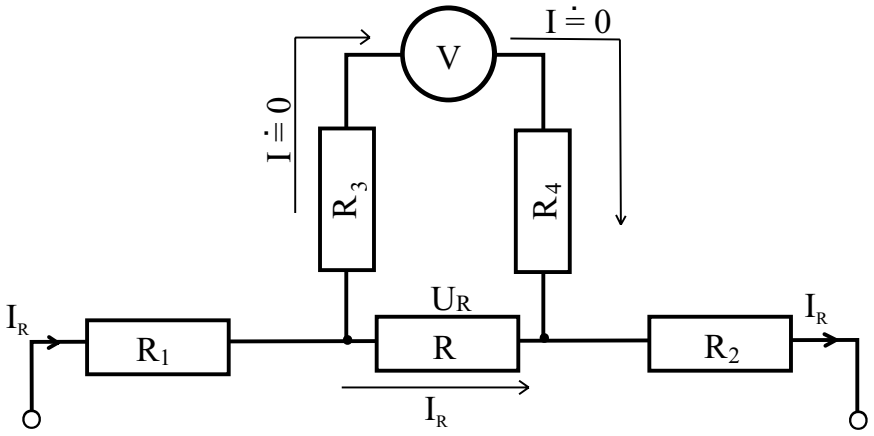

Figure 13: *Four-terminal pair measurement method.* R_1 and R_2 represent the impedances due to contacts and wires, respectively. Due to a high internal resistance of the voltmeter, the current flowing through R_3 and R_4 is negligible.

is designed to permit stable and accurate impedance measurements, without any mutual inductance or interference of measurements signals [22, 23].

Hewlett Packard 4284*A* precision LCR-meter uses the auto-balancing bridge method together with the four-terminal pair measurement method, depicted in Figure 13: two resistors, R_3 and R_4, are used in order to account for impedances due to contacts and wires, represented by R_1 and R_2, respectively. The voltage on R, which in this circuit represents the sample, is:

$$U_R = I_R R \left(1 - \frac{R + R_3 + R_4}{R_{VOLTMETER}}\right). \tag{64}$$

By taking into account the resistance of the voltmeter [23],

$$R_{VOLTMETER} = 10^{11}\Omega \implies \frac{R + R_3 + R_4}{R_{VOLTMETER}} = 0, \tag{65}$$

the current through the resistor is indeed:

$$I_R = \frac{U_R}{R}\ . \tag{66}$$

With preciseness of 0.05 % in the frequency range between 20 Hz and 2 MHz, the LCR-meter has the advantage in low as well as in high impedance measurements. If extensions are used, five-terminal and shielded two-terminal measurements are possible (see Figure 6–12 in Reference 23).

3.2 Nonlinear dielectric constant measurements

In order to determine the dielectric nonlinearity

$$a_3 = \frac{\varepsilon_3}{\varepsilon_0^3 \varepsilon^4}, \tag{67}$$

simultaneous measurements of temperature-dependence of the linear, ε_1, and the nonlinear, ε_3 dielectric constant have been performed using a circuit, depicted in Figure 14. The sample, C_X, is connected in parallel to known capacitance $C_0 \gg C_X$ and U_{AC} is applied to the sample. Capacitors $C_1 \gg C_0$ and $C_2 \gg C_0$ are in the circuit in order to protect the apparatuses from high external DC electric fields (source U_{DC}) during such measurements.

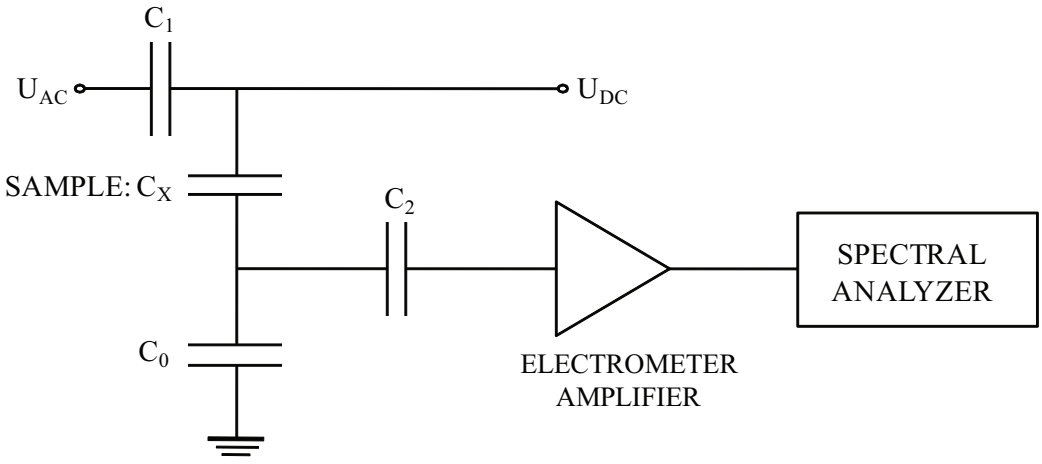

Figure 14: *Circuit used for measuring the nonlinear dielectric constant.* If a spectral analyser is used in combination with this circuit, simultaneous measurements of the linear and the nonlinear dielectric constant can be performed.

The response of the systems is amplified by an electronic signal amplifier and then measured by the Hewlett Packard 35665*A* Dynamic Signal Analyzer, which enables simultaneous measurements of the first, U_1, the third, U_3, and the fifth, U_5 harmonic dielectric responses. Then the linear, ε_1, and the nonlinear, ε_3, dielectric constants were calculated from relations:

$$\varepsilon_1 = \frac{C_0}{C_X} \cdot \frac{U_1}{U_0 - U_1} \tag{68}$$

and

$$\varepsilon_3 = \frac{4U_3}{U_1} \cdot \frac{\varepsilon_1}{E^2}, \tag{69}$$

in which E is the external electric field applied to the sample [25]. If $U_5 \approx U_3$, the nonlinear dielectric constant was calculated using the relation:

$$\varepsilon_3 = \frac{4C_0}{C_{X0}} \cdot \frac{d^2}{(U_0 - U_1)^3}\left(U_3 - \frac{5}{16}U_5\right), \tag{70}$$

where d is the sample thickness and C_{X0} is the capacitance, calculated using Equation 47 and sample dimensions.

The advantage of the simultaneous measurement is that, in comparison to separate measurement runs, the error in the subsequent computation of the ratio $a_3 = \varepsilon_3/\varepsilon_0^3\varepsilon^4$ is reduced. In this computation, the real part of the linear and the absolute value, ε_3, of the third-order nonlinear dielectric constant were used [25].

3.3 Temperature stabilization

Figure 15 depicts the schematic of the circuit used for temperature stabilization. The lock-in bridge is based on the Wheatstone bridge (Figure 11) and is composed of (i) a temperature sensor, R_X, which is a Pt1000 resistor, located in the probe, (ii) a resistor decade box, R_3, which is connected to the computer and enables the user to set the target desired temperature in the probe, and (iii) two 500 Ω resistors, R_1 and R_2.

The bridge is powered by the reference signal, outputted from the phase detector. The output signal is set to be positive, if $R_X < R_3$. A second output signal from the phase detector is run over a signal power amplifier and used to power the heater in the probe.

A Pt100 resistor, connected to the Keithley 196 System DMM, is used to determine the current temperature inside the probe [25]. Using the lock-in bridge technique and the probe, depicted in Figure 16, the temperature in the range of 80–450 K can be stabilized within 5 mK.

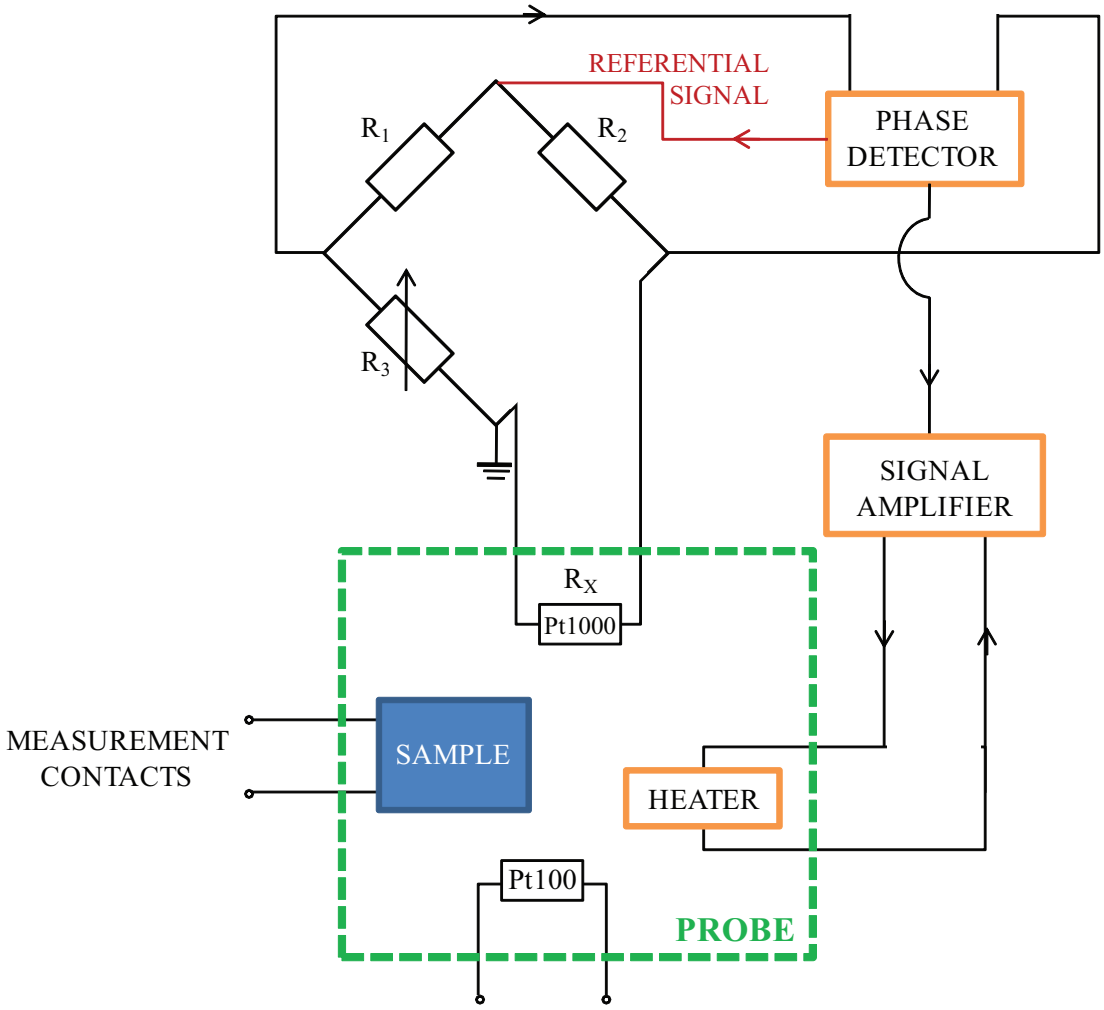

Figure 15: *Schematic of the circuit used for temperature stabilization.* The elements within the dashed green box are located within the probe.

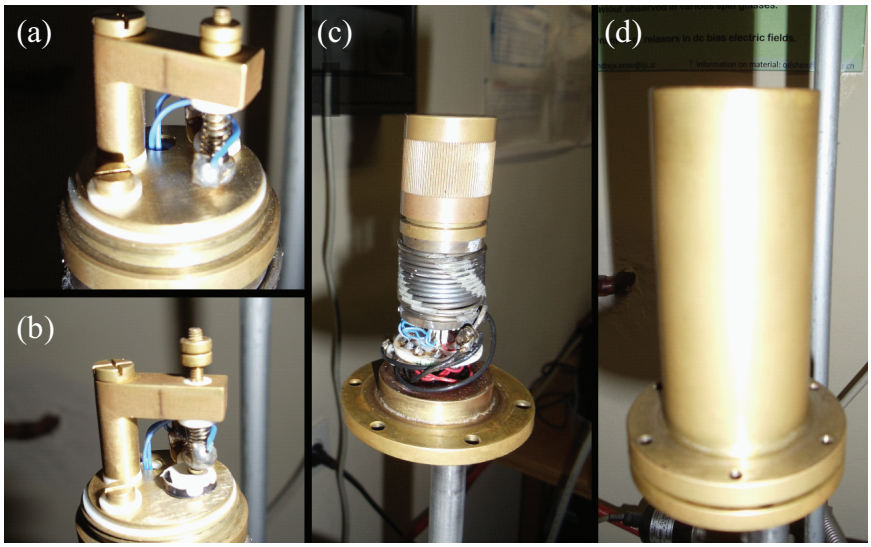

Figure 16: *The Probe.* The pictures show an empty probe (a), a sample in the probe (b), the inner shield over the probe (c) and the outer shield over the probe (d). The contacts and the shields of the probe are made of brass.

4 Dielectric investigations of $CaCu_3Ti_4O_{12}$ ceramic thin films

The chapter is dedicated to $CaCu_3Ti_4O_{12}$ ceramic thin films and core-shell structured ceramic materials in general. The beginning of the chapter serves as a brief historic overview of the scientific interest in the $CaCu_3Ti_4O_{12}$ system. The second part of the chapter focuses on modelling the temperature- and frequency-dependent dielectric response of core-shell structures in terms of the equivalent circuit. The rest of the chapter presents the results of the study of the influence of preparation conditions on the distinctive contributions to the dielectric behaviour of $CaCu_3Ti_4O_{12}$ thin films. The experimental work presented in this chapter was done in collaboration between the Condensed Matter Physics Department, F5, and the Electronic Ceramics Department, K5, of the Jožef Stefan Institute.

4.1 Overview

Over the last few decades, heterogeneous ceramic materials, such as $CaCu_3Ti_4O_{12}$ (CCTO) [15], $Gd_{0.6}Y_{0.4}BaCo_2O_{5.5}$ [18] and (Sr,La)$NbO_{3.5-x}$ [26] have been intensively studied due to very high values of the dielectric constant that reveal immense potential for the use of these materials in various modern electronic and electromechanical applications. Due to very high values of the dielectric constant (a nearly constant dielectric permittivity of several 10^3 was measured in CCTO bulk at 1 kHz in a temperature range between room temperature and 570 K [27, 28]), CCTO bulk, thick or thin films have intensively been studied in the last decennium [15–17, 27–30]. The origin of such high values has at first been attributed to either (i) the intrinsic effect, due to the perovskite-like crystal structure of CCTO, or (ii) the extrinsic effect, i.e., the insulating grain boundaries and semiconducting grains that form an effective circuit of parallel capacitors [27].

In initial research, an intrinsic mechanism was proposed in order to explain the physical origin of the measured Debye relaxation with $\varepsilon \sim 10^5$ at temperatures above 100 K and its drop for three orders of magnitude at temperatures below 100 K for the optical response of CCTO single crystals [29]: CCTO has perovskite-like atomic structure(see Figure 17), in which the lack of a fourfold axis disables cubic symmetry of the Ti^{4+} cations , and thus a ferroelectric phase transition based on the displacement of Ti^{4+} from the octahedron is much less likely than in a perovskite (a large enough TiO_6 octahedral tilt actually affects the transition into a ferroelectric state [27]). With increasing temperature, the Ti^{4+} cations could not displace off centre along a fourfold axis as they would in a perovskite, but only along their one threefold axis, thereby creating tension on the Ti–O and causing the octahedra to tilt. As no ferroelectric transition was observed, as well as no distortions in the crystal structure (which would be due to the changes in the TiO_6 octahedral tilt), the only thing that the intrinsic effect could explain is the origin of high values of the dielectric constant at high frequencies at high temperatures, where dielectric permittivity is almost temperature independent [29]. The measured Debye relaxation from Fig. 2 in Reference 29 has later successfully been modelled in terms of an equivalent circuit, depicted in Figure 10a, with only $\varepsilon_\infty = 80$. This showed that a non-intrinsic mechanism in fact governs the dielectric

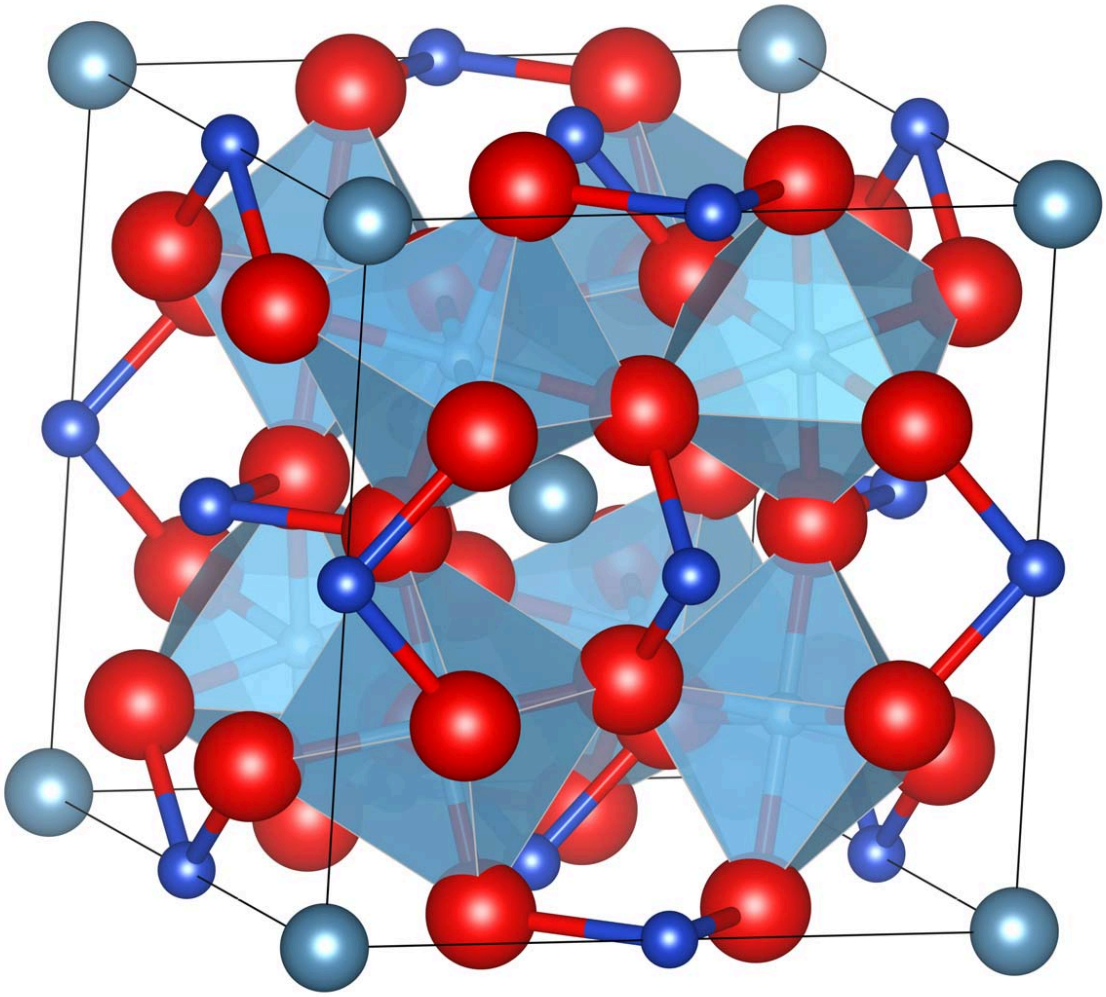

Figure 17: *Unit cell of $CaCu_3Ti_4O_{12}$.* A unit cell of CCTO, in which the atoms are plotted according to their ionic radius [31,32], shown as TiO_6 octahedra (Ti atoms in the octahedra are grey), Cu atoms (dark blue) bonded to four oxygen atoms (red) and Ca atoms (light blue) without bonds. The black lines are a guide for the eye.

properties of CCTO single crystal [15,30]. In further studies, dielectric spectroscopy turned out to be a powerful tool for revealing the electrical heterogeneities in the microstructure, i.e., the core-shell structure, as the origin of such high values, which are almost constant in a broad frequency and temperature range [15–17,30,33–37].

Analysis in terms of the equivalent circuit is a straightforward approach to understanding the dielectric behaviour: Elements of the equivalent circuit are used to describe distinctive contributions to the dielectric response, i.e., analysis in terms of an equivalent circuit enables separation and characterization of distinctive contributions to the dielectric response [14,15]. In our studies, the dielectric response of core-shell structured ceramic material was modelled in terms of an equivalent electric circuit with elements that describe distinctive contributions of grains and grain boundaries. By taking into account a proper temperature dependence of individual elements of the circuit, the temperature and frequency dependent dispersive dielectric behaviour, typically observed in these materials, was obtained. In addition, the use of analysis in terms of the equivalent circuit as a data rescue tool was presented for cases in which detected dielectric data are compromised by resistance or resonance of the measuring setup. It was shown that even small values of resistance or inductance result in an artificial relaxation or resonance in the detected dielectric response and the influence of parasitic inductance and resistance of the measuring setup on measured dielectric response

was presented [1].

Recent reports indicate that dielectric behaviour of CCTO ceramics and thin films can be influenced by the preparation conditions [15,34,38]. We studied the influence of preparation conditions on dielectric properties of CCTO by performing detailed dielectric investigations in a broad temperature and frequency range. Experimental results, obtained in various CCTO thin films prepared by chemical solution deposition, and analysis in terms of the equivalent circuit reveal that the preparation conditions govern the distinctive contributions of insulating grain boundaries and semiconducting grains in different temperature and frequency ranges. With proper post-annealing process, dielectric constant of ∼3000 was obtained in films with thickness below 500 nm. Additional analysis of the electrical conductivity revealed that 1-dimensional variable range hopping is the dominating transport mechanism in CCTO thin films [2,39].

4.2 Equivalent circuit modelling of core-shell structured ceramic materials

In the simplest case of core-shell structured ceramic materials, two constituents govern the dielectric response: conducting grains and insulating grain boundaries. Figures 18 and 19 show temperature and frequency dependence of ε' and ε'', respectively, for data obtained in CCTO ceramic thin films [1,2], which is similar to the case of single crystals, where the non-intrinsic origin of colossal values of dielectric permittivity is due to the crystal structure that consists of bulk material and surface layers, i.e., Schottky diode that was formed at the semiconductor-metal interface [15]. Equivalent circuit used for analysis of such systems is composed of two leaky capacitors connected in series, as shown in Figure 10a: G_{BULK} and G_{SL} represent the conductance and C_{BULK} and C_{SL} the capacitance of bulk material and surface layers, respectively, and $C_{SL} \gg C_{BULK}$. The reciprocal value of the complex impedance of such equivalent circuit is:

$$\frac{1}{Z} = \left(\frac{1}{G_{BULK} + i\omega C_{BULK}} + \frac{1}{G_{SL} + i\omega C_{SL}} \right)^{-1} \tag{71}$$

and can be rewritten to form from Equation 53, so that:

$$\begin{aligned} \frac{1}{Z} &= G_{MEAS} + i\omega C_{MEAS} = \\ &= \frac{((G_{BULK} + i\omega C_{BULK})(G_{SL} + i\omega C_{SL}))\,(G_{BULK} + G_{SL} - i\omega(C_{BULK} + C_{SL}))}{(G_{BULK} + G_{SL})^2 + \omega^2\,(C_{BULK} + C_{SL})^2}. \end{aligned} \tag{72}$$

The characteristic frequency of the artificial Debye relaxation, derived from Equation 72 at $G_{BULK} \gg G_{SL}$ and $C_{BULK} \ll C_{SL}$, is [1]:

$$\omega \simeq 1/(C_{SL} R_{BULK}), \tag{73}$$

in which $R_{BULK} = 1/G_{BULK}$ represents the resistance of the bulk and C_{SL} the capacitance of the electrode-bulk interface or grain boundaries. If R_{BULK} and, concomitantly, the characteristic frequency of this artificial Debye's response follow the Arrhenius law (Equation 59), then, with increasing temperature giant surface layer/grain boundary contributions are detected up to higher frequencies. Thus, the temperature dependence of the conductivity of the bulk in Equation 72 is assumed to be the usual Arrhenius expression [1]:

$$1/G_{BULK} = R_{BULK} = R_0 \exp\left(-T/T_0\right). \tag{74}$$

The choice of parameters G_{BULK}, C_{BULK}, G_{SL}, and C_{SL} for modelling does not influence the obtained Debye-like behaviour as long as $C_{BULK} \ll C_{SL}$ and $G_{BULK} \gg G_{SL}$.

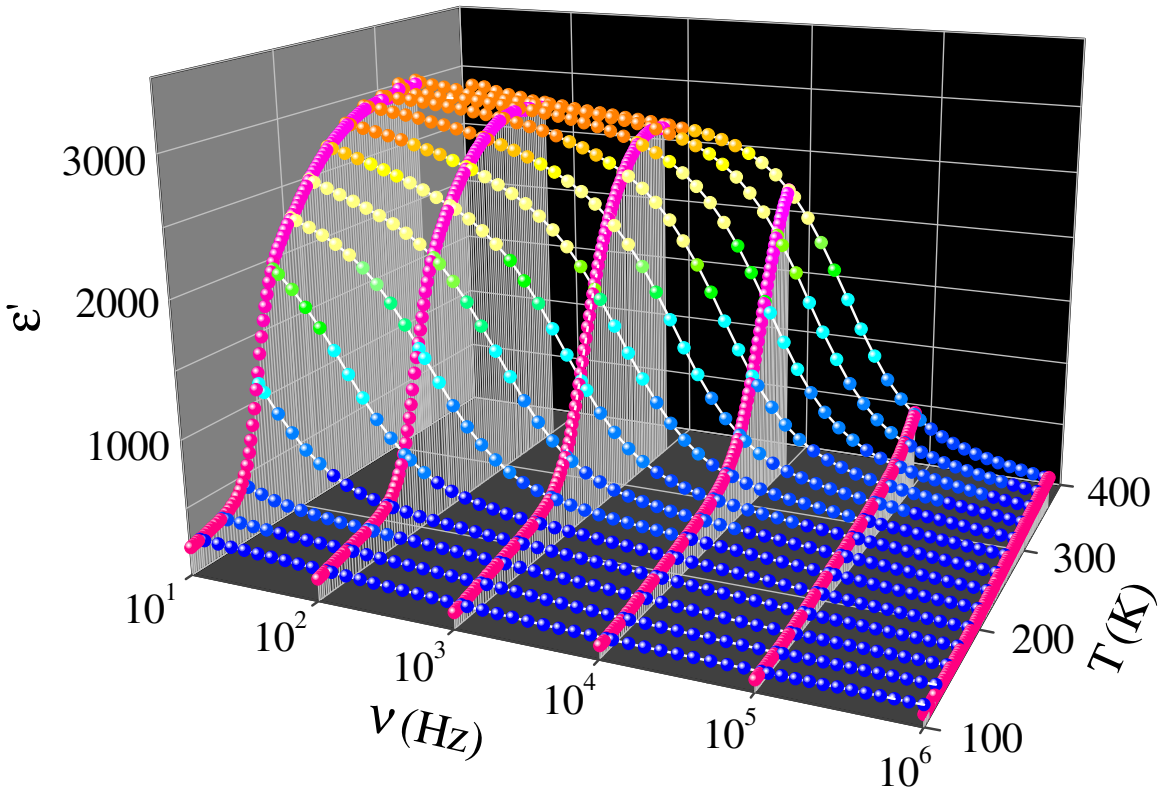

Figure 18: *Temperature- and frequency-dependent ε' of CCTO thin film.* Experimentally detected ε' vs. temperature and frequency in CCTO ceramic thin films, prepared by chemical solution deposition and post-annealed in flowing nitrogen atmosphere. Solid lines are a guide for the eye.

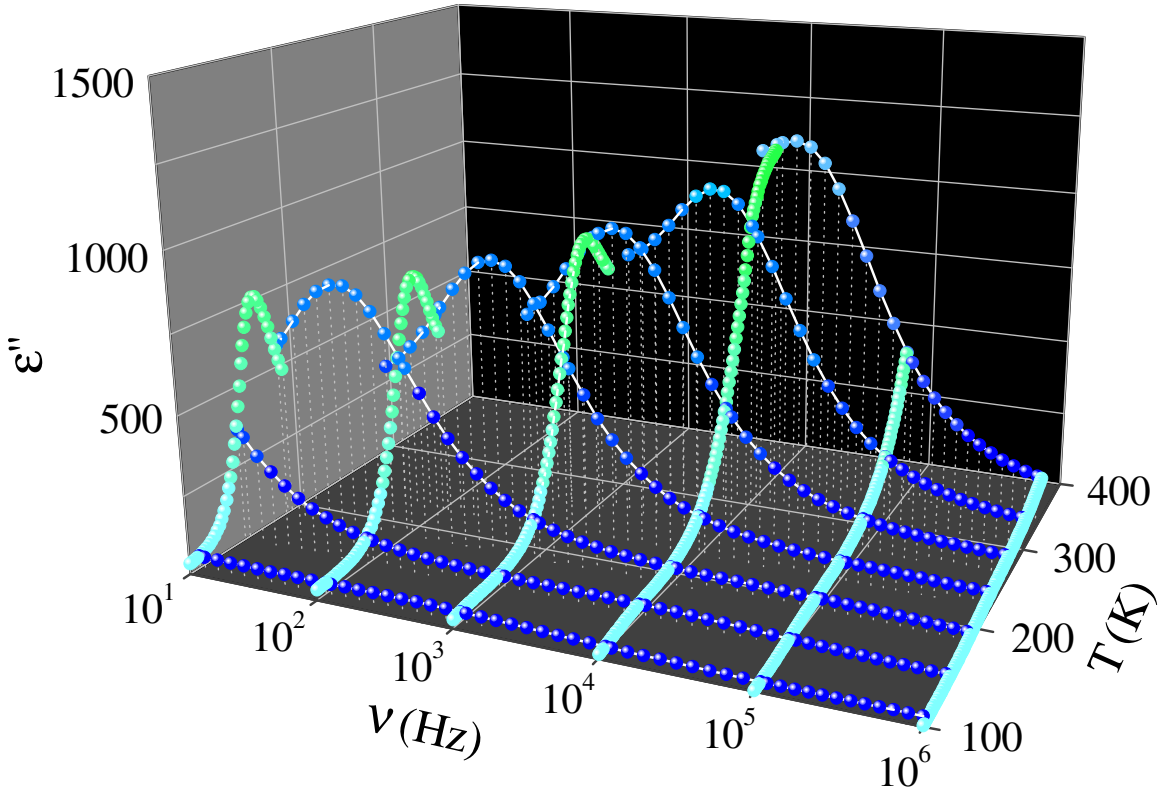

Figure 19: *Temperature- and frequency-dependent ε'' of CCTO thin film.* Experimentally detected ε'' vs. temperature and frequency in CCTO ceramic thin films, prepared by chemical solution deposition and post-annealed in flowing nitrogen atmosphere. Dashed lines are a guide for the eye.

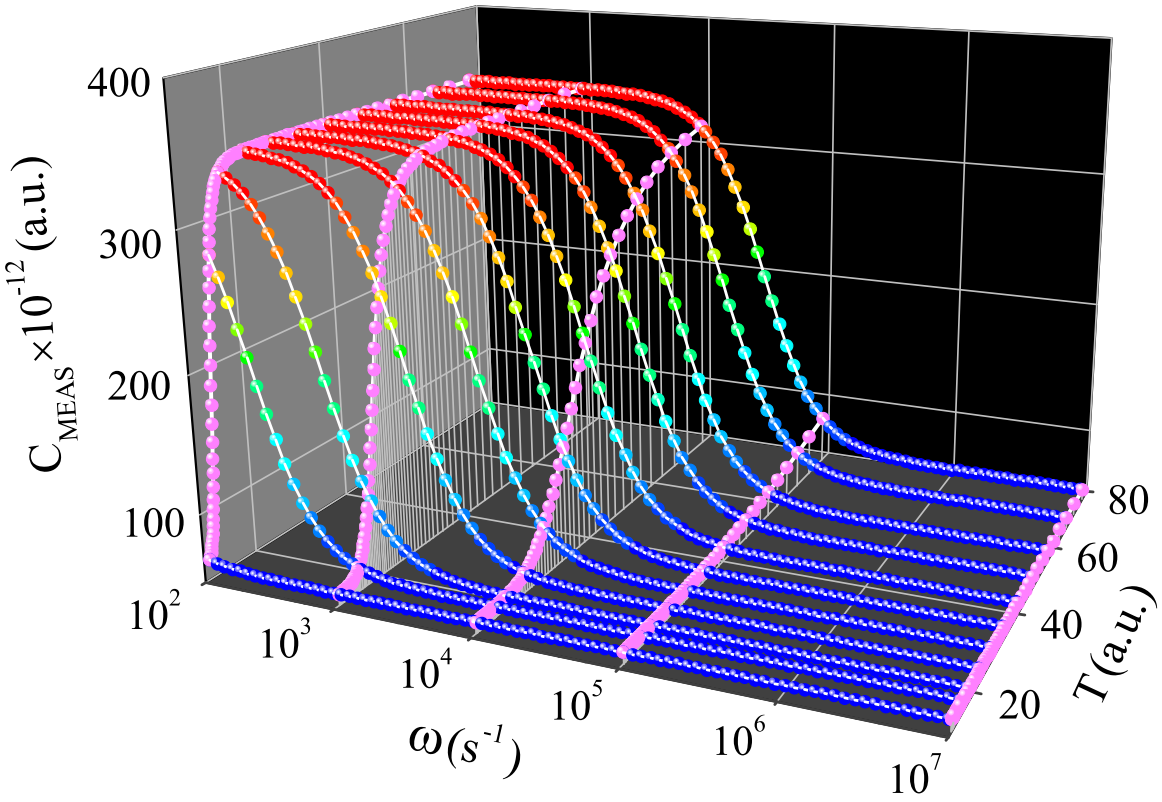

Figure 20: C_{MEAS} *vs. frequency and temperature.* Modelled plot of C_{MEAS} from Equation 72 vs. frequency and temperature. Solid lines are a guide for the eye.

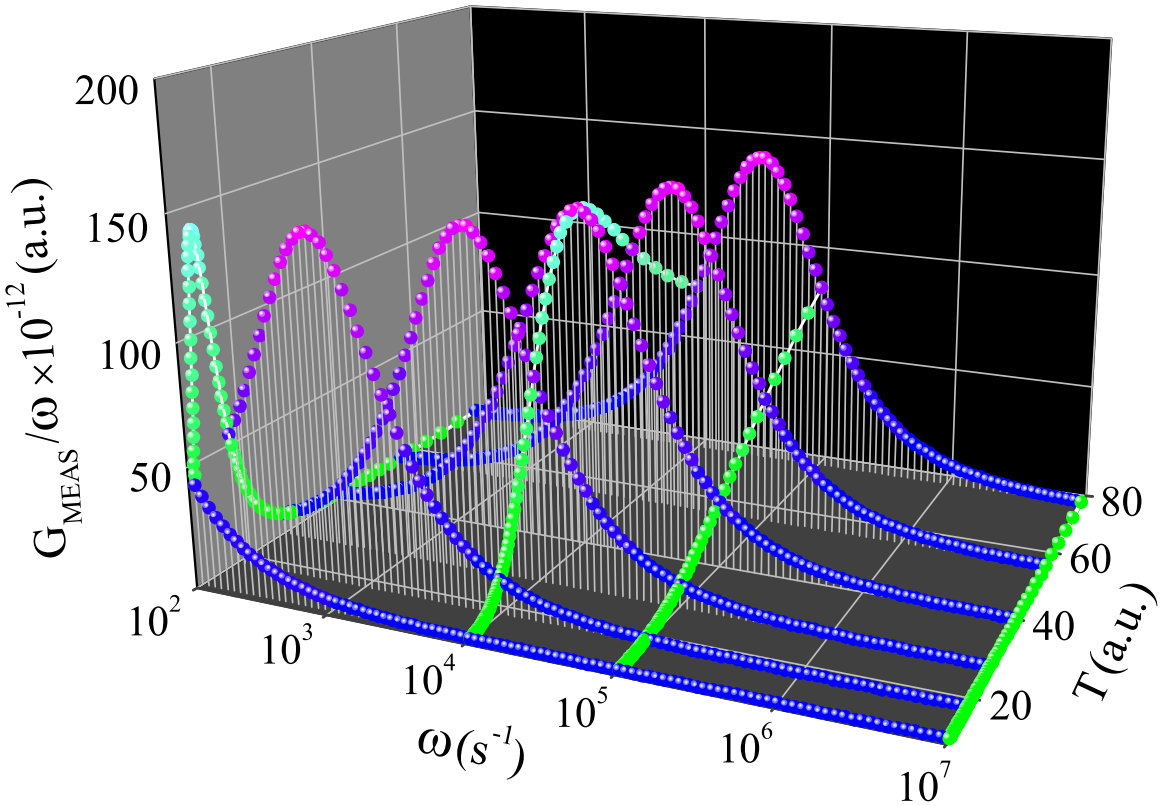

Figure 21: G_{MEAS}/ω *vs. frequency and temperature* Modelled plot of G_{MEAS}/ω from Equation 72 vs. frequency and temperature. Solid lines are a guide for the eye.

As the result, temperature dependencies of C_{MEAS} and G_{MEAS}/ω in Figures 20 and 21 reveal an artificial Debye relaxation: at a fixed value of frequency the measured capacitance drops from C_{SL} at higher temperatures to C_{BULK} at lower temperatures, and, concomitantly, the characteristic temperature drop increases with frequency, which is indeed the experimental case reported in core-shell structured ceramic materials. [15, 18, 26]. Due to clarity, a simpler, two-dimensional, view of the modelled plots of C_{MEAS} and G_{MEAS}/ω vs. frequency and temperature is depicted in Figure 22.

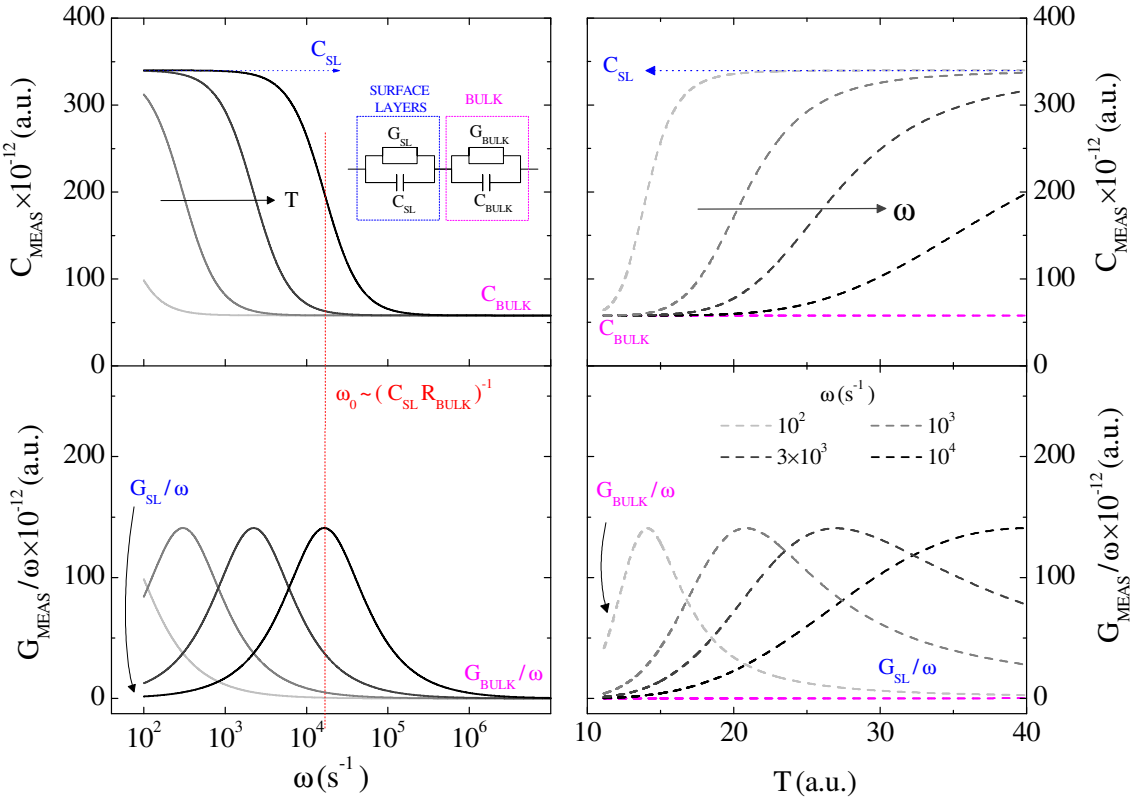

Figure 22: *C_{MEAS} and G_{MEAS}/ω vs. frequency and temperature* Modelled plots of C_{MEAS} and G_{MEAS}/ω from Equation 72 vs. frequency (left) and temperature (right). The inset shows the equivalent circuit composed of two leaky capacitors connected in series, representing the surface layers/grain boundaries and the bulk/grains.

4.3 Influence of preparation conditions on distinctive contributions to dielectric behaviour of $CaCu_3Ti_4O_{12}$ thin films

In order to investigate the influence of preparation conditions on dielectric behaviour of CCTO thin films, high-resolution dielectric investigations in a broad frequency and temperature range were performed. This section shows that (i) insulating grain boundaries and semiconducting bulk grains individually determine the dielectric behaviour of CCTO thin films in different temperature and frequency regions and (ii) by manipulating the conditions under which the thin films are prepared, their dielectric properties can be controlled. In addition, it is shown that in the case of CCTO thin film, prepared on a nucleation layer, the dielectric response is determined by the microstructure consisting of large grains that extend throughout the whole thickness of the film.

4.3.1 Experimental procedure

4.3.1.1 Processing and structural characterization

CCTO thin films were prepared from the nitrate-alkoxide based solution. Titanium n-butoxide (99.9+%, Alfa Aeser) and a mixture of calcium nitrate tetrahydrate (99.9995%, Alfa Aeser) and copper nitrate hemipentahydrate (99.999%, Alfa Aeser) were separately dissolved in 25 ml and 50 ml of 2-methoxyethanol (99.3%, Sigma Aldrich), respectively, and mixed. The solution was heated for 30 min at 323 K. The concentration of the final light blue solution was 0.4 M. The CCTO solution was spin-coated onto platinized silicon substrates (100 nm Pt/10 nm $TiO_2/SiO_2/Si$, Aixacct) at 3000 rpm/30 s, dried at 523 K for 2 min, and pyrolyzed at 623 K for 5 min. The procedure was repeated six or twelve times and the respective films are further denoted as 6- or 12-layer films. The films were annealed at 1023 K for 15 min in a rapid thermal annealing (RTA) furnace. Selected films were post-annealed in a tube furnace at 773 K for 8 h in flowing nitrogen, air, or oxygen atmospheres. In addition, some CCTO thin films were prepared on a nucleation layer. In order to obtain the nucleation layer, CCTO solution was spin-coated onto platinized silicon substrates (100 nm Pt/10 nm $TiO_2/SiO_2/Si$, Aixacct) at 3000 rpm/30s, dried at 523 K for 2 min, and annealed at 1023 K for 5 min. In further text, CCTO films with a nucleation layer will be referred to as 1+X-layer films, where 1 represents the nucleation layer and X is 6 or 12, with respect to the number of the procedure repetitions [2].

The films were characterized by X-ray diffraction (XRD, PANalytical X'pert Pro diffractometer, $CuK_{\alpha 1}$ radiation). The data were collected in the 2θ-range from 15° to 55°, with a step of 0.034° and an exposure time of 100 s per step. The phases were identified using the PDF–2 database [40] and the microstructure was analysed by field emission scanning electron microscopy (FE-SEM, Supra 35 VP, Carl Zeiss) [2].

4.3.1.2 Dielectric characterization

Figure 23 depicts CCTO thin films with sample thickness in the range of 200–600 nm and sputtered upper Cr/Au electrodes with 0.4 mm diameter (RF-magneton sputtering, 5Pascal) that were used for dielectric measurements. The complex dielectric constant from Equation 14 was measured by Novocontrol Alpha High Resolution Dielectric Analyzer in a frequency range of 1 Hz–3 MHz. The amplitude of the probing AC electric signal was 50 mV. The data were obtained in the temperature range of 90–410 K during cooling with temperature change rate of $\Delta T/\Delta t = 0.5$ K/min. Temperature of samples was stabilized within 10 mK using a lock-in bridge technique with a Pt100 resistor as a thermometer [2, 39].

4.3.2 Results and discussion

4.3.2.1 Materials properties

Figure 24 shows the XRD patterns of RTA- and post-annealed 6- and 12-layer CCTO thin films, which could be indexed with the randomly oriented $CaCu_3Ti_4O_{12}$ phase (JCPDF 75-2188) [40]. Among the detected low-intensity peaks, the peak at 27.54° could be assigned to TiO_2 (rutile, JCPDF 89-4921) [40] and the one at 35.29° to CuO (JCPDF 89-5899) [40]: both peaks are known from reports on the processing of CCTO powder [41] and solution-derived thin films [42]. Note that the peak at 35.29°, assigned to CuO, and the trace impurities are much more pronounced in 12-layer post-annealed films [2].

Microstructures of RTA-annealed CCTO thin films are collected in Figure 25. The fraction-surface micrographs in Figures 25a, c and e reveal (i) no layered structure of the films (a layered structure could have been expected due to CCTO solution being dried and pyrolyzed in several layers onto the nucleation layer or the substrates) and (ii) an appreciable amount of porosity [2]. Similar as in solution derived films [43], porosity is the

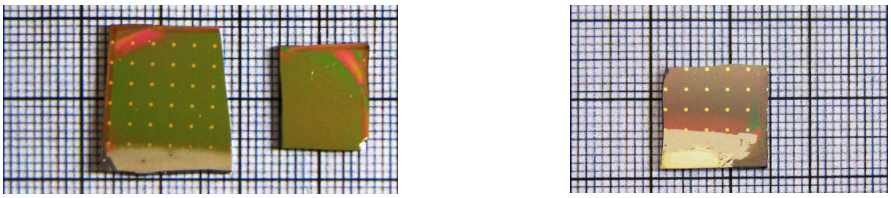

(a) 6-layer CCTO thin films (b) 12-layer CCTO thin film

Figure 23: *CCTO thin films.* CCTO thin films, prepared for dielectric measurements. In subfigure a), a sample without sputtered electrodes is shown (right). Although there is a difference in colour between the 6-layer (a) and 12-layer (b) samples, the preparation conditions did not notably influence the physical appearance of samples.

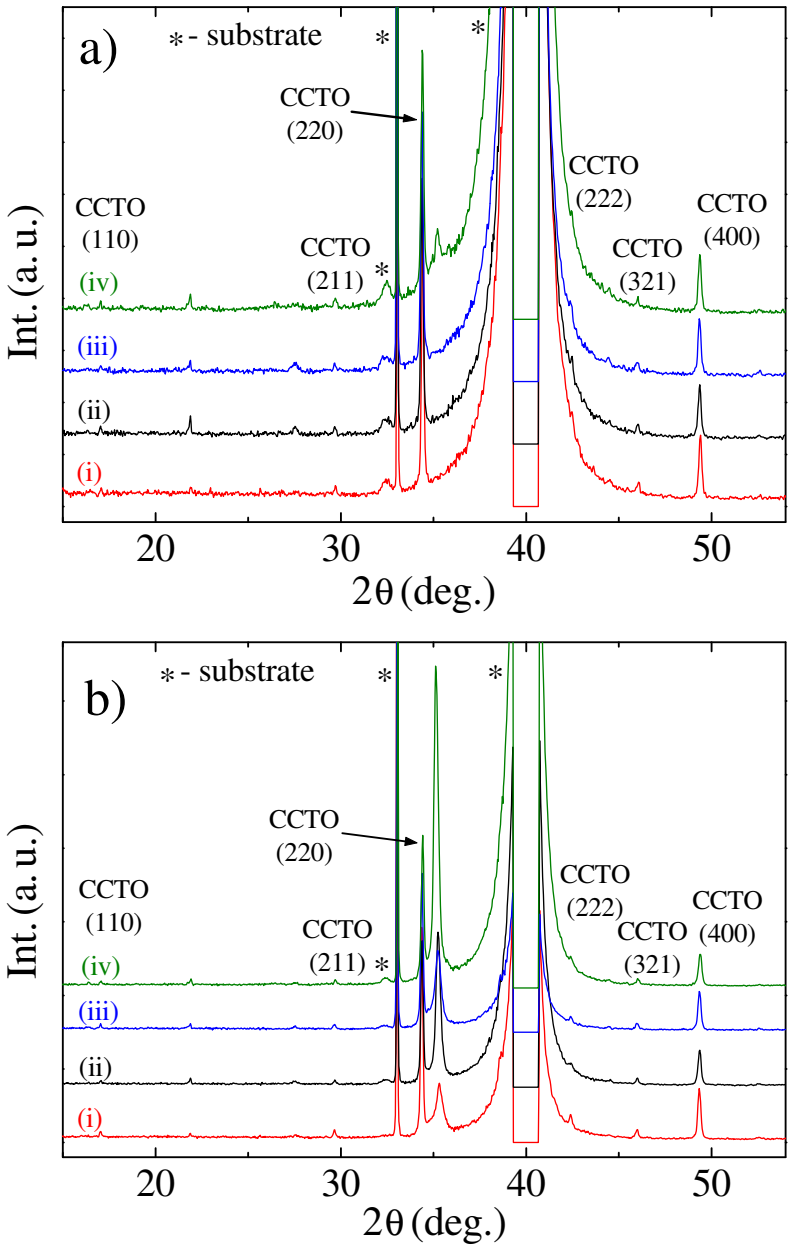

Figure 24: *XRD patterns of CCTO thin films.* XRD patterns of a) 6- and b) 12-layer CCTO films, which were (i) RTA-annealed and post-annealed in flowing (ii) nitrogen, (iii) air, or (iv) oxygen atmosphere.

main microstructural feature in the case of CCTO thin films. Even so, there is not much porosity in the plane-view micrographs (e.g., see Figure 25b), which could indicate different conditions of the consolidation at the film surface in comparison with the film interior.

In 6- and 12-layer films, the size and the shape of the grains are unrecognizable from the fracture-surface micrographs (Figures 25a and c); however, grains of either a few nm or a few 10 nm in size are visible in plane-view only (Figures 25b and d) revealing a bimodal grain-size distribution, which could be correlated to the presence of impurities [43]. Similar microstructural features (porosity and bimodal grain-size distributions) were observed in all 6- and 12-layer post-annealed films. It should also be stressed that the measurements of the sample thickness with the profilometer (Taylor Hobson Form Talysurf) reveal an increase in the thickness after post-annealing: The thickness of RTA-annealed films increased from 270 or 550 nm to 300 or 610 nm after post-annealing for 6- or 12-layer films, respectively [2].

In 1+6-layer film, both, fracture-surface and plane-view micrographs (Figures 25e and f) reveal grains of several 100 nm in size. The microstructure is, however, completely different from that of films without a nucleation layer: In this case, a single grain extends through

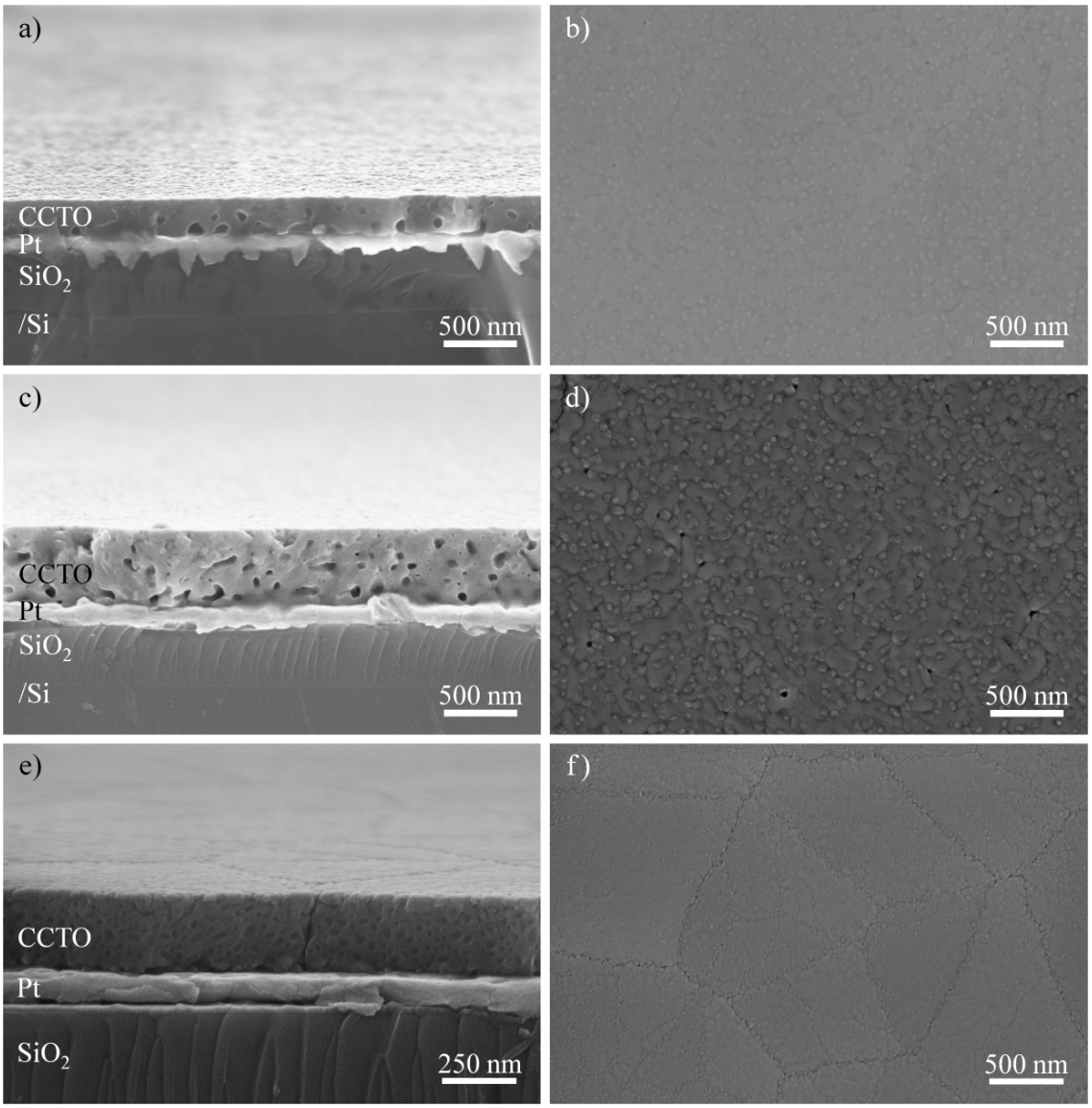

Figure 25: *Fracture-surface and plane-view FE-SEM micrographs of CCTO thin films.* Fracture-surface and plane-view FE-SEM micrographs of RTA-annealed 6-layer (a and b), 12-layer, (c and d), and 1+6-layer (e and f) CCTO thin films.

the whole thickness of the film [2].

4.3.2.2 Temperature-dependent dielectric behaviour of CCTO thin films

Figure 26 shows the dielectric constant data as a function of the temperature, obtained at several measuring frequencies between 1 Hz and 3 MHz, for RTA-annealed 12- and 6-layer CCTO thin films. In the 12-layer film, a typical main plateau, i.e., relatively high and almost temperature-independent ε' values of ~ 2200 in the high-temperature range, arises due to grain boundary contributions [2]. The additional high-temperature increase of ε' at lower frequencies is due to the increasing electrical conductivity. This contribution is more conspicuous from the increase of $\varepsilon''(T)$. In the 6-layer, i.e., thinner film, in which the $\varepsilon' \sim 1400$ plateau arises due to the contributions of the grain boundaries, the $\varepsilon' \sim 1700$ plateau can be attributed to contribution of surface layers and the high-temperature increase of ε'' at lower frequencies is due to the increasing electrical conductivity. The contributions of the surface layers are naturally present also in a ceramic sample, and it is also well known that they suppress the dielectric response of thin films [30]. Comparison of both dielectric responses at a discrete value of frequency reveals that (i) ε' main plateau has higher values and (ii) the drops in the value of ε', accompanied by peaks in ε'', occur at higher temperatures in the case of the 12-layer film.

The dielectric constant of 12- and 6-layer films that were post-annealed at various oxygen partial pressures is shown in Figures 27 and 28. In spite of some porosity, which was (in this case) not modelled by our equivalent circuits, but undoubtedly alters the dielectric response, i.e., decreases the dielectric constant, with proper post-annealing process, for a

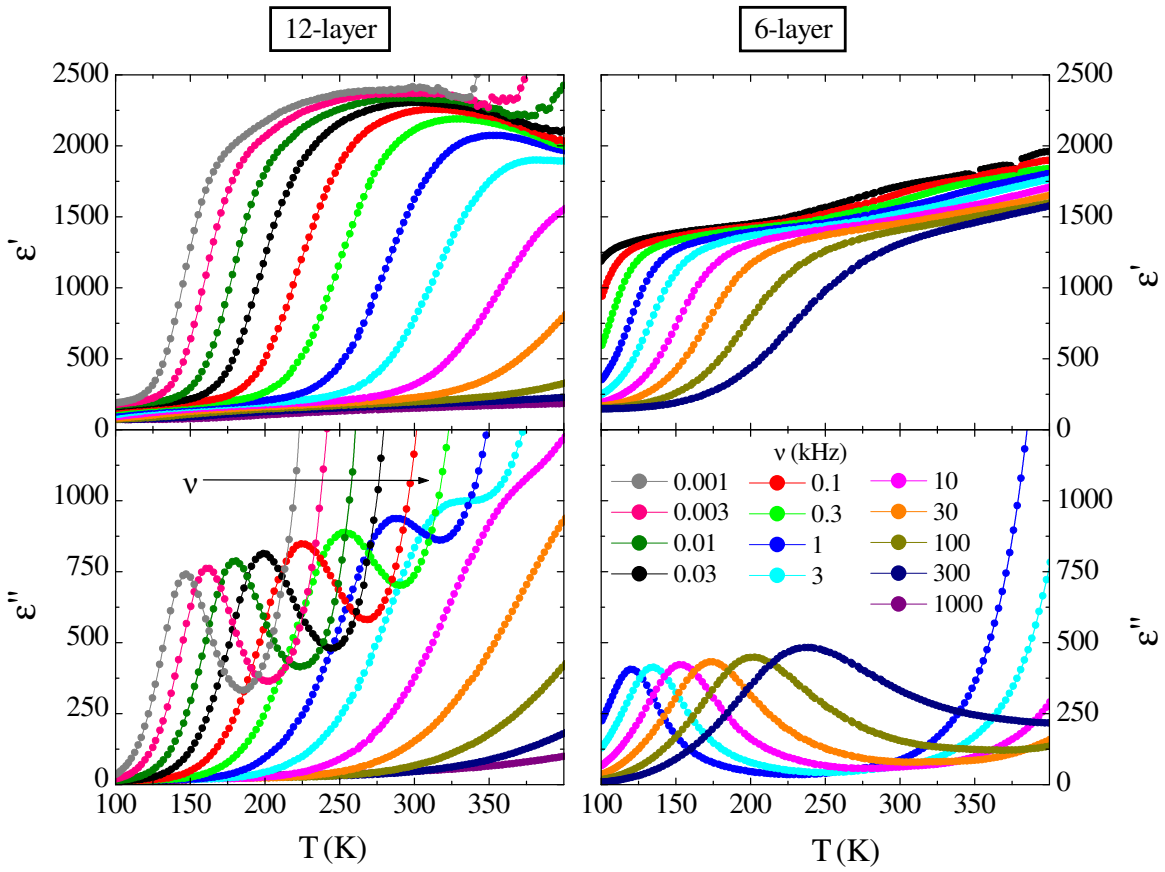

Figure 26: *Temperature-dependence of RTA-annealed CCTO thin films.* The real, ε', and the imaginary, ε'', parts of the complex dielectric constant, obtained in RTA-annealed 12- (left) and 6-layer (right) CCTO thin film at various frequencies.

thin film very high dielectric constant of ~ 3000 was obtained [2]. While at low temperatures the bulk values are almost the same (~ 110), comparison of samples, prepared under the same conditions (e.g., Figures 27a and 28a), reveals much higher ε' plateau values for thicker 12-layer samples. In fact, the plateau ε' values, arising from the grain boundaries, is in 6-layers films only ~ 1500 (Figure 28a) and ~ 1250 (Figure 28b). The influence of the surface layers was expected to be much more pronounced in thinner samples, which is indeed the experimental case: Another dispersive anomaly (due to the influence of the surface layers), which further increases ε' values, can clearly be seen [2].

Post-annealing strongly affects main plateau values and the temperature of their drop. In comparison to the RTA-annealed samples, main plateau values increase and the temperature of their drop shifts towards lower temperatures after post-annealing in nitrogen. After post-annealing in air or atmosphere with high oxygen partial pressure, however, main plateau values decrease and the temperature of their drop shifts towards higher temperatures. These differences in ε' can be attributed to either (i) changes in geometry that are due to electrical heterogeneities in the microstructure (e.g., different distributions of Cu^+ and Cu^{2+} within grains and grain boundaries of CCTO, which could perhaps imply that post-annealing changes the thickness of grain boundaries and thus vales of C_{GB} and characteristic frequency from Figure 22 or (ii) differences in conductivity of both grains and grain boundaries and concomitantly their influence on ε' via the Kramers-Kronig relations [1,2]. It should also be stressed that differences in the dielectric response are much more pronounced in thicker samples, as the influence of surface layers suppresses the dielectric response of thinner samples.

The distribution of Cu^+ and Cu^{2+} ions could in fact be the reason for the core-shell structure, i.e., electrical heterogeneities in the microstructure of CCTO thin films: Cu^+ ions are distributed on the edges and Cu^{2+} in the centres of the grains, where there are, concomitantly, more Ti *3d* electrons available, which increase the conductivity. Thus, the preparation conditions could influence the electrical heterogeneities in the microstructure due to the reactions that affect copper ions in CCTO during sintering in air and post-annealing in an atmosphere that contains a certain percentage of oxygen. Oxidation numbers of CCTO are $Ca^{2+}Cu_3^{2+}Ti_4^{4+}O_{12}^{2-}$. During sintering, a slight reduction of Cu^{2+} to Cu^+ occurs, which is compensated by a slight substitution of Ti^{4+} ion on Cu site in a way that the average oxidation state of 2 is maintained and the overall charge of the compound is balanced. This can occur at temperatures as low as 700 K upon heating oxides in air [38,44]. Then, during post-annealing, reaction

$$Cu^+ \xrightarrow{0_2} Cu^{2+} \tag{75}$$

takes place due to the presence of oxygen in the annealing atmosphere, causing Cu^+ to revert back to Cu^{2+} [44]. Such a scenario would result in different distributions of Cu^+ and Cu^{2+} within grains and grain boundaries of CCTO after the post-annealing process, and, concomitantly, should show in the dielectric response as changes in main plateau vales and the temperature of their drop. However, at this point it should be mentioned that alternative explanations for the influence of preparation conditions on dielectric behaviour of CCTO bulk and thin film exist, based on oxygen vacancies [38] or copper-less grains [34].

If the above proposed scenario is considered, then CCTO thin films that were post-annealed in flowing air or oxygen atmospheres should have lower grain boundary contributions, i.e., lower ε' values than samples that were not post-annealed, and the temperature of the drop in ε' at a given frequency should take place at a higher temperature. This indeed is the experimental case in, e.g., Figures 27b and c. On the other hand, ε' values of samples, post-annealed in nitrogen, are higher in comparison to samples that were not post-annealed. Since a very small percentage of oxygen exists in flowing nitrogen atmosphere, a smaller number of Cu^+ ions take part in the reaction in Equation 75 than in the cases, where samples were post-annealed in air or oxygen enriched atmospheres. Instead, the re-

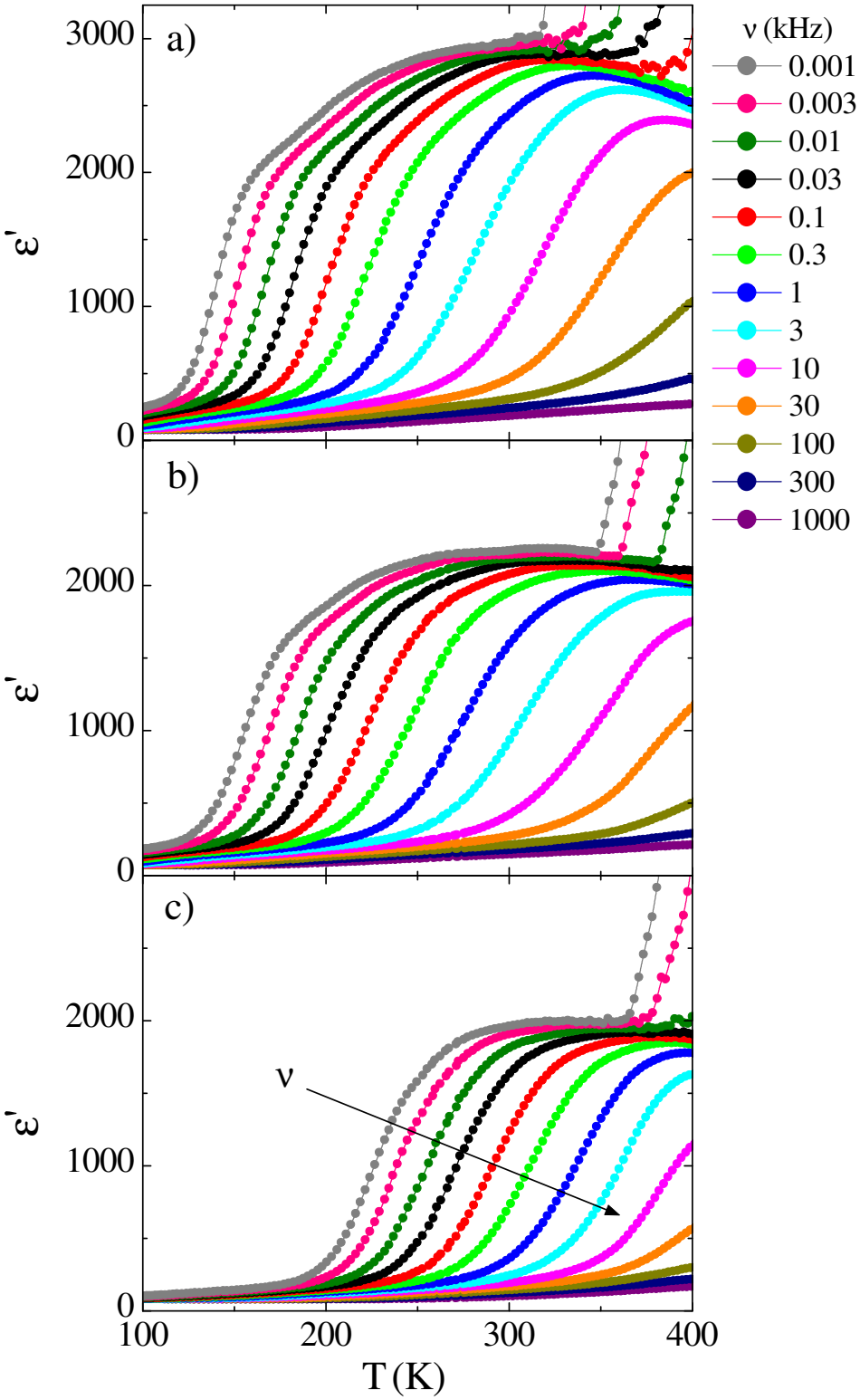

Figure 27: *Temperature-dependence of 12-layer CCTO thin films.* Dielectric constant vs. temperature of 12-layer films, post-annealed in flowing a) nitrogen, b) air and c) oxygen atmosphere.

duction of Cu^{2+} to Cu^{+}, which already took place during sintering, occurs again, more Cu^{+} ions form and, concomitantly, more liberated electrons go into Ti *3d* conduction band. It was shown that samples, which were post-annealed in flowing nitrogen atmosphere, indeed exhibit higher electrical conductivity [2].

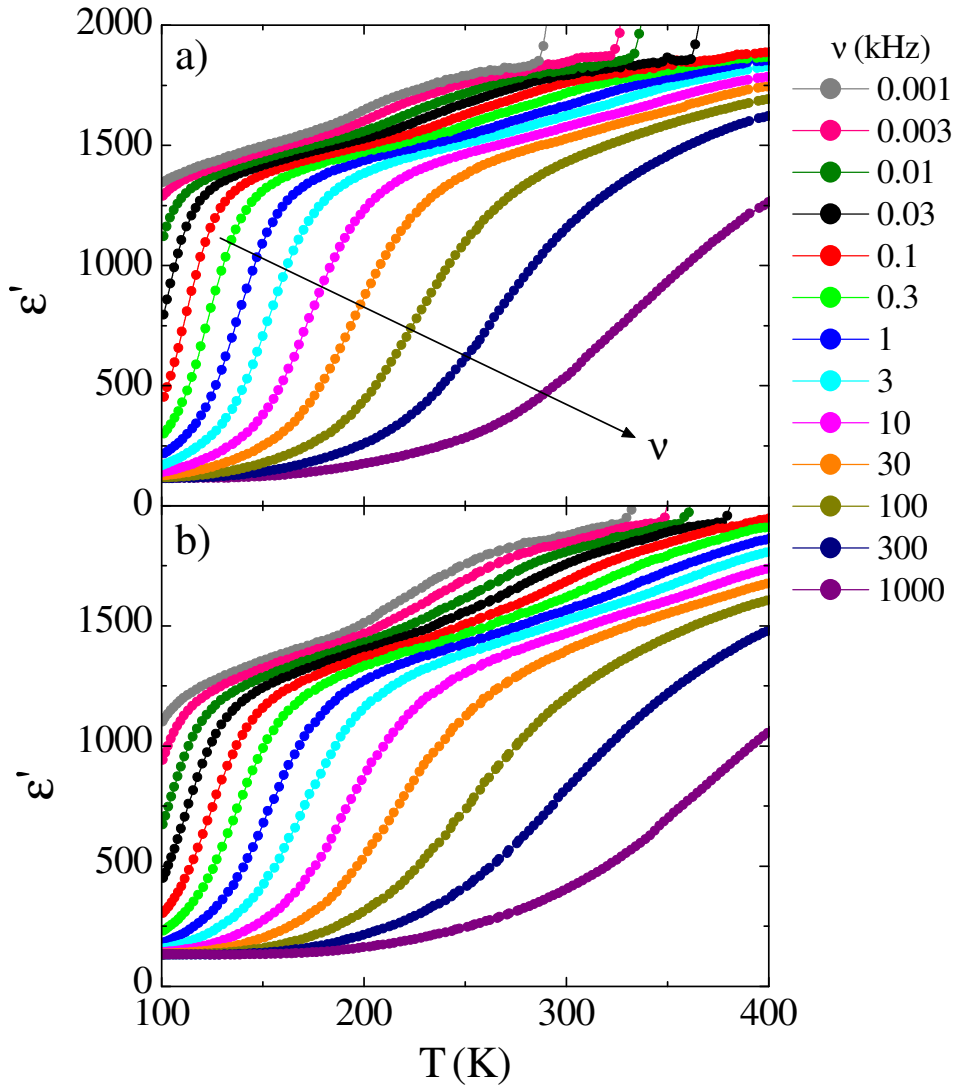

Figure 28: *Temperature-dependence of 6-layer CCTO thin films.* Dielectric constant vs. temperature of 6-layer films, post-annealed in flowing a) nitrogen and b) oxygen atmosphere.

4.3.2.3 Frequency-dependent dielectric response and the analysis of the electrical conductivity

Figure 29 depicts frequency-dependence of the complex dielectric constant and the electrical conductivity (see Equation 51), measured at several temperatures, for the case of a 6-layer film, post-annealed in flowing nitrogen atmosphere. For frequencies above 1 MHz, a resonance that is due to the piezoelectric effect, which is typical for thin samples (thickness of the measured sample is only 260 nm), was detected. A similar frequency-dependent response was obtained in all 6-layer samples [39].

Figure 30 shows the complex dielectric constant and electrical conductivity as a function of the frequency for several measuring temperatures between 90 and 410 K for 12-layer thin film that was post-annealed in the lowest oxygen partial pressure. An artificial Debye relaxation occurs, similar to the one depicted in Figure 22 for the case of CCTO single crystal, only in this case the main plateau values at low frequencies are due to grain boundary (and not surface layer) contributions [15]. The typical drop in ε' takes place at lower frequencies for lower temperatures (as R_{BULK} increases) and the values of conductivity decrease with decreasing temperature. These ε' data are in Figure 31 compared to ε' data, obtained in samples that were post-annealed in various oxygen partial pressures. Main plateau values are higher for samples that were post-annealed in lower oxygen partial pressure and the

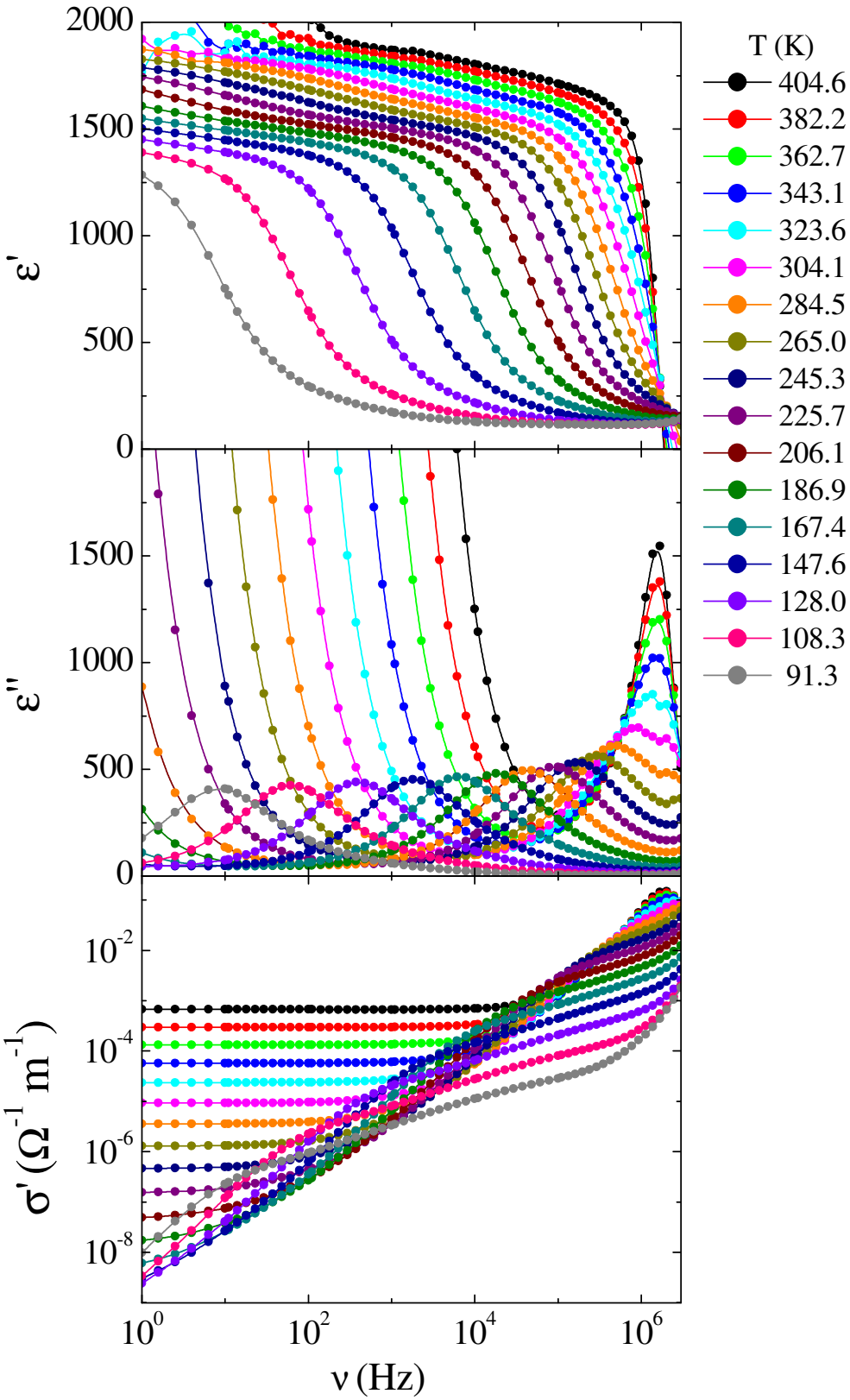

Figure 29: *Frequency-dependence of 6-layer CCTO thin film, post-annealed in N_2.* ε', ε'' and σ' vs. frequency, detected at several measuring temperatures in 6-layer film, post-annealed in flowing nitrogen atmosphere.

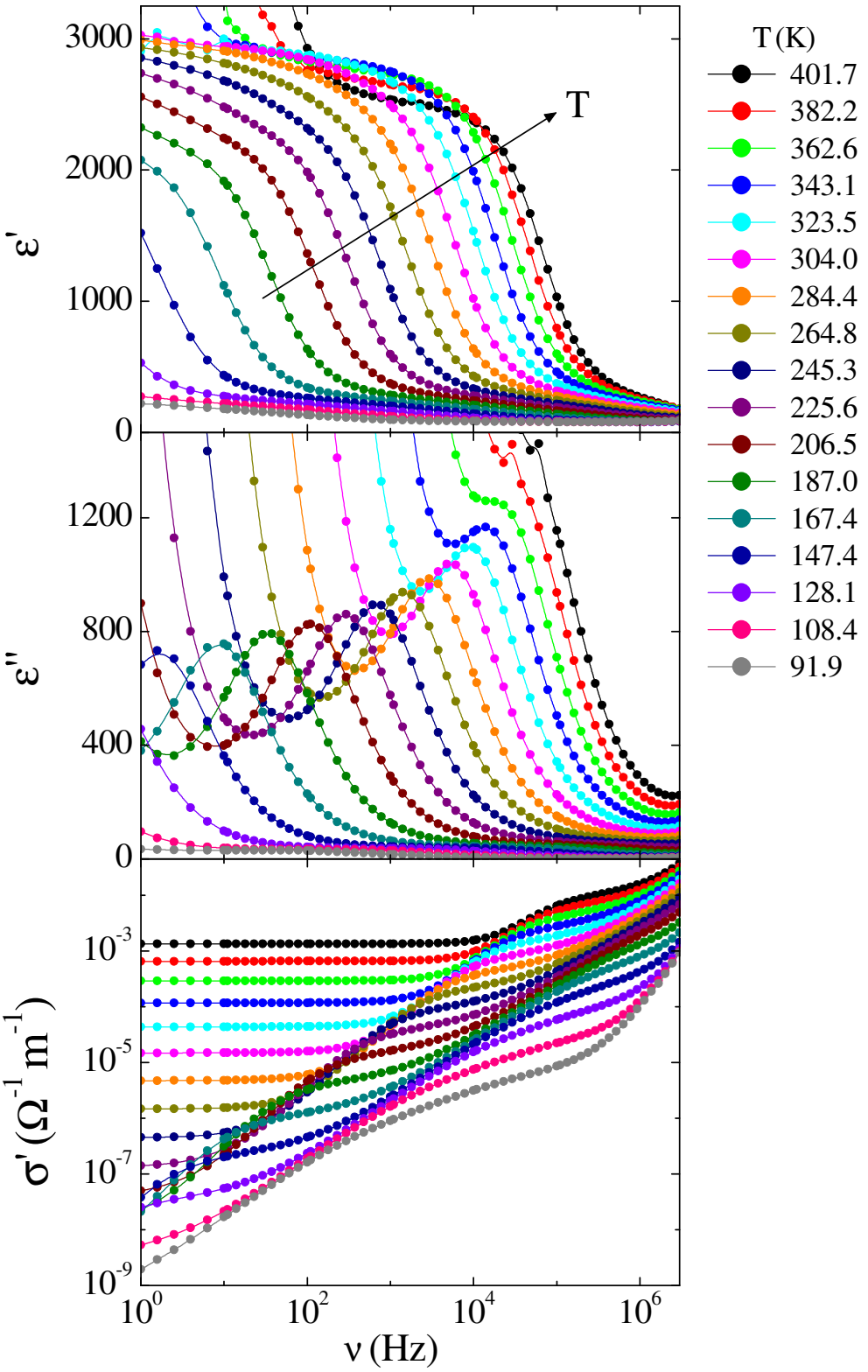

Figure 30: *Frequency-dependence of 12-layer CCTO thin film, post-annealed in* N_2. ε', ε'' and σ' vs. frequency, detected at several measuring temperatures in 12-layer film, post-annealed in flowing nitrogen atmosphere.

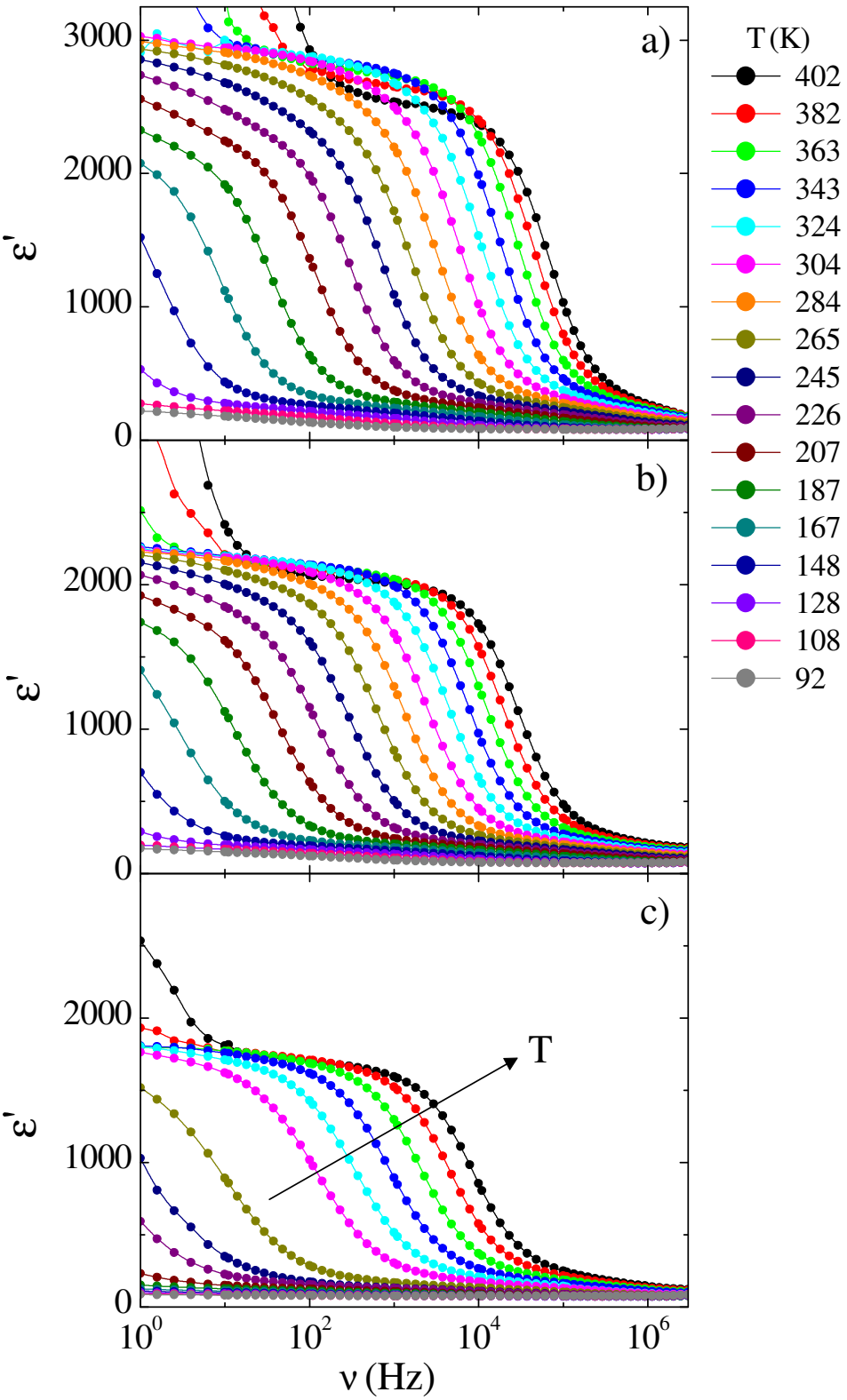

Figure 31: *Frequency-dependence of 12-layer CCTO thin films.* ε' vs. frequency, detected at several measuring temperatures in the 12-layer films, post-annealed in flowing a) nitrogen, b) air, and c) oxygen atmosphere.

frequency of their drop takes place at lower frequencies for samples that were post-annealed in higher oxygen partial pressure, which is consistent with the dielectric data, obtained in the same samples as a function of the temperature (see Figure 27). Similar results were obtained for 6-layer samples; however, analysis in terms of the equivalent circuit was performed on 12-layer samples only. Attempts to model the dielectric behaviour of any 6-layer film were hindered by several variables that would occur in the model due to the influence of the grain boundaries, the surface layers and the resonance, which in term complicated the modelling process to the point, at which it was no longer possible to distinguish between various contributions to the dielectric response [2].

In Figure 32, the electrical conductivity is shown as a function of the frequency at a measuring temperature of 304 K for 12-layer samples that were post-annealed in flowing nitrogen, air and oxygen atmosphere. The solid lines present the analysis in terms of the equivalent circuit from Figure 10c. The inset shows values of the DC conductivity, obtained from the fit with Equation 58, revealing higher values of σ_{DC} for samples that were post-annealed in lower oxygen partial pressure. In addition, contributions of grain boundaries to σ' (step from σ_{DC} plateau at $\sim 10^4$ Hz to values measured at lower frequencies - see Fig. 3 in Reference 15 for a more detailed overview) are higher for samples that were post-annealed in lower oxygen partial pressure. These results indicate that the conductivity of both, grains and grain boundaries, increases by post-annealing in oxygen deprived atmospheres.

Full analysis in terms of the equivalent circuit was performed on the sample with the highest values of the dielectric constant (Figures 27a and 30 show the dielectric response of the analysed film). Experimental $\varepsilon'(\nu)$ and $\sigma'(\nu)$ data have been fitted to Eqation 58 at several measuring temperatures, and the variable range hopping (VRH) model (Equation 61) was applied. Results of these analysis are shown in Figures 33 and 34. Figure 33 depicts the values of the DC conductivity as a function of $T^{-\frac{1}{2}}$ and the solid line presents the analysis in terms of the one-dimensional VRH model ($d = 1$). The inset features the fitting UDR parameter s as a function of the temperature, revealing $s < 1$ through the entire temperature

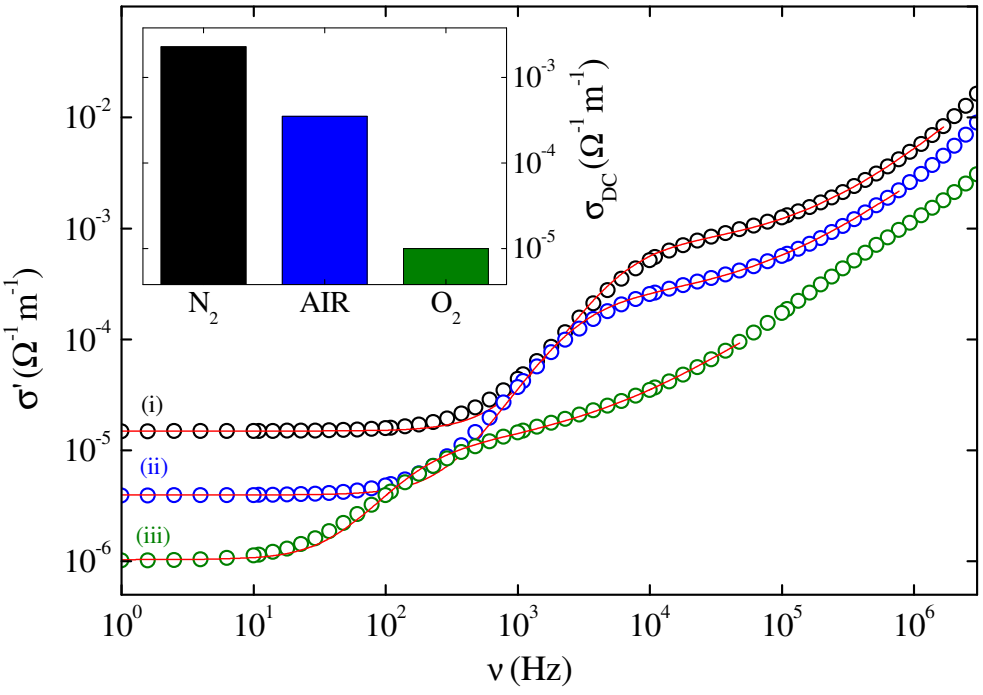

Figure 32: *σ' vs. frequency at 304 K in 12-layer films.* σ' as a function of frequency at a measuring temperature of 304 K in 12-layer films, post-annealed in flowing (i) nitrogen, (ii) air, and (iii) oxygen atmosphere. Solid lines are fits to the equivalent circuit model (Equation 58). The inset shows the values of σ_{DC}, obtained from the fits for each film.

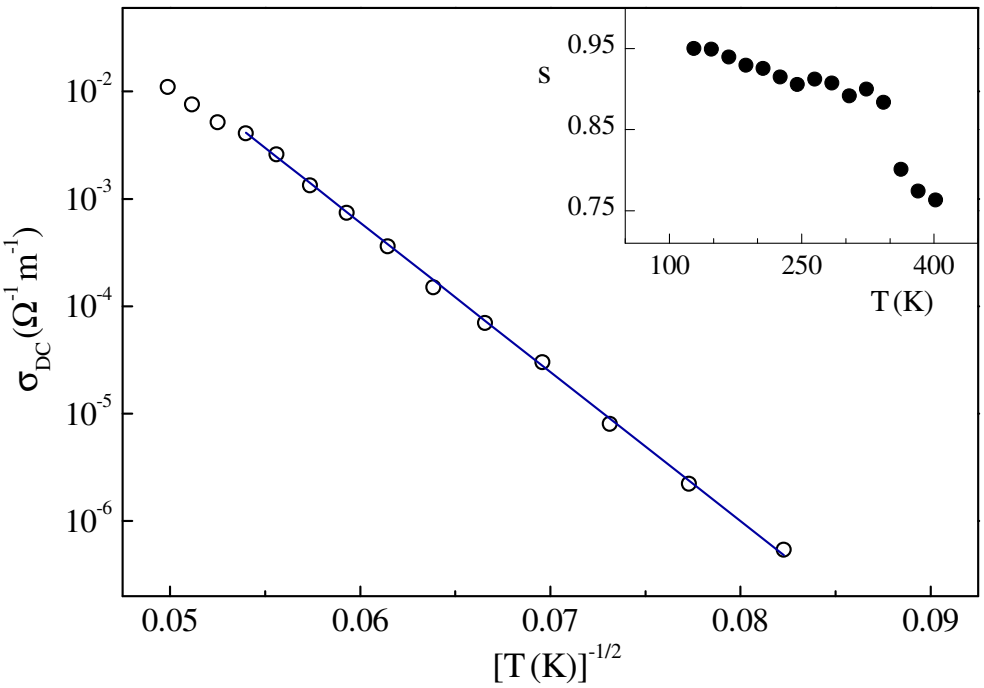

Figure 33: *1D hopping of localized charge carriers.* σ_{DC} as a function of $T^{-\frac{1}{2}}$, obtained by full analysis in terms of the equivalent circuit on 12-layer film that was post-annealed in nitrogen atmosphere. The solid line is the fit to Eq. 61, using $d = 1$ (1D hopping of localized charge carriers). The inset features fitting UDR parameter s as a function of the temperature.

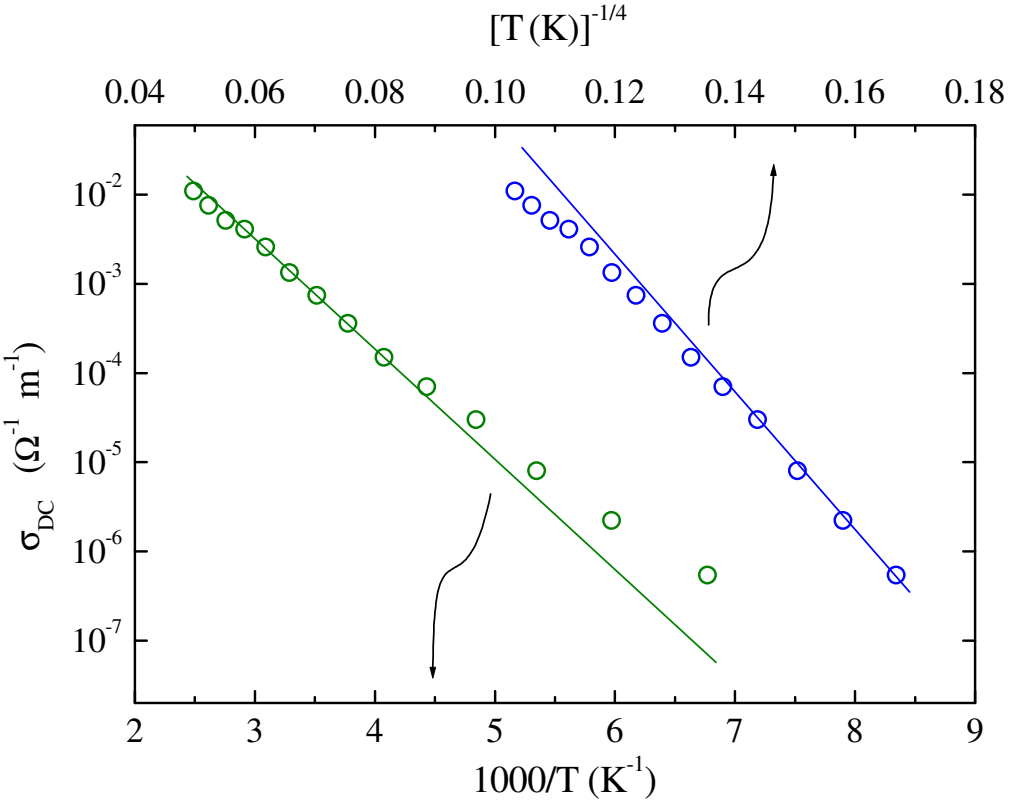

Figure 34: *Arrhenius dynamics and 3D VRH.* σ_{DC} as a function of $1000/T$ (green) and $T^{-\frac{1}{4}}$ (blue), obtained by full analysis in terms of the equivalent circuit on 12-layer film that was post-annealed in nitrogen atmosphere. The solid lines are the fit to Equation 61, using $d = 0$ (green, Arrhenius dynamics) and $d = 3$ (blue, 3D hopping of localized charge carriers).

interval. Figure 34 depicts results obtained by using $d = 0$ and $d = 3$ in the VRH model, which could hint that thermally activated Arrhenius-type behaviour governs the charge transport at higher temperatures, while 3D VRH of charge carriers between localized states dominates the charge transport at lower temperatures. However, this would contradict the fact that UDR behaviour, which is typical for hopping or tunneling of localized charge carriers and not thermally activated behaviour, was observed at all temperatures (see inset to Figure 33). It can thus be concluded, that 1D VRH is the dominating charge transport behaviour in CCTO thin films (in addition, results of VRH model with $d = 2$ revealed no clear evidence of two-dimensional hopping of localized charge carriers) [2].

4.3.2.4 Samples with a nucleation layer

Big grains in the 1+X-layer film (see Figures 25e and f) form an effective circuit composed of a set of leaky capacitors, connected in parallel, where the number of the leaky capacitors equals the number of the grains. Such an equivalent circuit would give a very smoothed $\varepsilon^*(T)$ response in comparison to that of any of the equivalent circuits featured in Figure 10, which indeed is the experimental case.

Figure 35 shows the dielectric response as a function of the temperature at several mea-

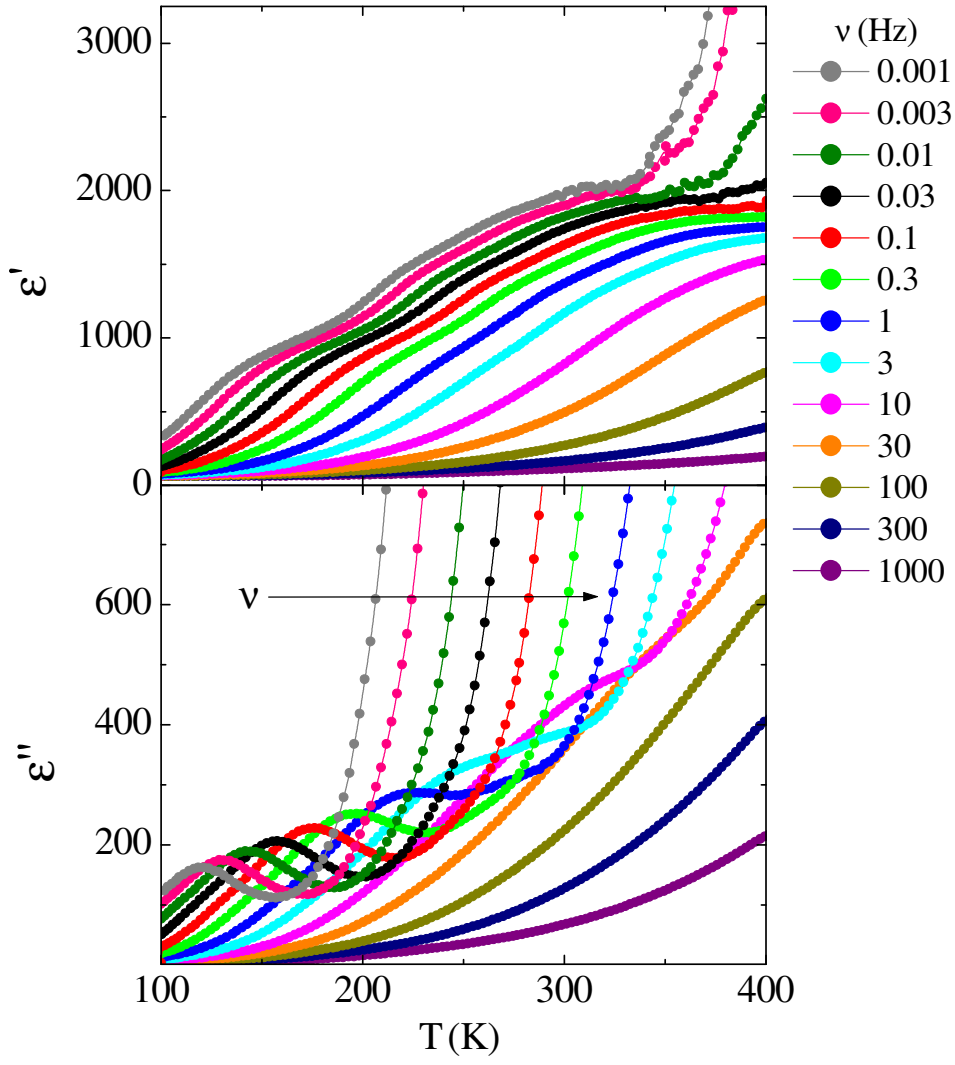

Figure 35: *Temperature-dependence of a sample with a nucleation layer.* Dielectric response of 1+12-layer RTA-annealed CCTO thin film, where single grains expand through the whole thickness of the film.

suring frequencies between 1 Hz and 1 MHz for 1+12-layer RTA-annealed CCTO thin film, revealing a smoothed dielectric response, i.e., ε' drop takes place over a broad temperature range. The comparison of dielectric response of 1+12-layer film to all other 12-layer films (see Figures 26 and 27) reveals that in the 1+12-layer film (i) ε' values are similar to that of 12-layer film that was post-annealed in the highest oxygen partial pressure, (ii) ε' drop takes place over a larger temperature range and it ends at lower temperatures than in any other case at all frequencies and (iii) the peaks in ε'' at any frequency take place at the lowest temperatures among all 12-layer thin films [2].

5 Relaxor reduced poly(vinylidene fluoride-trifluoroethylene) copolymer system

The chapter is dedicated to relaxor reduced poly(vinylidene fluoride-trifluoroethylene) copolymer, i.e., a new class of relaxor systems, and the studies of the influence of DC bias electric field on Vogel-Fulcher dynamics in relaxor ferroelectrics. The first part of the chapter presents a brief historic overview of scientific research and development of relaxor poly(vinylidene fluoride-trifluoroethylene)-based copolymer systems. Then chapter focuses on the properties of a new class of relaxor polymers, the reduced poly(vinylidene fluoride-trifluoroethylene) copolymer, and the results of the study of the influence of DC bias electrical field on the Vogel-Fulcher dynamics in the organic and the inorganic relaxor systems. The last part of this chapter presents the results of electromechanical measurements, conducted in the reduced P(VDF-TrFE) copolymer system. The experimental work presented in this chapter was done in collaboration with the groups of Prof. Dr. Qun-Dong Shen from the Nanjing University in China and Prof. Dr. Horst Beige from the Martin Luther University in Halle, Germany.

5.1 Overview

Over the last few decades, ferroelectric and relaxor polymers based on poly(vinylidene fluoride-trifluoroethylene) [P(VDF-TrFE)] copolymer have been of great interest for a broad range of applications, as they exhibit strain levels far above those of traditional piezoceramic materials [45, 46], fast response speeds [47, 48], high electric energy density with fast discharge speed [49] and large electrocaloric effect near room temperature [50]. Relaxor ferroelectrics in general attract a considerable amount of attention due of their unique physical properties [51]: (i) the absence of long range ferroelectric order in zero electric field at any temperature and (ii) a ferroelectric phase, which is formed by cooling the relaxor in an electric field higher than the critical field [52, 53]. The relaxor state is in fact usually described as a network of randomly interacting polar nanoregions (PNRs) that are embedded in a highly polarizable medium and upon cooling undergo a freezing transition into a glassy nonergodic state [52, 54].

In the beginning of the millennia, giant electrostriction in electron-irradiated P(VDF-TrFE) copolymer [47] and in terpolymer with chlorofluoroethylene, poly(vinylidene fluoride-trifluoroethylene-chlorofluoroethylene) [P(VDF-TrFE-CFE)] [48], was detected. It was shown that these systems exhibit an identical macroscopic dielectric properties as inorganic relaxors [55], which suggested that high-energy electron irradiation [47] or introduction of an additional monomer, such as chlorofluoroethylene (CFE) [48] converts the coherent polarization domain (all-trans chains) in normal ferroelectric P(VDF-TrFE) into nanopolar regions, thereby transforming the material into a relaxor system [55] and an ultrahigh strain response in relaxor polymers is generated due to expansion of the polar regions under an external electric field, coupled with a large difference in the lattice strain between the polar and the nonpolar phases [47].

At this stage, some basic structural properties of ferroelectric and relaxor polymers

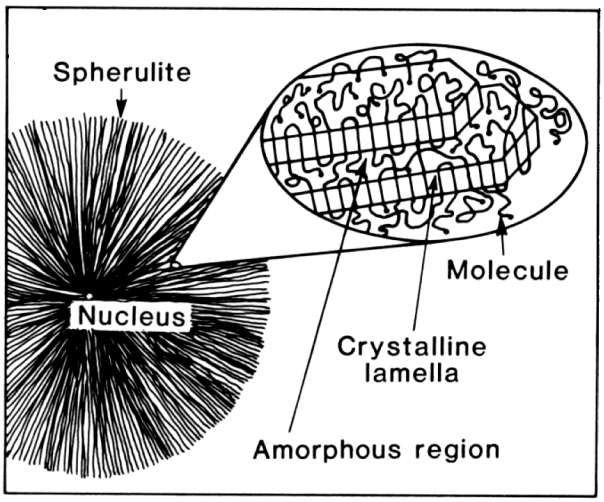

Figure 36: *Schematic representation of the structure of polymer spherulites.* Heterogeneous structure of PVDF and of ferroelectric and relaxor polymers in general [45].

will be presented. The first known relaxor polymer was in fact poly(vinylidene fluoride) [(PVDF)], molecular formula of which is $(CH_2–CF_2)_n$, which exhibits one of the strongest piezoelectric and pyroelectric activity among polymers [45]. After melt-solidification, within the so-called spherulites, crystalline lamellas are formed within the amorphous regions (see Figure 36). The most favourable torsional bond arrangements have substituents at 180° to each other (called trans or t) or at ±60° (called gauche or $g^{\pm}$), although actual torsional angles commonly somewhat deviate from these values [45]. Figure 37a and b illustrate a sequence of three t bonds and a g^+tg^- bond sequence, respectively.

PVDF has three known chain conformations: All-trans (i.e., ttt), tg^+tg^- and $tttg^+tttg^-$ (in all cases, slight deviations from the 180° and the ±60° angle exist). The first two conformations, depicted in Figures 37c and d, respectively, are the most common [45]. Polymer

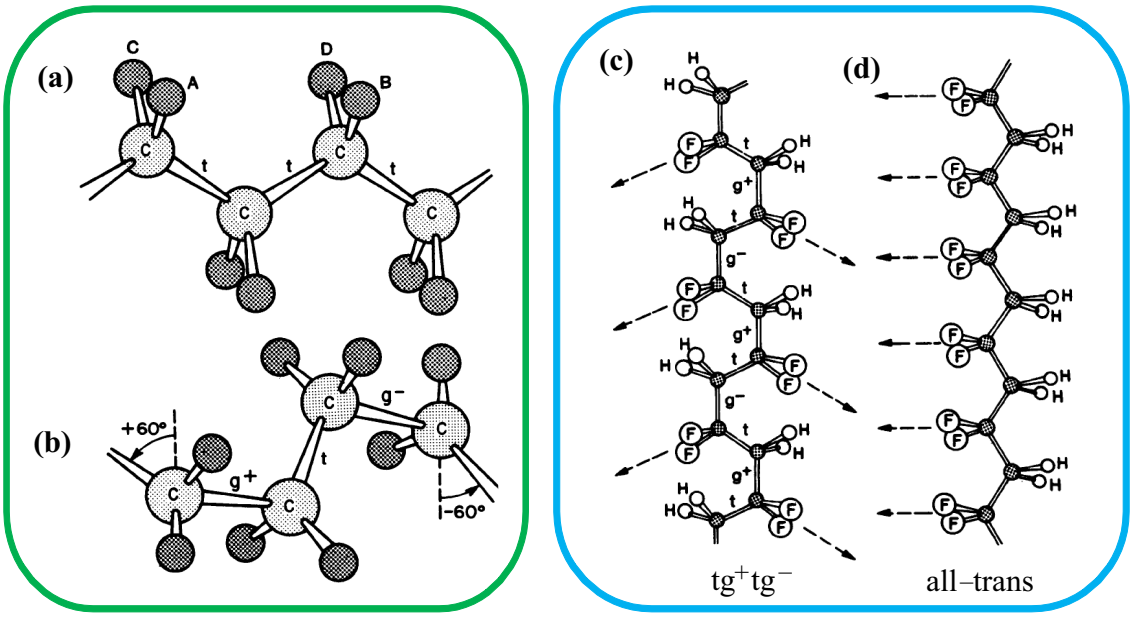

Figure 37: *Schematic representation of polymer chain segments in different conformations.* Schematic representation of ttt (a) and g^+tg^- (b) polymer chain segments and a schematic depiction of the two most common crystalline chain conformations in PVDF: (c) tg^+tg^- and (d) all-trans. The arrows in (c) and (d) indicate the projections of the $–CF_2$ dipole directions on planes defined by the carbon backbone [45].

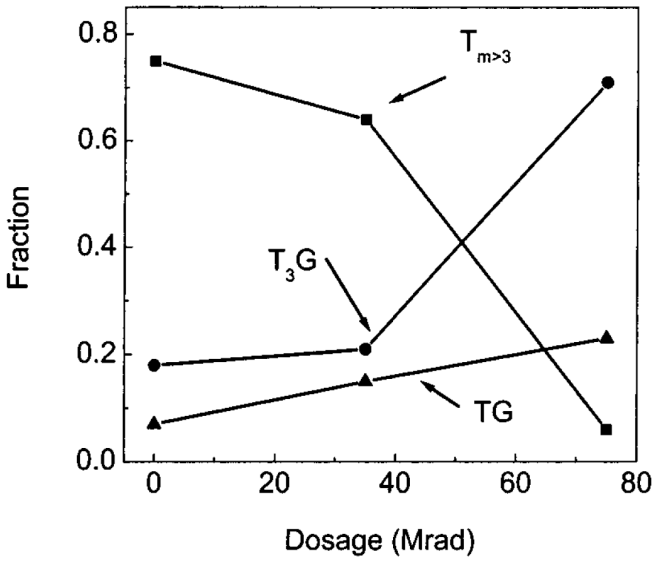

Figure 38: *Fourier transform infrared spectroscopy data of P(VDF-TrFE) copolymer film.* FT-IR data of P(VDF-TrFE) 68/32 copolymer film at room temperature: Fraction of different conformations in film vs. irradiation dose [56].

chains that are in the all-trans conformation have all dipoles essentially normal to the molecular axis and, thusly, in term form a polar conformation. The tg^+tg^- chain conformation is also polar, however, due to the inclination of the dipole moments, it has components of the net moment both parallel and perpendicular to the chain axis (see Figure 37c). It should be noted that PVDF melt-solidifies into a tg^+tg^- chain conformation, in which the lattices are crystallographically packed so as to cancel each other's dipole moment, i.e., PVDF melt-solidifies in a non-polar phase. However, by mechanical stretching, the tg^+tg^- chain conformations can be transformed into all-trans chain conformations. The latter is the most highly polar phase of the PVDF: its unit cell consists of two all-trans chains packed with their dipoles pointing in the same direction [45]. On the other hand, P(VDF-TrFE), which consists of –[CH_2–CF_2]– and –[CHF–CF_2]– monomers, spontaneously crystallizes into a *ttt* chain conformation and, concomitantly, has better ferroelectric properties than PVDF.

In inorganic relaxors, the typical relaxor structure (polar clusters in a non-polar matrix) forms due to structural disorder (random distribution of different ions on the same crystallographic site). In relaxor polymers, however, the disorder must first be introduced into the ferroelectric system of a given polymer system: either by high-energy electron irradiation or by introduction of the third bulky monomer, which contains Cl atoms (e.g., chlorofluoroethylene, –[CFCl–CH_2]–, or chlorotrifluoroethylene, –[CFCl–CF_2]–, monomers) that are much larger than any other atom in the original chain and thus prevent all-trans chain conformation between two neighbouring monomers. Both mentioned approaches favour the non-polar trans-gauche chain conformations over the polar all-trans conformations, as shown in Figure 38 [56] and Table 1 [48].

Table 1: *Comparison of molecular conformations in relaxor polymers.* Comparison of all-trans, $tttg^+tttg^-$ and tg^+tg^- molecular conformations in three polymers [48].

sample	% $t_{m>3}$	% $tttg^+tttg^-$	% tg^+tg^-
P(VDF-TrFE) 65:35	75	18	7
P(VDF-TrFE-CTFE)	34	61	5
P(VDF-TrFE-CFE)	36	55	9

Relaxors are in general characterized by a broad frequency dispersion in the complex dielectric constant, logarithmic polarization decay and slowing dynamics that signals the onset

of freezing [54, 57]. For example, in inorganic systems, relaxor behaviour (usually correlated with the cationic disorder in the same crystallographic site – in fact, only disordered ferroelectric systems show relaxor behaviour), was detected predominantly in lead-containing ternary compounds and solid solutions [52–54, 57–59]. At the freezing temperature T_f the longest relaxation time in the system diverges, while the bulk of the relaxation spectrum remains active [57]. The characteristic relaxation time diverges at a somewhat lower temperature T_0 according to the Vogel-Fulcher relation (see Equation 60). Although this empirical law has experimentally been observed in a variety of systems, its derivation at the mesoscopic level has just recently been proposed [21]. Furthermore, it has been argued that (i) the external electric field induces a ferroelectric order and (ii) the dielectric relaxation time in relaxors is governed by the mechanism of growth and percolation of PNRs [60], with an appropriate correction of the local electric field inside a PNR if bias field is applied. This correction has theoretically been determined by the anharmonic polarization term in the free energy functional: The relaxation time then follows a modified Vogel-Fulcher law with T_0 depending on the applied field and nonlinear susceptibility [5].

At this point, some typical features, detected in the $\varepsilon^*(T)$ spectra of P(VDF-TrFE)-based systems, should be stressed: the most distinctive feature in the ferroelectric P(VDF-TrFE) is a frequency-independent peak in both, ε' and ε'', at $T_c \approx 350$–380 K (depending on the VDF to TrFE ratio), which denotes the phase transition from the distorted trans-gauche paraelectric to all-trans ferroelectric phase, occurring in the crystalline region of the copolymer [55, 61–63]. The second feature is a dielectric relaxation in the temperature region of 275–335 K [61–63]. This so-called β-process is without ambiguity associated with the dynamic manifestation of the glass transition in the amorphous phase of copolymer, i.e., a transition from the glassy to rubbery state [62–64]. Earlier studies have shown that the temperature dependence of the characteristic relaxation time of this β-relaxation is of the WLF-type (Williams, Landel and Ferry), thus being clearly different than the Arrhenius-type relaxation process, which also occurs at low-temperatures in the crystalline region of the copolymer [63].

In the relaxor P(VDF-TrFE)-based systems up to now only one, broad dispersive maximum has been observed (see Figure 39). Similar as in dipolar glasses and inorganic relaxor systems, this typical relaxor feature is a result of the fact that ε' at a certain temperature, which depends on the experimental time scale (i.e., frequency), starts to deviate from its static value. The static dielectric constant indeed does not show any anomaly, which was also confirmed by measurements of the static dielectric constant via the charge accumulation technique in the P(VDF-TrFE-CFE) terpolymer [55].

As already pointed out, it is well known, from X-ray, heat capacity and infrared investigations, that poly vinylidene fluoride [PVDF] and its copolymers are semicrystalline systems comprising noncrystalline, i.e., amorphous regions, and crystalline regions with a spontaneous polarization associated with parallel packing of all-trans polymer chains [45, 61]. On heating, the amorphous region undergoes a transition from glassy to a rubbery state below room temperature, while the crystalline region adopted ferroelectric phase undergoes a transition into a paraelectric phase and finally melts [61]. Introduction of defects results in the coexistence of polar and nonpolar phases within the same crystalline region [65], and, concomitantly, the ferroelectric peak transforms into a typical relaxor frequency-dependent dielectric maximum [66], which usually completely overrides the dielectric anomaly due to the glass-to-rubber (i.e., glassy) transition in the amorphous matrix. The latter is, however, almost uninfluenced by introduction of defects. This in term means that the typical dielectric maximum, up to now observed in relaxor polymers is comprised of two dynamics: the relaxor dynamics in crystalline regions and the glassy transition in the amorphous matrix, i.e., the β-relaxation in the dielectric spectra of P(VDF-TrFE-CFE) terpolymer (see Figure 39) is overlapped by a relaxor dielectric dispersion [3, 4, 6, 67–69]. Similar as in inorganic relaxors, this peak is a consequence of polar nanoregions' dynamics and does not denote

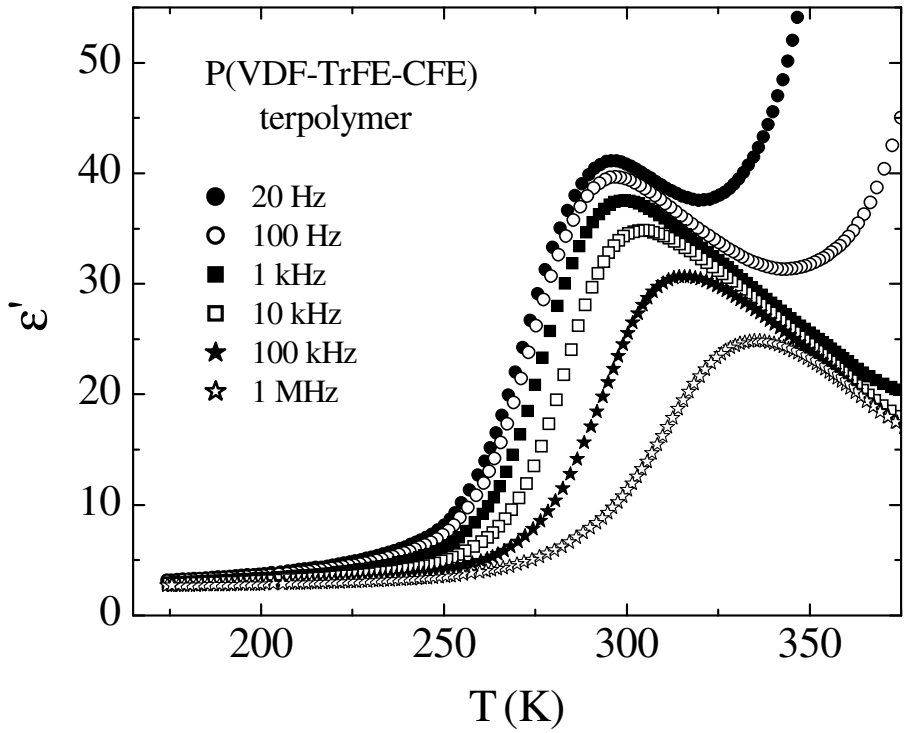

Figure 39: *Temperature dependence of the real part of the complex dielectric constant of a relaxor polymer.* ε' vs. temperature, measured at different frequencies in relaxor P(VDF-TrFE-CFE) terpolymer [3].

any phase transition, just as being the case in dipolar glasses [70]. Alas, dielectric analysis of relaxor polymers has been incomplete until now: data interpretation and understanding were complicated by the fact that two similar types of dynamics take place in the same temperature range [3, 67].

In order to investigate both, relaxor and glassy dynamics separately, we performed high-resolution dielectric measurements in a new class of relaxor P(VDF-TrFE) copolymer, synthesized via reductive dechlorination from the poly(vinylidene fluoride-chlorotrifluoroethylene) [P(VDF-CTFE)] copolymer [3]. The reduced P(VDF-TrFE) copolymer system is very attractive for high-temperature applications: Not only that relatively high dielectric constants (for a polymer system) are obtained around 375 K, it also exhibits a high melting point of ~ 475 K [71]. In this system relaxor peaks take place at much higher temperatures than those of previously reported relaxor polymers: Here they remain in the temperature region of a previous ferroelectric phase transition and, concomitantly, take place at much higher temperatures than is the temperature of the glass transition in the amorphous matrix [71]. Analysis of the experimental data revealed that the relaxor dielectric dynamic in the reduced P(VDF-TrFE) copolymer, i.e., the dynamics which is now not influenced by separate processes in the amorphous matrix, is indeed almost identical to that observed in classical relaxor systems, such as lead magnesium niobate, and, furthermore, reminiscent of the dynamic behaviour observed in various spin glasses [3]. In addition, electromechanic measurements were performed.

We also studied the influence of DC bias electrical field on the Vogel-Fulcher dynamics in organic and inorganic relaxor systems: In order to experimentally detect changes in dynamics of relaxors due to a DC bias electric field, we performed measurements of the dielectric response of the polymeric relaxor, reduced P(VDF-TrFE) copolymer, and the archetypal inorganic relaxor lanthanum-modified lead zirconate titanate ceramics $Pb_{1-x}La_x(Zr_yTi_{1-y})_{1-x/4}O_3$ ($x = 0.09$, $y = 0.65$, denoted as 9/65/35 PLZT). The majority of investigations were performed on the reduced P(VDF-TrFE) copolymer system and the results

of the analysis were compared to the newly derived mesoscopic model from reference 5 [4].

5.2 Experimental procedure

5.2.1 Material preparation

Reduced P(VDF-TrFE) was prepared as follows: 1.0 g of P(VDF-CTFE) 66/34 copolymer and 88.6 mg of AIBN in tetrahydrofuran was stirred at 333 K for 30 min, then tri(n-butyl)tin hydride (4.52 mmol) was added. The solution was kept stirring at 333 K for 24 h. P(VDF-TrFE) was then collected by precipitation and dried in vacuum. Finally, copolymer films were prepared by solution cast method, using dimethylformamide as the solvent, followed by further annealing at 413 K [3].

5.2.2 Dielectric measurements

For dielectric measurements, surfaces of the 20 μm thick polymer films were covered by sputtered gold or silver paint electrodes (see Figures 40a and b). Figure 41 shows that the use of either silver paste (full circles) or gold sputtered electrodes (empty circles, solid lines are a guide to the eye) does not affect the dielectric response of the investigated system. Complex linear dielectric constant from Equation 14 was measured in the frequency range of 20 Hz–1 MHz by using HP4282 Precision LCR Meter. The amplitude of the probing AC electric signal was 0.1 V. The real part of the complex AC conductivity was calculated using Equation 51. After heating the samples up to 420 K, the DC bias electric field was (optionally) applied and then the dielectric response was detected during cooling runs with the rate of -0.5 K/min. The temperature of the samples was stabilized within 10 mK by using lock-in bridge technique with a platinum resistor Pt100 as a thermometer. A similar experimental procedure was used for the polished platelet-shaped sample, cut from the hot pressed 9/65/35 PLZT ceramics.

Similar heating/cooling procedure was used for the third-order nonlinear dielectric response measurements, which were carried out at various frequencies, by using the HP35665A Dynamic Signal Analyzer. Here, the first and the third harmonic dielectric responses were measured simultaneously, which, in comparison to separate measurement runs, reduces errors in the subsequent calculation of the ratio $a_3 = \varepsilon_3/\varepsilon_0^3\varepsilon^4$ (Equation 67). In this computation, the real part of the linear and the absolute value, ε_3, of the third-order nonlinear dielectric constant were used (their values were calculated from Equations 68 and 69, respectively; See section 3.2 for a more detailed description).

5.2.3 Electromechanical measurements

Electromechanical characterization has been performed in the laboratories of Prof. Dr. Horst Beige at the Martin Luther University in Halle, Germany. Equipment based on a capacitance detector was used for measurements of the polarization and the electrically induced strain. In this setup, depicted in Figure 42, the sample is placed in series with a movable air capacitor within a HF resonance circuit. A change of the sample thickness causes a change of the capacity and therefore frequency modulation of the HF circuit. After the demodulation, a voltage proportional to the strain of the sample can be measured. By using a quartz crystal connected in series with the sample, the strain in the direction of the applied measuring field of the sample can be obtained for various frequencies and voltage amplitudes by a compensation technique. Samples were measured at room temperature and at 353 K under DC electric fields of 25–125 and 25–60 MV/m, respectively. The hysteresis loop and the dielectric constant of the sample were measured by probing frequencies of 1.7, 17 and 170 Hz using a Sawyer-Tower circuit with an electrometer amplifier. A more detailed review of the experimental setup is available in references 72 and 73.

(a) Silver paint electrode

(b) Sputtered gold electrode

Figure 40: *Reduced P(VDF-TrFE) copolymer films.* Reduced P(VDF-TrFE) copolymer films with silver paint (a) and sputtered gold electrodes (b), prepared for dielectric measurements.

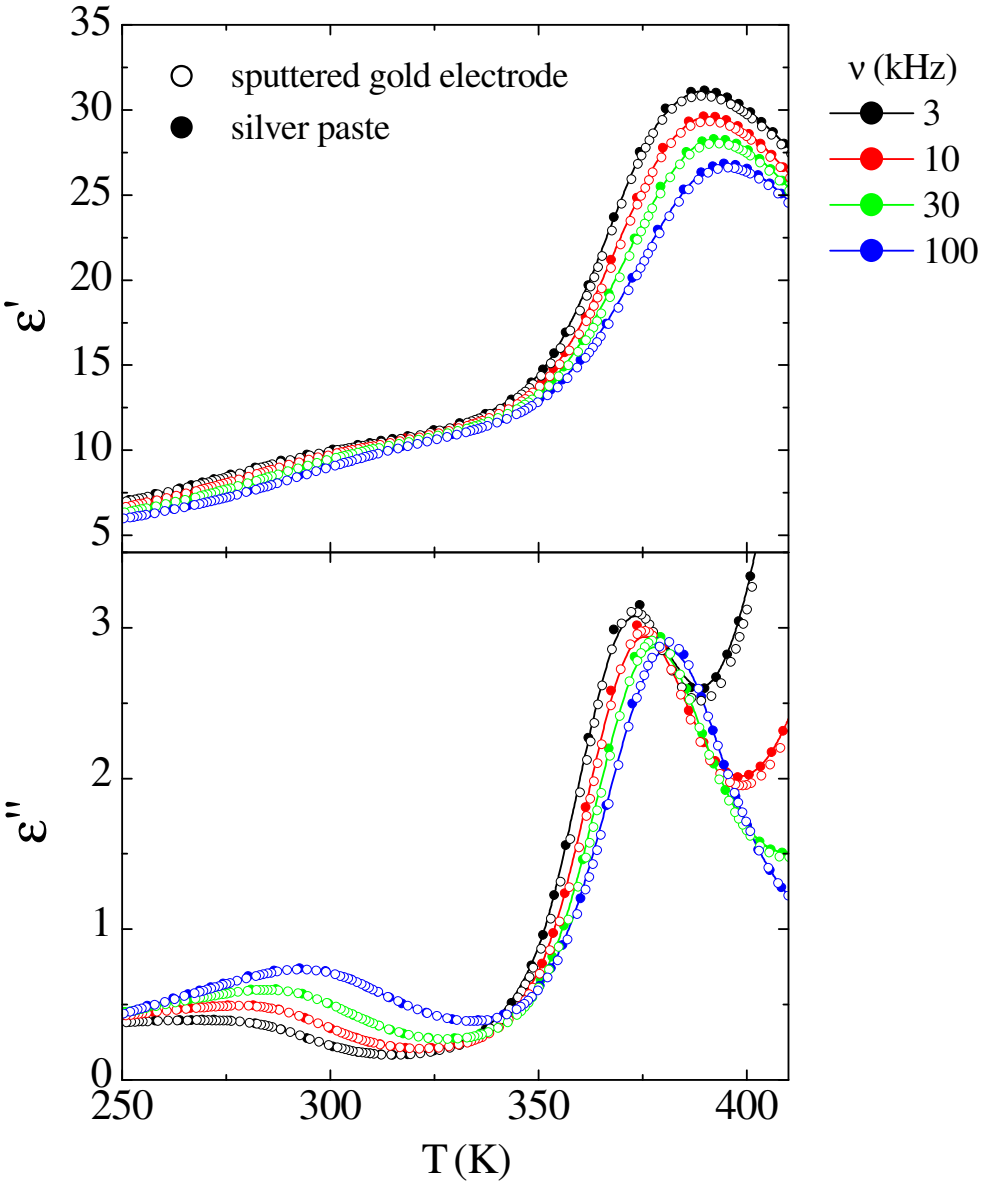

Figure 41: *Temperature-dependent dielectric response, detected using different electrodes.* The temperature-dependencies of the real, ε', and imaginary, ε'', part of the complex dielectric constant, measured at various frequencies in the reduced P(VDF-TrFE) copolymer with silver paste (full circles) and sputtered gold electrodes (empty circles). Solid lines are a guide to the eye.

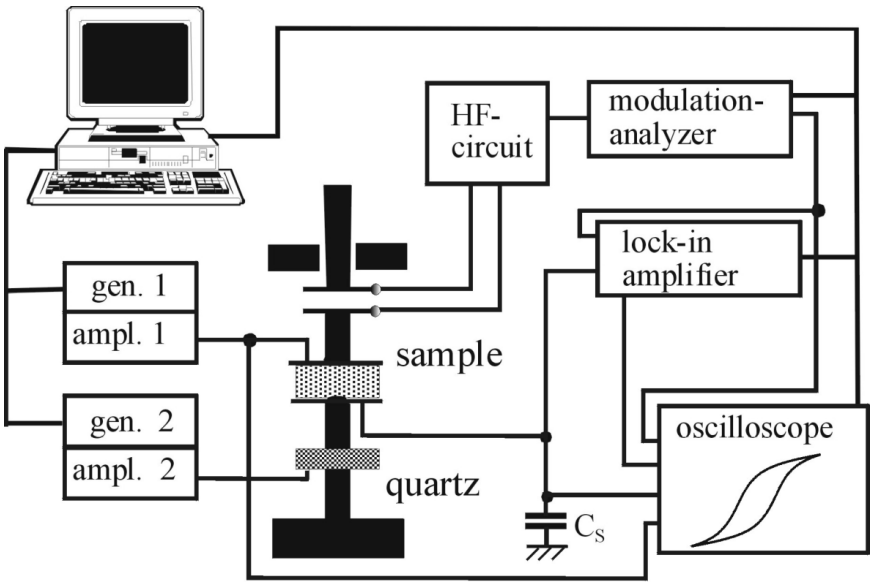

Figure 42: *Schematic of the experimental setup used for temperature stabilization.* Schematic representation of the experimental setup at Physics Department of the Martin Luther University in Halle, Germany. This setup can be used for simultaneous detection of induced strain and electric polarization, as well as for measurements of piezoelectric constants.

5.3 Results and discussion

This section presents the results of investigations of the dielectric properties of a new class of relaxor polymers, the reduced P(VDF-TrFE) copolymer system. Measurements and analysis of temperature- and frequency-dependent linear dielectric response of reduced P(VDF-TrFE) copolymer in several DC bias electric fields, as well as the nonlinear dielectric response are presented. The results of the analysis of the influence of DC bias electrical field on the Vogel-Fulcher dynamics in this organic relaxor system are presented and compared to that of an archetypal inorganic relaxor lanthanum-modified lead zirconate titanate ceramics $Pb_{1-x}La_x(Zr_yTi_{1-y})_{1-x/4}O_3$ ($x = 0.09$, $y = 0.65$, denoted as 9/65/35 PLZT). In addition, the results of measurements of the electromechanical response of the reduced P(VDF-TrFE) copolymer are shown.

5.3.1 Contributions of distinctive dynamic processes to dielectric response of relaxor reduced P(VDF-TrFE) copolymer

5.3.1.1 Linear dielectric behaviour

Figure 43 shows the temperature dependence of the real, ε', and imaginary, ε'', parts of the complex linear dielectric constant, measured at several different frequencies in the reduced P(VDF-TrFE) copolymer in zero DC bias field. Two dispersive dielectric anomalies, one in the temperature region of 350–400 K and the other in the temperature region of 275-335 K, can clearly be seen.

Due to different synthetic process, the reduced copolymer possesses different chain structure compared with that from the normal polymerized system. Infrared spectroscopy data clearly revealed head-to-head (H–H) and tail-to-tail (T–T) linkages in this system [71]. The reduced P(VDF-TrFE) copolymer thus possesses high degree of T–T and H–H defects, depicted in Figure 44, which are very different from the predominate head-to-tail (H–T) chain arrangement in the normal polymerized P(VDF-TrFE) copolymers. A large content of H–H and T–T defects in the copolymer breaks coherent ferroelectric domains and is most probably responsible for the observed high-temperature relaxor behaviour [3], which, however,

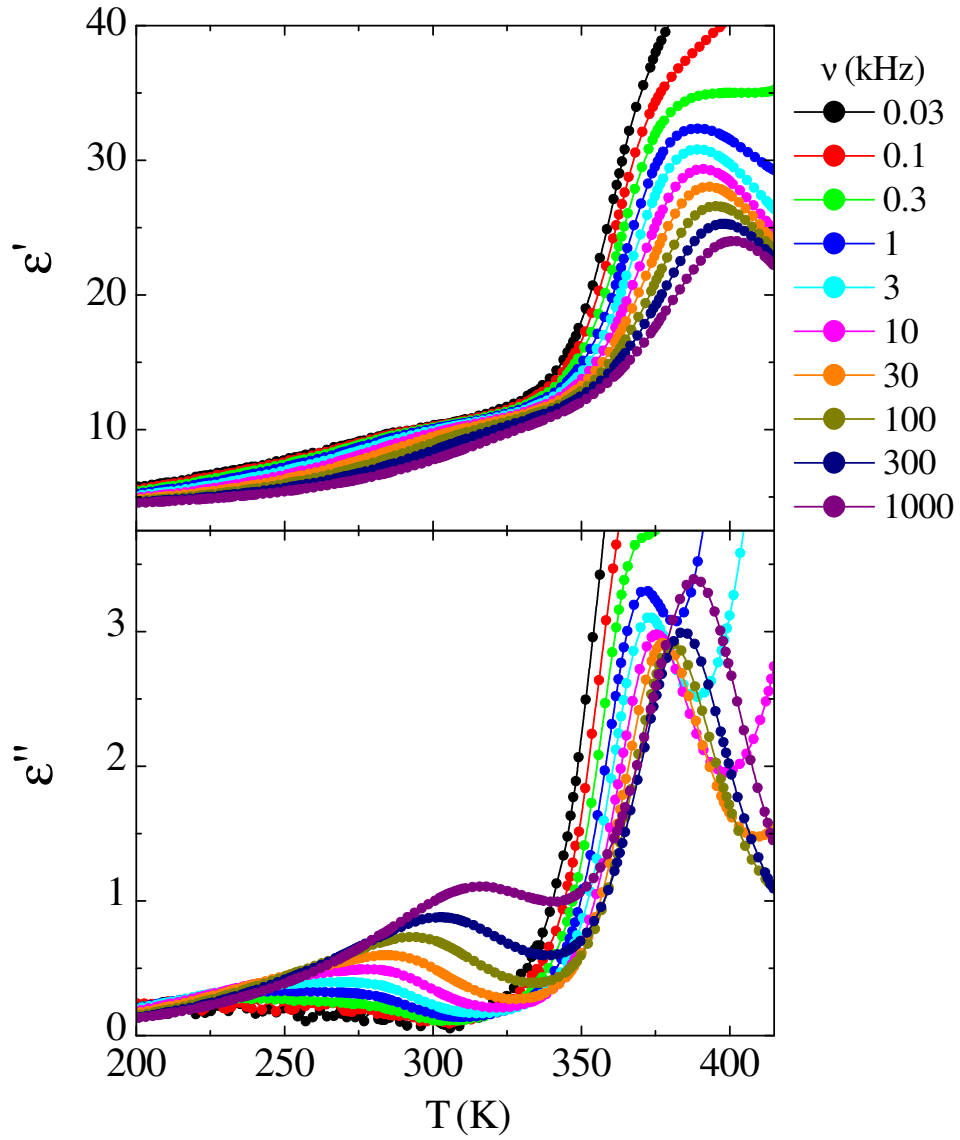

Figure 43: *Temperature-dependence of the reduced P(VDF-TrFE) copolymer in zero DC bias field.* Temperature dependence of ε' and ε'', detected at various frequencies in the reduced P(VDF-TrFE) copolymer in zero DC bias field.

does not shift to lower temperatures and remains in the temperature region of a previous ferroelectric phase transition (350–380 K) and is, concomitantly, not influenced by dynamic processes in the amorphous matrix (275–335 K).

It should be stressed here once again that relaxor polymers are usually obtained by introducing disorder into ferroelectric systems. First attempts by using high-energy electron irradiation [47] or γ-irradiation [74] indeed successfully transformed the long-range all-trans ferroelectric ordering into trans sequences of shorter correlation length and moreover, nonpolar trans-gauche conformation has been induced. This scission of ferroelectric ordering occurred mainly due to double C=C bonds and consequently, a typical relaxor structure, polar nanoregions in the nonpolar matrix, was formed. Unfortunately, the radiation also induced several other defects, for example, by breaking of C–H and C–F bonds different free radicals were formed [75]. Thus further processing of relaxor polymers involved introduction of monomers with large chlorine atoms [48], which, due to their size, prevent formation of long-range ordered all-trans chains and favour trans-gauche conformation. This noninvasive procedure is almost free of other undesirable defects and thus resulted in an almost ideal relaxor dielectric response (see Figure 39). A similar response has also been detected here,

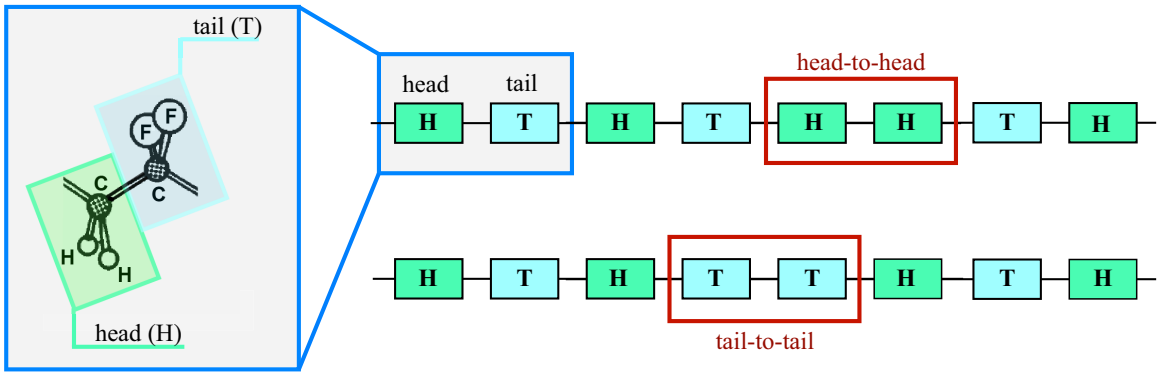

Figure 44: *Schematic representation of H–T chain arrangements and H–H and T–T defects.* Schematic representation of head-to-tail (H–T) chain arrangements and head-to-head (H–H) and tail-to-tail (T–T) defects. On the left side, positions of the head and the tail are schematically shown for the monomer of PVDF.

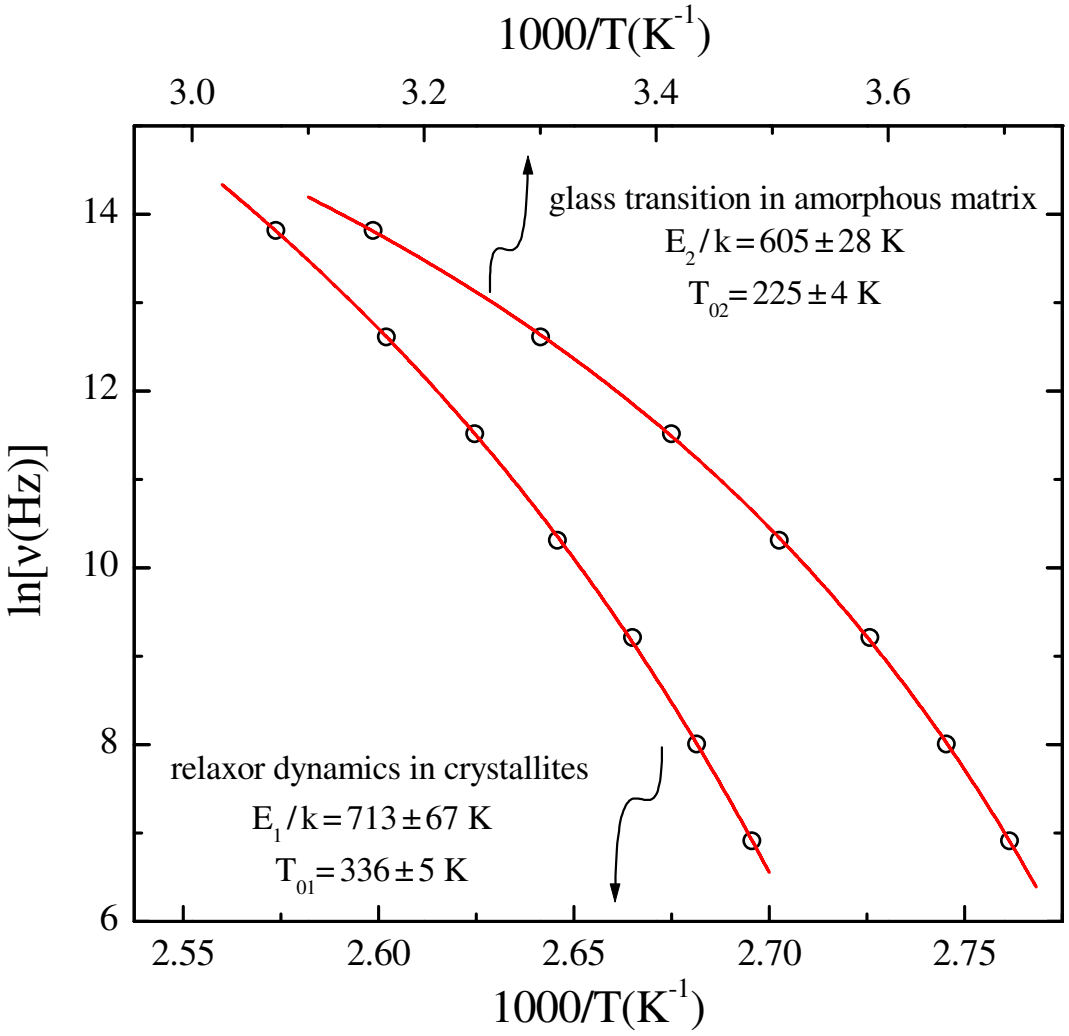

Figure 45: *The Vogel-Fulcher dependence of the characteristic relaxation times in zero DC bias field.* The Vogel-Fulcher dependence of the characteristic relaxation times for the (i) relaxor dynamics in the crystalline part of the system and (ii) glass-to-rubber transition in the amorphous matrix.

in the reduced P(VDF-TrFE) system, which means that processing most probably did not introduce additional defects to H–H and T–T linkages, which are in fact responsible for the relaxor structure and thus for the observed dielectric response. Indeed, the electrical conductivity is higher than in relaxor terpolymers ($\varepsilon''(T)$ curves in Figure 43 increase at higher temperatures even when measured at 30 kHz), but this can also be due to the fact that the relaxor response is obtained at much higher temperatures in this system in comparison with conventional terpolymers, which certainly implies higher electrical conductivity.

Characteristic relaxation frequencies, determined from peaks in $\varepsilon''(T)$ (Fig. 45), for both processes follow the Vogel-Fulcher law (Equation 60) with the Vogel-Fulcher temperatures of $T_{01} = 336 \pm 5$ K and $T_{02} = 225 \pm 4$ K for relaxor dynamics in the crystalline regions and glass-to-rubber transition in the amorphous matrix, respectively. Such a dependence is typical for relaxor (and glassy) systems, and as there is also no sign of any frequency-independent anomaly, we can conclude that during preparation P(VDF-TrFE) has been completely transformed from the ferroelectric into a relaxor system [3, 67].

The frequency dependence of ε' and σ', measured at various temperatures in zero DC bias field, is shown in Figure 46. The ε' data are presented on a logarithmic scale. Indeed, such

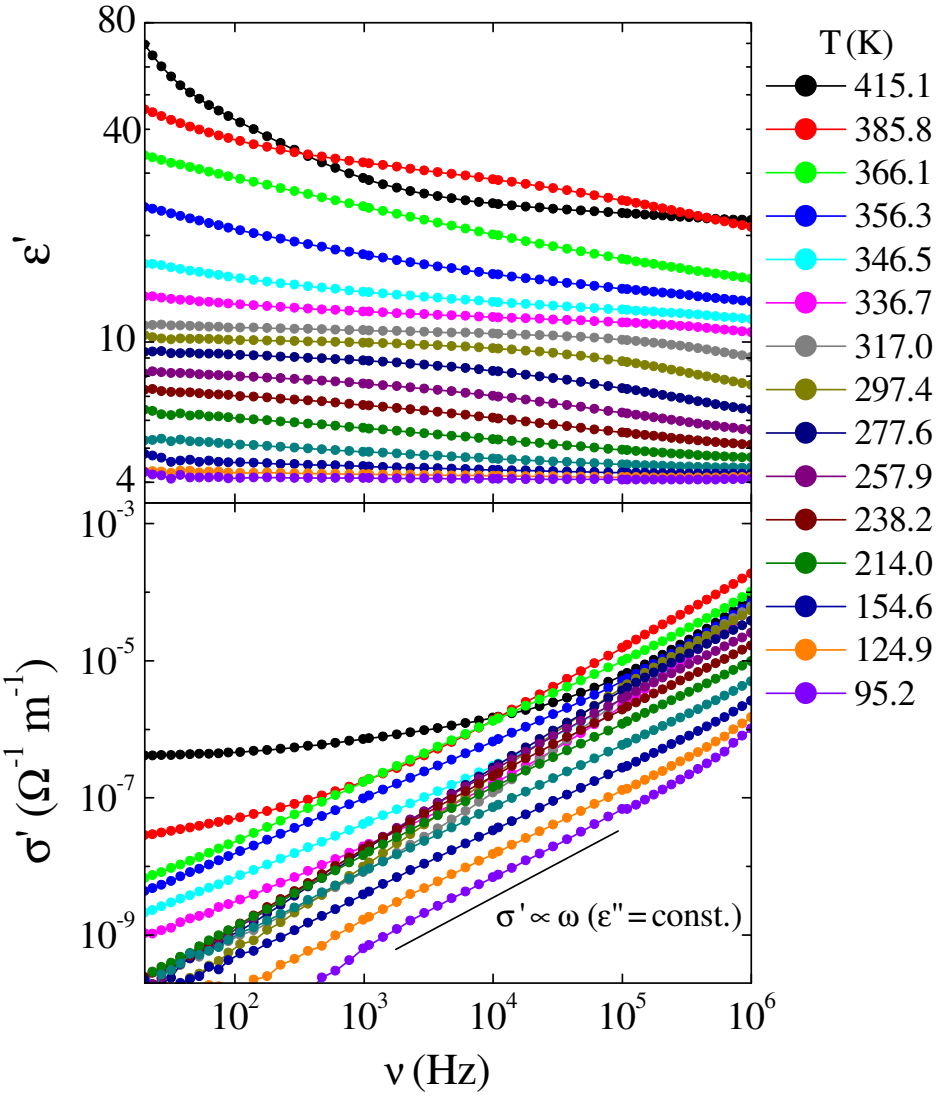

Figure 46: *Frequency-dependence of the reduced P(VDF-TrFE) copolymer in zero DC bias field.* Frequency dependence of ε' and σ', measured at various temperatures in the reduced P(VDF-TrFE) copolymer in zero DC bias field. The solid line in the lower frame demonstrates the constant dielectric losses dependence.

a representation does not reveal different contributions to the measured response so clearly as the linear one. However, main contributions to the measured response have already been revealed from the temperature-dependent data: relaxor dynamics in the crystalline regions and glass-to-rubber transition in the amorphous matrix. This representation clearly shows that already at $\sim$ 100 K the measured value is only $\varepsilon' \sim 4$. Furthermore, this value is independent of the measuring frequency, and the same applies to the measured ε'' data at this temperature. In order to demonstrate this, the solid line in the lower frame of Figure 46, representing constant dielectric losses dependence, is plotted. This, very low, frequency-independent ε^* data indicates that all major polar processes, connected with the above mentioned relaxor and glassy dynamics, are already terminated, and that at temperatures below 100 K only high-frequency non-polar processes contribute to the dielectric response.

This is further supported in Figure 47, which depicts the frequency dependent data, obtained in the temperature range of 228–288 K, in the ε'', ε' plane. In this temperature range there still exists a strong polar contribution, originating from the glassy transition in the amorphous matrix, to the measured dielectric response. Solid lines through the experimental data in Figure 47 are fits to the Cole-Cole expression from Equation 35. More importantly, results of the analysis reveal almost temperature-independent value of $\varepsilon_\infty \sim 4$ in the temperature range where polar processes govern the dielectric response, which is of the same value as ε' response measured at all frequencies at $\sim$ 100 K. As ε_∞ by definition takes into account only high-frequency nonpolar processes, this result thus confirms the conclusion, brought already from Figure 46, that all polar processes in this system terminate down to $T \sim 100$ K [3].

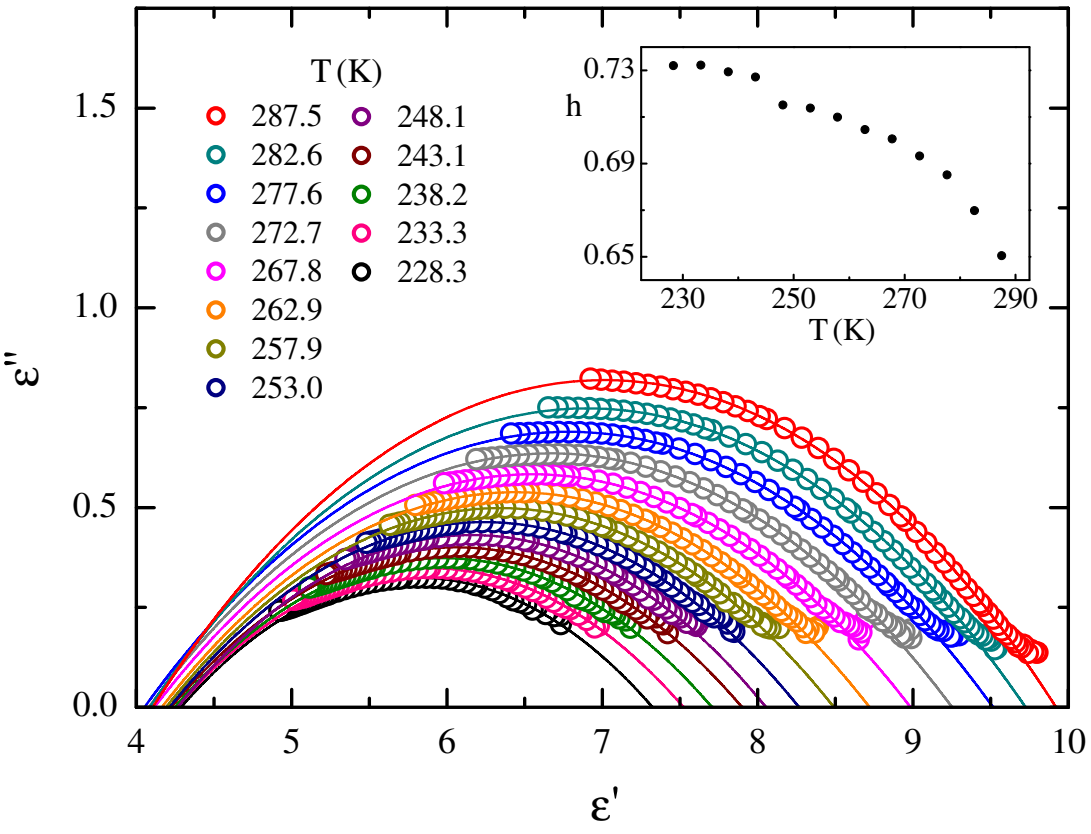

Figure 47: *Frequency-dependent ε^* obtained in zero DC bias field represented in ε'', ε' plane.* Measured values of ε'' plotted vs. ε' at various temperatures in the range, where dynamics in the amorphous matrix dominates the dielectric response. Solid lines through the experimental data are fits to the Cole-Cole expression (Equation 35). The inset shows the temperature dependence of the polydispersivity of the relaxation spectrum.

5.3.1.2 Nonlinear dielectric behaviour

Figure 48 shows the temperature dependence of the third-order nonlinear dielectric constant ε_3 and dielectric nonlinearity a_3 from Equations 69 and 67, respectively. The scaling theory of the second order phase transition gives the following for a ferroelectric (FE) system [76]:

$$a_3^{FE} \propto (T - T_C)^{\gamma - 2\beta}, \tag{76}$$

in which γ is defined by $\chi_1 \propto (T - T_C)^{-\gamma}$ and β is the order-parameter critical exponent, $\eta \propto (T - T_C)^{\beta}$. In general, $\gamma - 2\beta > 0$ for cubic systems at spatial dimensionality $d = 3$ (e.g., mean-field approximation with $\gamma = 1$ and $\beta = \frac{1}{2}$ gives $\gamma - 2\beta = 0$), and concomitantly, the coefficient a_3^{FE} decreases on approaching T_C from above and should vanish at T_C. In a spin glass (SG) or dipolar glass (DG), however, χ_3 behaves according to [77, 78]:

$$\chi_3 \propto (T - T_f)^{-\gamma_3} \tag{77}$$

with $\gamma_3 > 0$, whereas χ_1 remains finite at T_f. Thus [57]:

$$a_3^{SG} = \frac{\chi_3}{\chi_1^4} \propto (T - T_f)^{-\gamma_3}, \tag{78}$$

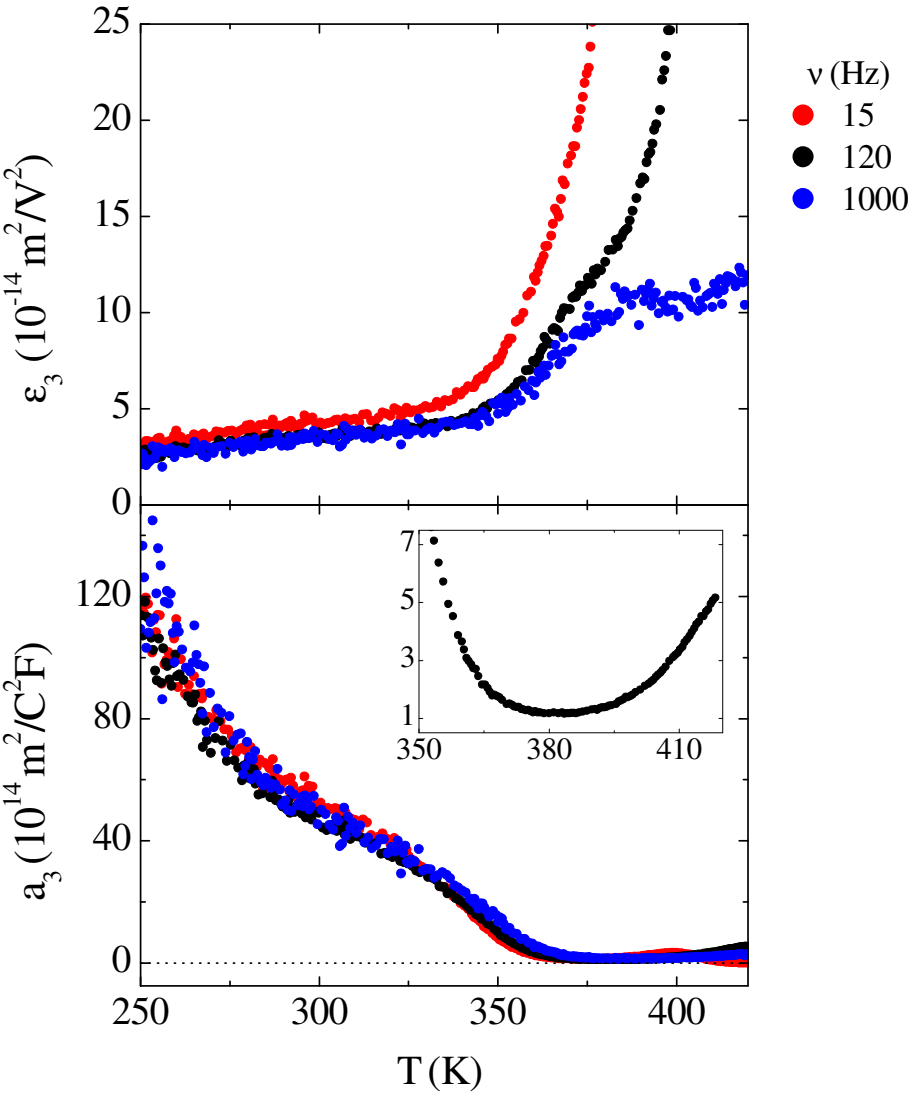

Figure 48: *Nonlinear dielectric response of reduced P(VDF-TrFE) copolymer.* Temperature dependence of the third-order nonlinear dielectric constant ε_3 and dielectric nonlinearity a_3, measured at three different frequencies. The inset shows a paraelectric-to-glass crossover in the $a_3(T)$ in the temperature region, where relaxor dynamics dominates the dielectric response.

i.e., the dielectric nonlinearity coefficient diverges at the freezing transition.

On the other hand, it has been shown that in relaxors a_3 undergoes a crossover from decreasing paraelectric-like to increasing glass-like temperature behaviour when approaching the freezing transition from above [79–82]. Such a dependence is also in accordance with the predictions of the spherical random-bond-random-field model of relaxor ferroelectrics [79]. The inset to Figure 48 shows exactly such a crossover in the $a_3(T)$ in the temperature region, where relaxor dynamics dominates the dielectric response, which confirms the absence of the long-range order and a relaxor nature of the reduced P(VDF-TrFE) copolymer system [3].

5.3.2 Influence of DC bias electric field on Vogel-Fulcher dynamics in relaxor ferroelectrics

The influence of DC bias electric field on the dielectric response of the reduced P(VDF-TrFE) copolymer is depicted in Figure 49. For the relaxor contribution both, ε' and ε'', decrease and the peaks occur at lower temperatures, while there is almost no influence of the bias field on the glassy processes in the matrix. The electrical conductivity astonishingly

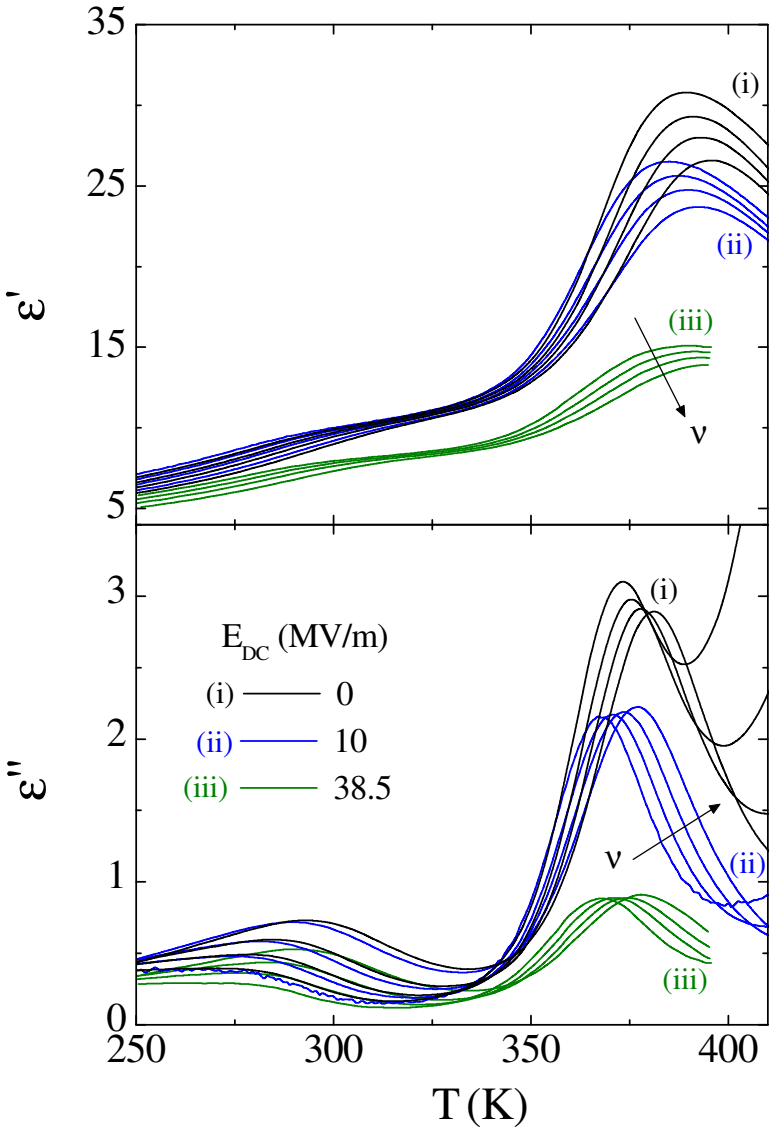

Figure 49: *Temperature-dependent dielectric response of reduced P(VDF-TrFE) copolymer in DC bias electric field.* Temperature dependencies of $\varepsilon'$and ε'', measured at 3 kHz, 10 kHz, 30 kHz and 100 kHz in zero, 10 MV/m and 38.5 MV/m DC bias electric fields.

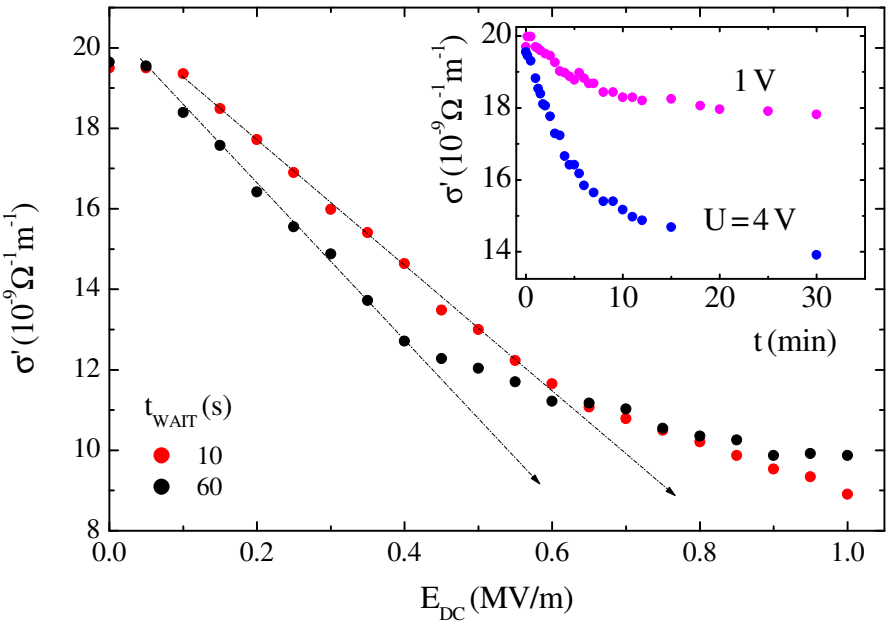

Figure 50: *Electrical conductivity of relaxor reduced P(VDF-TrFE) copolymer vs. DC bias electric field.* The electrical conductivity at 110 Hz as a function of the DC bias electric field, detected with two different field change rates. The waiting time between two subsequent points was either 10 s or 60 s. The arrows point towards anticipated AC conductivity blocking field. The inset shows the time-decreasing of the AC conductivity under applied bias voltages of 1 V and 4 V, corresponding to the DC bias fields of 0.05 MV/m and 0.2 MV/m, respectively.

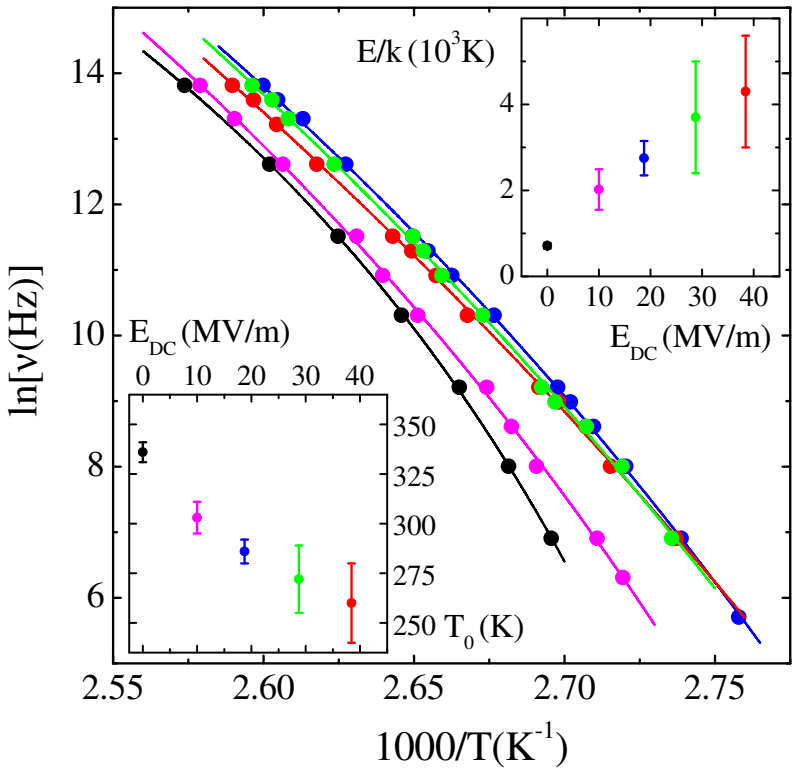

Figure 51: *Vogel-Fulcher plot of characteristic relaxation times, obtained in organic relaxor in different DC bias fields.* The Vogel-Fulcher dependence of the characteristic relaxation time for the relaxor dynamics in the relaxor reduced P(VDF-TrFE) copolymer, obtained from peaks in $\varepsilon''(T)$ in different DC bias electric fields. The insets show the DC bias field dependence of the activation energy (upper inset) and Vogel-Fulcher temperature (lower inset).

decreases in the DC bias electric field: A strong increase of $\varepsilon''(T)$ curves in zero bias field at the highest temperatures, which is due to the increasing conductivity, is almost completely suppressed by the applied electric field [4, 68].

This effect is thoroughly demonstrated in Figure 50. The main frame shows decreasing of the electrical conductivity at 400 K when DC bias field increases. The conductivity remains low after removal of the bias field, however, it can be restored to the initial value by applying AC voltage of the same level as previously applied DC bias [4]. Obviously, charge carriers, which are responsible for the AC electrical conductivity, migrate in a DC bias electric field and become pinned, probably mainly at the electrode-sample interface, while the AC electric field unpins them and restores the conductivity. A similar space charge blocking effect on AC electrical conductivity has already been found in various ionic conductors [85] and thin ceramic films [86]. This is throughout a dynamic process, thus determination of any blocking field (indicated by arrows in Figure 50, which extend the initial linear dependence) is strongly influenced by the measurement rate. The inset to Figure 50 shows that, at high temperatures, even very low bias voltages in a few minutes effectively block the AC electrical conductivity of the reduced P(VDF-TrFE) copolymer.

Decreasing of ε' values in a DC bias electric field as seen in Figure 49 could thus be the result of either (i) the nonlinear dielectric contribution, i.e., the third order nonlinear dielectric susceptibility χ_3 affects polarization and thus detected linear dielectric constant via relation $P = \chi_1 E + \chi_3 E^3 + \cdots$ (see Equation 4) or (ii) decreasing electrical conductivity, which also affects the real part of the complex linear dielectric constant via the Kramers-Kronig relations [4]. The data in Figure 51 reveal that the decreasing of ε' values in a DC bias electric field in fact occurs due to the nonlinear dielectric contribution. The dielectric response, as shown in Figure 49, has been measured in the reduced P(VDF-TrFE) copolymer

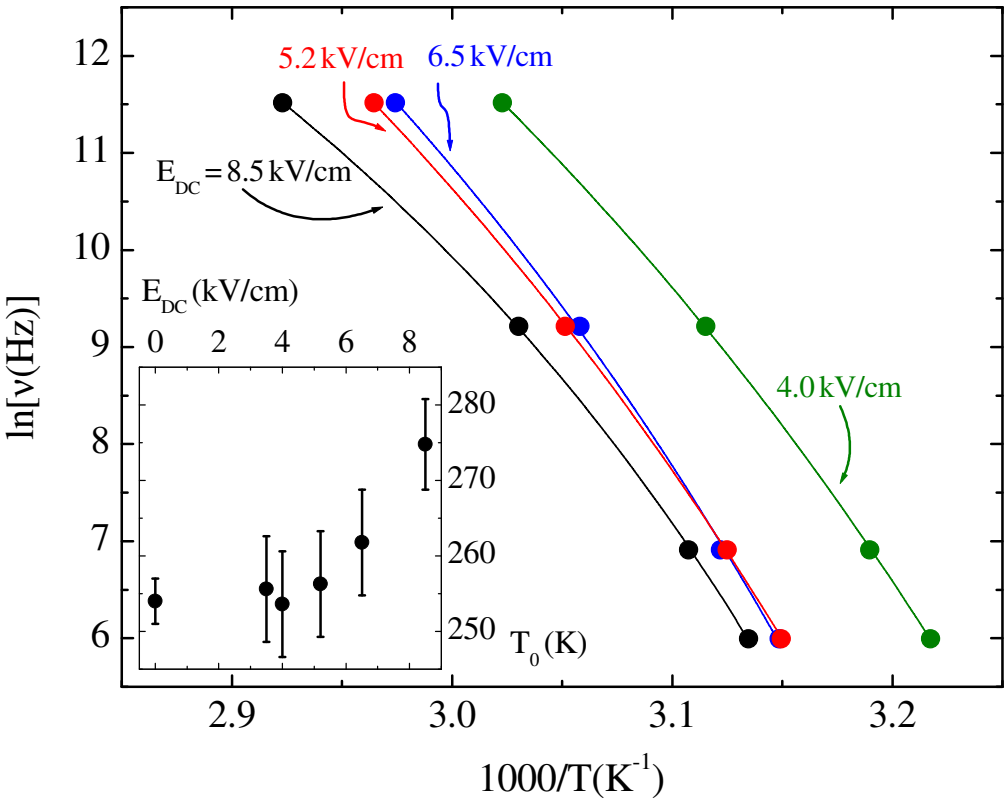

Figure 52: *Vogel-Fulcher plot of characteristic relaxation times, obtained in inorganic relaxor in different DC bias fields.* The Vogel-Fulcher dependence of the characteristic relaxation time for the relaxor 9/65/35 PLZT ceramics obtained from peaks in $\varepsilon''(T)$ in different DC bias electric fields. The inset shows the DC bias field dependence of the Vogel-Fulcher temperature.

in several DC bias electric fields and Figure 51 shows the Vogel-Fulcher analysis of the characteristic relaxation time behaviour for the relaxor dynamics. The upper inset to Figure 51 shows that the activation energy strongly increases on increasing DC bias field, while the lower inset shows that the Vogel-Fulcher temperature strongly decreases. This suggests a negative nonlinear dielectric contribution, as variation of T_0 in DC bias electric fields is directly proportional to the value of parameter b_e from the inverted $P(E)$ relation $E = (\varepsilon_0\chi_1)^{-1}P + b_eP^3 + \cdots$ and thus, as $b_e = \chi_3/(\varepsilon_0\chi_1)^4$, also to χ_3 [5].

This result has been further confirmed by dielectric investigations of the relaxor 9/65/35 PLZT ceramics in DC bias electric fields and the analysis of the characteristic relaxation time behaviour [4]. It is namely known that the nonlinear dielectric response in this system increases the static polarization (the limiting value is $-\chi_3 = 6.4 \times 10^{-19}$ AsmV^{-3} [87]). Indeed, as can be seen in Figure 52, the Vogel-Fulcher temperature in PLZT, contrary to the reduced P(VDF-TrFE) copolymer, increases with increasing DC bias electric field. Furthermore, the activation energy systematically decreases from $E/k \sim 1400$ K without DC bias field to $E/k \sim 700$ K in the DC bias field of 8.5 kV/cm. It should be stressed that, although there exist a critical DC bias field of ~ 5 kV/cm which induces long-range

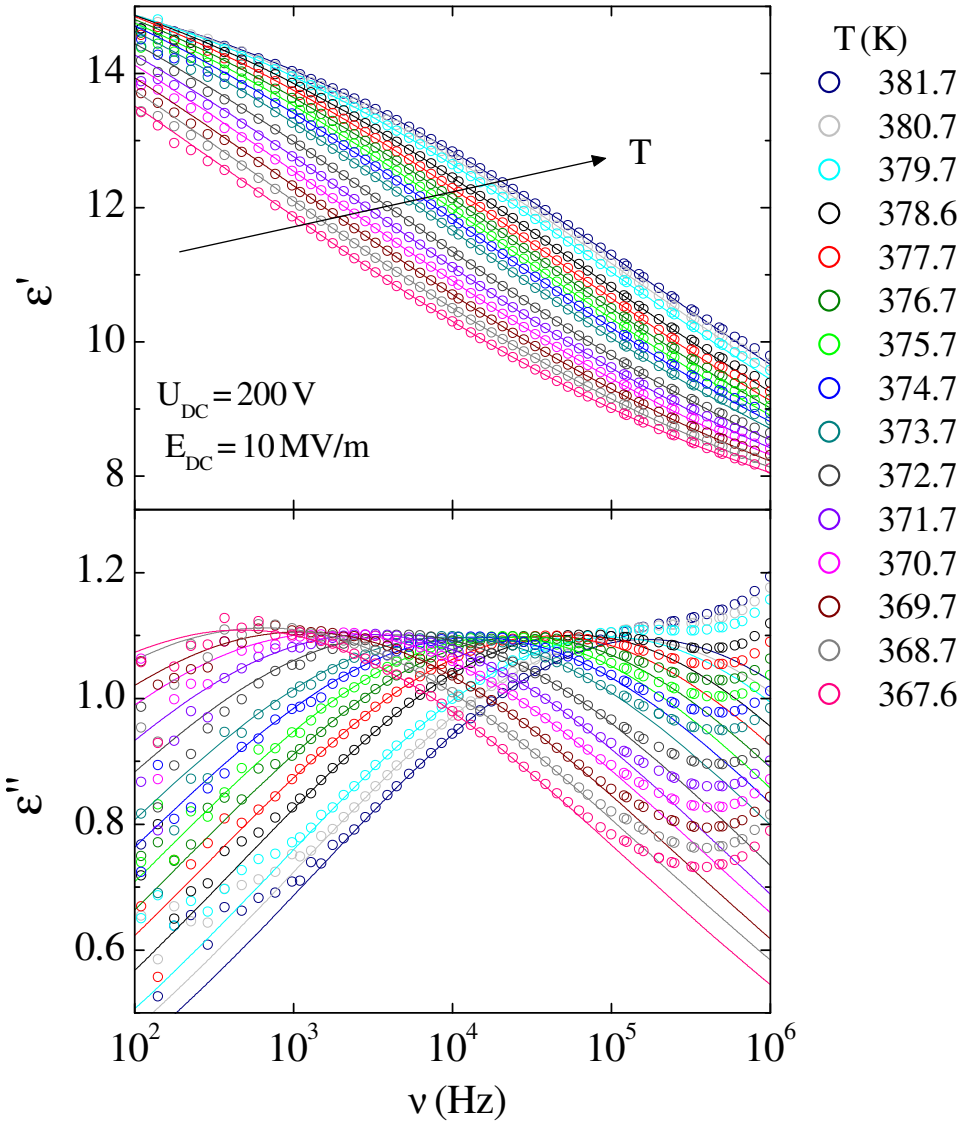

Figure 53: *Frequency-dependent dielectric response of reduced P(VDF-TrFE) copolymer in 10 MV/M DC bias electric field.* $\varepsilon'$and ε'' vs. frequency, obtained in 10 MV/m DC bias field at various temperatures. Solid lines represent the fit to the Cole-Cole expression from Equation 35.

ferroelectric order in this system, the relaxor dynamic peaks can still be studied using Vogel-Fulcher analysis, as they occur at temperatures around 350 K while the ferroelectric state appears below ~ 250 K [52].

In general, parameters of the Vogel-Fulcher relation (Equation 60) T_0 and E/k, obtained from peaks in $\varepsilon''(T)$ may be different from those obtained from analysis of the frequency-dependent permittivity using the Cole-Cole expression (Equation 35) [83,84]. It has already been shown that in zero DC bias field in classical relaxor terpolymers both processes give the same result [55], just like in inorganic relaxors [84], however, a DC bias field could influence the shape of the static dielectric constant. Figure 53 presents frequency-dependent dielectric response of the reduced P(VDF-TrFE) copolymer, obtained in 10 MV/m bias field at various temperatures. Solid lines through experimental data are fits to the Cole-Cole expression (Equation 35). Figure 54 shows the comparison of the Vogel-Fulcher analysis of the characteristic relaxation time behaviour for the relaxor dynamics, using data obtained in 10 MV/m DC bias field from (i) peaks in $\varepsilon''(T)$ and (ii) parameters obtained from analysis of $\varepsilon^*(\nu)$ using the Cole-Cole expression (Equation 35). It can clearly be seen that the Vogel-Fulcher parameters T_0 and E/k are, within experimental error, identical [68].

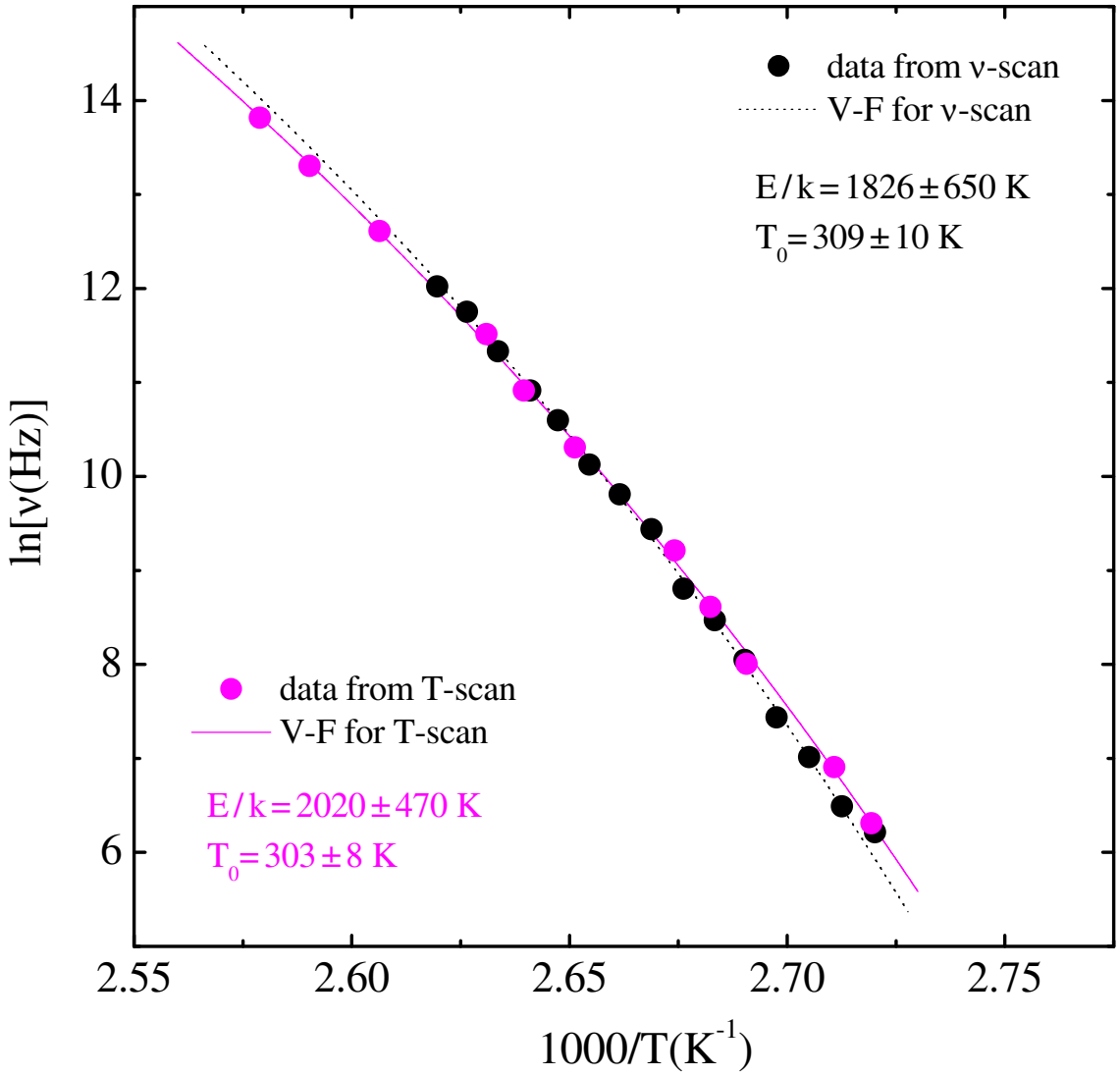

Figure 54: *Vogel-Fulcher plots of characteristic relaxation times of relaxor reduced P(VDF-TrFE) copolymer, obtained from $\varepsilon''(T)$ and $\varepsilon^*(\nu)$.* Comparison of Vogel-Fulcher plots, using characteristic relaxation times, obtained in 10 MV/m DC bias field from peaks in $\varepsilon''(T)$ and from Cole-Cole analysis of the frequency-dependent response in Figure 53.

5.3.3 Electromechanical response of relaxor reduced P(VDF-TrFE) copolymer

Investigations of the electromechanical properties of relaxor polymers have been attracting considerable attention, ever since the initial studies of the electron-irradiated P(VDF-TrFE) copolymer revealed giant electrostriction, which is two orders of magnitude larger than in inorganic piezoceramic and magnetostrictive materials and also considerably larger than in ferroelectric polymers ($-S_3 \sim 0.1$ %) [47]. In further studies, similar electromechanical properties were detected in relaxor terpolymers, in which the third monomer contains Cl atoms (e.g., chlorofluoroethylene or chlorotrifluoroethylene monomers) [48]. In light of these finds, we decided to conduct investigations of the electromechanical properties of the new class of relaxor polymers, the reduced P(VDF-TrFE) copolymer system, in collaboration with the group of Prof. Dr. Horst Beige from the Martin Luther University in Halle, Germany.

Measurements of the electromechanical response of the reduced P(VDF-TrFE) copolymer revealed (i) electrical breakdown field of 125 MV/m and 60 MV/m at room temperature and 353 K, respectively, and (ii) high-field-induced longitudinal strain of $\sim 2 \cdot 10^{-3}$ below 120 MV/m at room temperature (see Figure 55). Figure 56 depicts the measured hysteresis loops, obtained simultaneously with the strain loops (see the experimental procedure technique described in subsection 5.2.3) in the relaxor reduced P(VDF-TrFE) copolymer at room temperature at 17 Hz. Due to high electrical conductivity of the material at higher electric fields, which also influenced the shape of the hysteresis loops, the analysis of experimental data remained inconclusive. Similar hysteresis loops were detected at 1.7 and 170 Hz probing frequencies at room temperature and at 353 K (at the same probing frequencies).

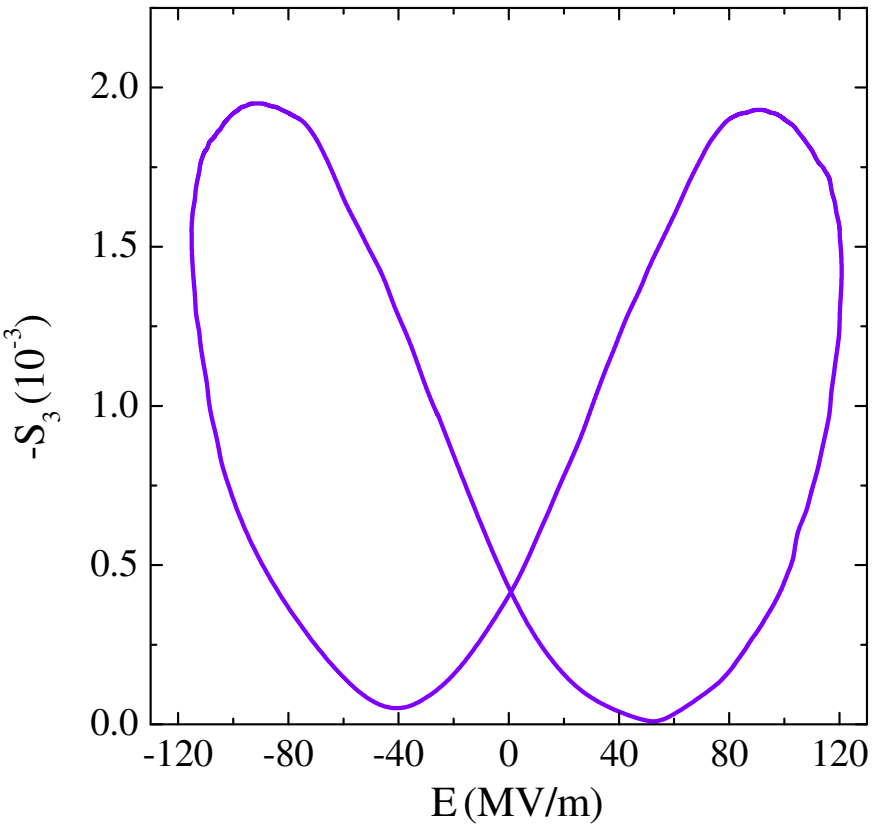

Figure 55: *Strain-field dependence of reduced P(VDF-TrFE) copolymer.* Strain-field dependence at room temperature, obtained using 17 Hz probing frequency.

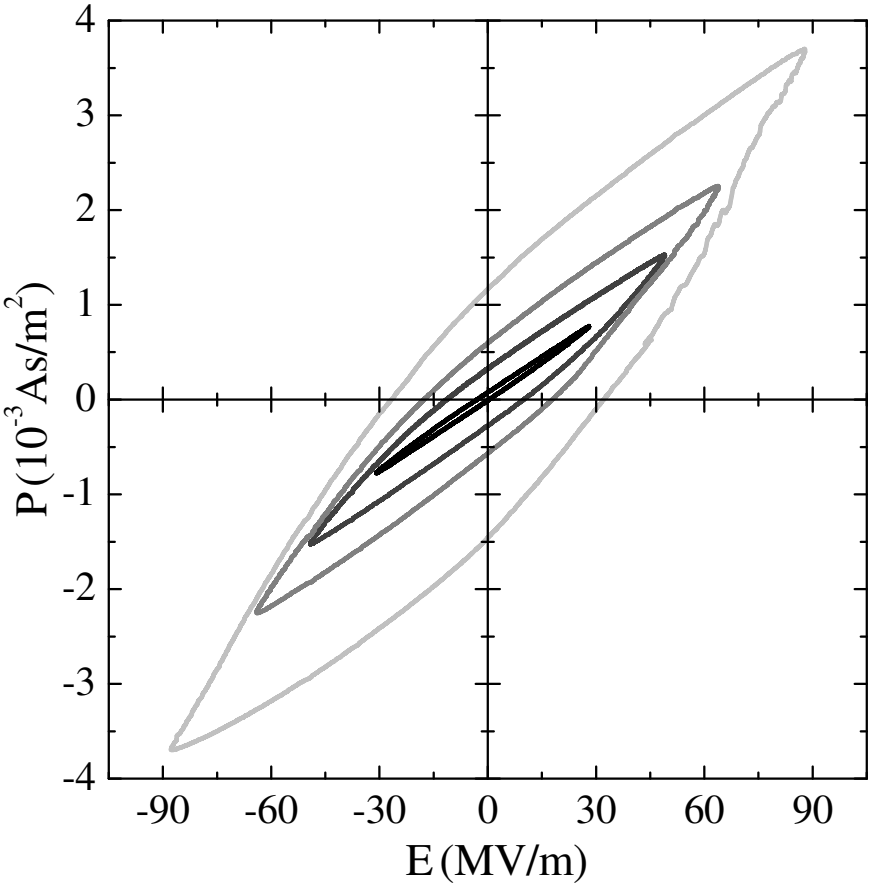

Figure 56: *Polarization hysteresis loops of reduced P(VDF-TrFE) copolymer.* Polarization hysteresis loops at room temperature, obtained using 17 Hz probing frequency.

6 Relaxor poly(vinylidene fluoride)-based terpolymer/copolymer blends on aluminium foil

This chapter is dedicated to relaxor poly(vinylidene fluoride)-based terpolymer/copolymer blends developed on aluminium foil and relaxor systems in general. The first part of the chapter is a short overview of research and development interest in polymer blends developed on a surface in general. In the second part of the chapter, structural, caloric and dielectric properties of relaxor poly(vinylidene fluoride-trifluoroethylene-chlorofluoroethylene) [P(VDF-TrFE-CFE)] (66.3/26.4/7.3 mol%) terpolymer and poly(vinylidene fluoride-chlorotrifluoroethylene) [P(VDF-CTFE)] (91/9 mol%) copolymer blends developed on aluminium foil are presented. In the last part of the chapter, the results of investigations of the influence that two different dynamic contributions, which superimpose in the detected dielectric response of a relaxor, could have on the characteristic relaxation times and, concomitantly, on the Vogel-Fulcher behaviour, are presented.

6.1 Overview

Relaxor polymers are very promising for a broad range of energy storage capacitor applications due to their unique physical properties [51, 58]. One of the advantages for use of polymers in such applications arises from the possibility of polymer film formation directly on a surface [88]. Active metals such as aluminium can be used for substrates, as they are less expensive than noble metals and mechanically more stabile than glassy carbon [88, 89]. And as has already been pointed out, investigations of relaxor P(VDF-TrFE-CFE) terpolymer have revealed high values of the dielectric constant at room temperature, fast response speeds, high strain levels and energy density, and large electrocaloric effect [49, 50, 90–92]. Figure 57 thus depicts an infographic on motivation for research and development of relaxor polymers on a metal surface.

Polymer blends exploit merits of both, base and additive polymer, as, due to the interference effect, properties of base polymer can be tailored and improved [93]. Recent studies show that polymer blends composed of P(VDF-TrFE-CFE) terpolymer as a base with a small amount of poly(vinylidene fluoride-chlorotrifluoroethylene) [P(VDF-CTFE)] copolymer (e.g., 5 or 10 mol %) as an additive have an even higher polarization response, energy density, elastic module and particularly important, a much higher electrical breakdown field than pure relaxor P(VDF-TrFE-CFE) system [50, 92, 93].

As mentioned in chapter 5, materials based on PVDF, its copolymers, or terpolymers are semi-crystalline systems, composed of crystalline regions embedded in an amorphous matrix [45, 61]. In most relaxor polymers, a broad relaxor peak is detected at lower temperatures than the previous ferroelectric peak and almost completely overrides the dielectric anomaly due to the glass-to-rubber transition in the amorphous matrix [3, 48, 55]. This complicates analysis and interpretation of dielectric results, since a typical detected dielectric maximum is not only due to relaxor dynamics in the crystalline region, but comprises also the contribution of glassy dynamics in the amorphous matrix.

We have studied structural and electrically-induced properties of relaxor polymer blend

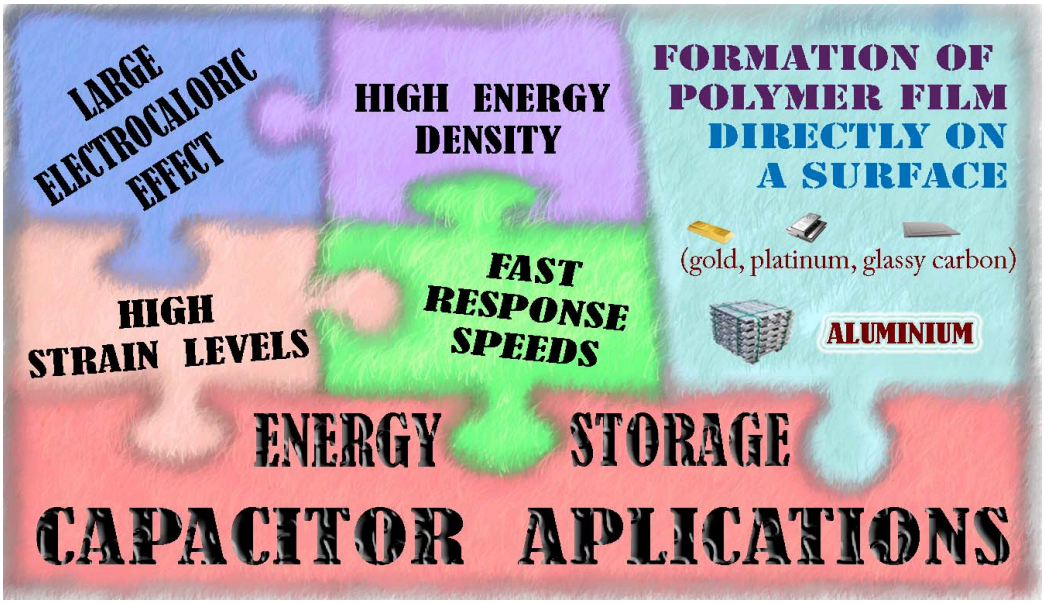

Figure 57: *Infographics on the motivation for research and development of polymers on a metal surface.*

films composed of P(VDF-TrFE-CFE) (66.3/26.4/7.3 mol %) terpolymer and P(VDF-CTFE) (91/9 mol %) copolymer on aluminium foil in terms of X-ray investigations, differential scanning calorimetry and detailed dielectric response analysis. We have furthermore calculated dielectric response of a relaxor polymer system in order to shed some light on the influence of two superimposed dynamics in detected dielectric response on the characteristic relaxation times and on the Vogel-Fulcher behaviour.

6.2 Structural and dielectric properties of poly(vinylidene fluoride)-based terpolymer/copolymer blends developed on aluminium foil

This section presents the results of the structural, caloric and dielectric measurements and analysis of relaxor polymer blend films composed of P(VDF-TrFE-CFE) terpolymer as the base and P(VDF-CTFE) copolymer as the additive, developed on aluminium surface.

6.2.1 Experimental procedure

6.2.1.1 Processing and structural characterization

P(VDF-TrFE-CFE) (66.3/26.4/7.3 mol %) terpolymer and P(VDF-CTFE) (91/9 mol %) copolymer were dissolved in dimethylformamide respectively. Then both solutions were mixed together with the copolymer weight content ranging from 0 % to 10 %. The final solutions were poured on several pieces of aluminium foil and dried at 333 K for 10 h in an air-circulation oven. Finally, the films were annealed at 378 K for 24 h in a vacuum oven.

Thermal analysis was performed on a Perkin-Elmer Pyris 1 differential scanning calorimeter (DSC) with a heating rate of 10 K/min. X-ray studies were carried out on a Bruker D8 Advance X-ray diffractometer equipped with a Cu source with an average wavelength of 1.542 Å.

6.2.1.2 Dielectric measurements

For dielectric measurements, surfaces of 3–4 μm thick polymer films were covered first by sputtered chromium (10 nm) for better adhesion of the final 100 nm thick sputtered gold electrodes (see Figure 58). Complex dielectric constant from Equation 14 was measured in the frequency range of 20 Hz–1 MHz by using an HP4282 Precision LCR Meter. The amplitude of the probing AC electric signal was 0.1 V. After heating the samples up to ≈350 K, the dielectric response was detected during cooling runs with the rate of 0.5 K/min. The temperature of the samples was stabilized within 10 mK by using lock-in bridge technique with a platinum resistor Pt100 as a thermometer.

(a) Pure terpolymer sample

(b) Copolymer-terpolymer blend

Figure 58: *Relaxor polymer films on a surface.* Relaxor P(VDF-TrFE-CFE) terpolymer (a) and P(VDF-TrFE-CFE) terpolymer-P(VDF-CTFE) copolymer blend films (b) on aluminium surface, prepared for dielectric measurements, with (right side) and without (left side) sputtered gold electrodes.

6.2.2 Results and discussion

6.2.2.1 Structural and caloric characterization

Figure 59 shows differential scanning calorimetry (DSC) traces of terpolymer samples blended with a different amount of copolymer. Each trace has two or more melting endothermal peaks. For pure terpolymer, the two endothermal peaks are caused by the melting of crystallites with different inclusion degree of CFE units: the peak at lower temperature indicates more CFE units are included in the crystallites and these defects can reduce the lattice positional ordering and result in the decrease of the melting temperature [94]. As the copolymer content increases, two apparent changes occur. First, both endothermal peaks of the terpolymer shift towards lower temperature. This indicates that the copolymer disturbs the crystallizing process of the terpolymer. The CTFE units may be included in the terpolymer crystallites thus introducing more defects into the crystallites, which can be corroborated by the XRD data. Another proof that the crystallizing process is disturbed is the decreased crystallinity (for binary blends being calculated through the total enthalpy method) listed in Table 2. Second, a new endothermal peak appears around 423 K, which can be attributed to

Table 2: *Total enthalpy change and DSC peak temperatures and the crystallinity of relaxor polymer films, developed on aluminium surface.* Total enthalpy change and DSC peak temperatures and the crystallinity of the P(VDF-TrFE-CFE) terpolymer film and its blends with 5 % and 10 % of the P(VDF-CTFE) copolymer. For comparison, data of pure copolymer are included.

sample	ΔH(J/g)	T_1(K)	T_2(K)	T_3(K)	X_C(%)
terpolymer	19.0	389.5	411.6	-	45.6
5 %-blend	17.1	389.2	408.8	-	41.0
10 %-blend	14.9	385.6	406.8	422.5	35.7
copolymer	31.5	417.7	437.8	-	75.5

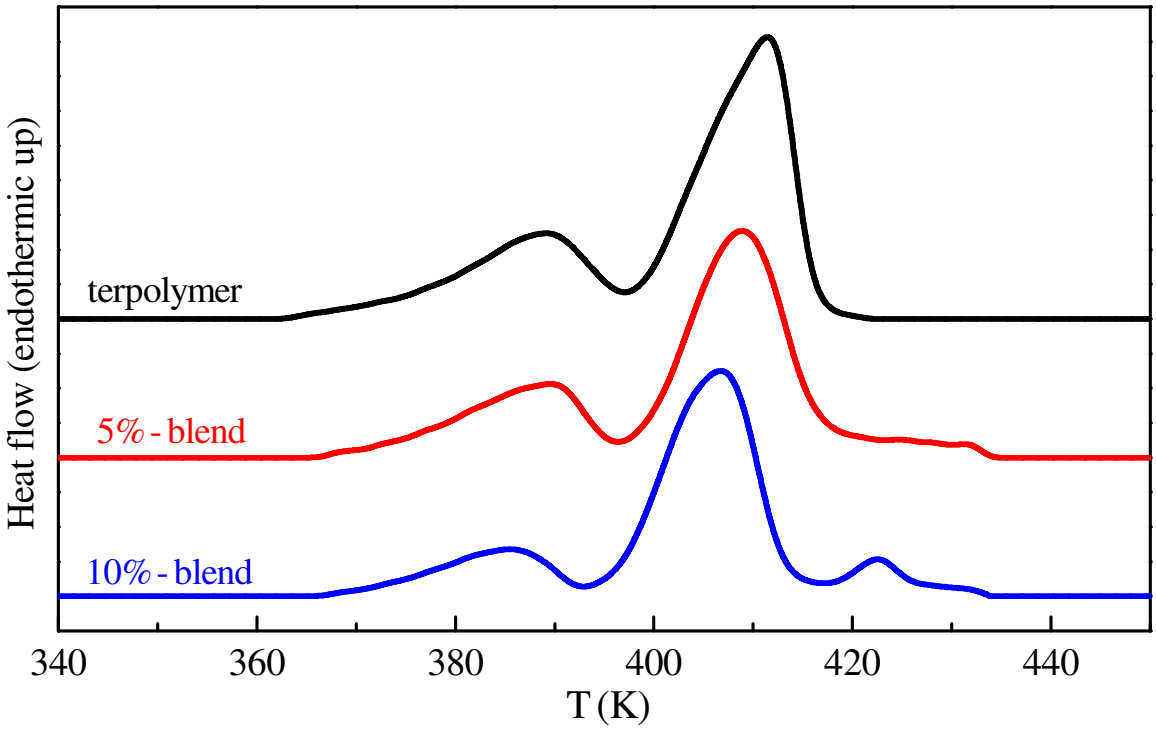

Figure 59: *DSC traces of relaxor polymer films, developed on aluminium surface.* DSC traces of the P(VDF-TrFE-CFE) terpolymer film (black) and its blends with 5 % (red) and 10 % (blue) of the P(VDF-CTFE) copolymer.

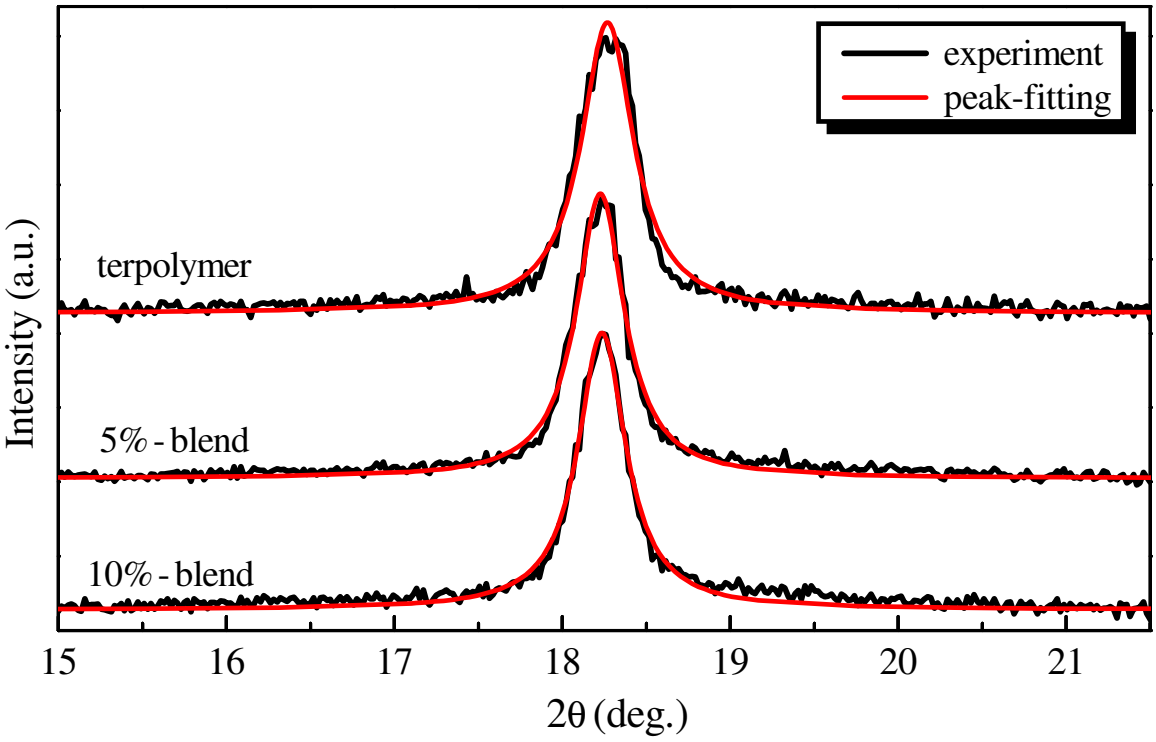

Figure 60: *XRD patterns of relaxor polymer films, developed on aluminium surface.* XRD patterns of the P(VDF-TrFE-CFE) terpolymer film and its blends with 5 % and 10 % of the P(VDF-CTFE) copolymer.

the melting of copolymer crystallites. This indicates that, particularly at higher content, the copolymer cannot totally co-crystallize with the terpolymer but is only partially embedded during crystallization of the terpolymer [6].

The XRD patterns are shown in Figure 60. Each sample exhibits only one peak, referent to the diffraction in planes (110,200) [95]. The detailed lattice parameters are listed in Table 3. With the increase content of copolymer, the lattice spacing is expanded from 4.85 Åto 4.86 Å, which is due to the incorporation of the CTFE units in the crystallites. The coherence lengths (L) perpendicular to the (110,200) planes, representing the sizes of crystallites in the terpolymer, were estimated using Scherrer equation [6]:

$$L = K\lambda/Bcos(\theta), \tag{79}$$

in which $K = 0.9$ is the shape factor, λ is X-ray wavelength, and B and θ are full width at half-maximum and angular position of the diffraction peaks, respectively. The coherence length increases from 21.2 nm for pure terpolymer to at least 23.2 nm for polymer blends. Both the enlarged coherence length and the expanded lattice spacing corroborate the DSC results that the addition of copolymer introduces more defects and distorts the crystalline ordering [6].

Table 3: *X-ray diffraction angle, lattice spacing, and the coherence length in relaxor polymer films, developed on aluminium surface.* X-ray diffraction angle, lattice spacing, and the coherence length in the P(VDF-TrFE-CFE) terpolymer film and its blends with 5 % and 10% of the P(VDF-CTFE) copolymer.

sample	2Θ(°)	d(Å)	L(nm)
terpolymer	18.27	4.85	21.2
5 %-blend	18.23	4.86	23.2
10 %-blend	18.24	4.86	23.3

6.2.3 Dielectric properties

Figure 61 depicts the dielectric constant data as a function of the temperature, obtained at several measuring frequencies between 30 Hz and 1 MHz, in terpolymer samples blended with a different amount of copolymer. A typical dispersive relaxor dielectric behaviour with relatively high maximum value of $\varepsilon' \sim 80$ in the low-frequency range around room temperature has been detected in the terpolymer film. Upon increasing mol % of P(VDF-CTFE) copolymer, values of both, ε' and ε'', decrease. This is in concurrence with the interference effect, as ε' values are lower in copolymer with respect to terpolymer [92]. Insets to Figures 61d–f show that characteristic relaxation frequencies, determined from peaks in $\varepsilon''(T)$, follow the Vogel-Fulcher law from Equation 60, as being typical for relaxors [55]. No notable differences within statistical error in the Vogel-Fulcher temperature and the activation energy between terpolymer and terpolymer/copolymer blends have been detected, indicating that the level of crystallization has no influence on the relaxor dielectric dynamics of the terpolymer film [6].

Figures 62, 63 and 64 depict the frequency-dependence of the complex dielectric constant and the electrical conductivity (see Equation 51), detected in the terpolymer film and its blends with 5 % and 10 % of the copolymer at various temperatures, respectively. Solid lines are a guide for the eye. Figure 65 shows a comparison of characteristic relaxation times of the terpolymer film, determined from $\varepsilon^*(\nu)$ data in Figure 62 by Cole-Cole fitting (Equation 35), denoted as ν-scan, to those determined from $\varepsilon''(T)$ from Figure 61d, denoted as T-scan. There is no essential difference between data obtained from both scans at temperatures above room temperature, however, ν-scan data no longer follow Vogel-Fulcher law below room temperature. Similar evolution of characteristic relaxation times has been observed

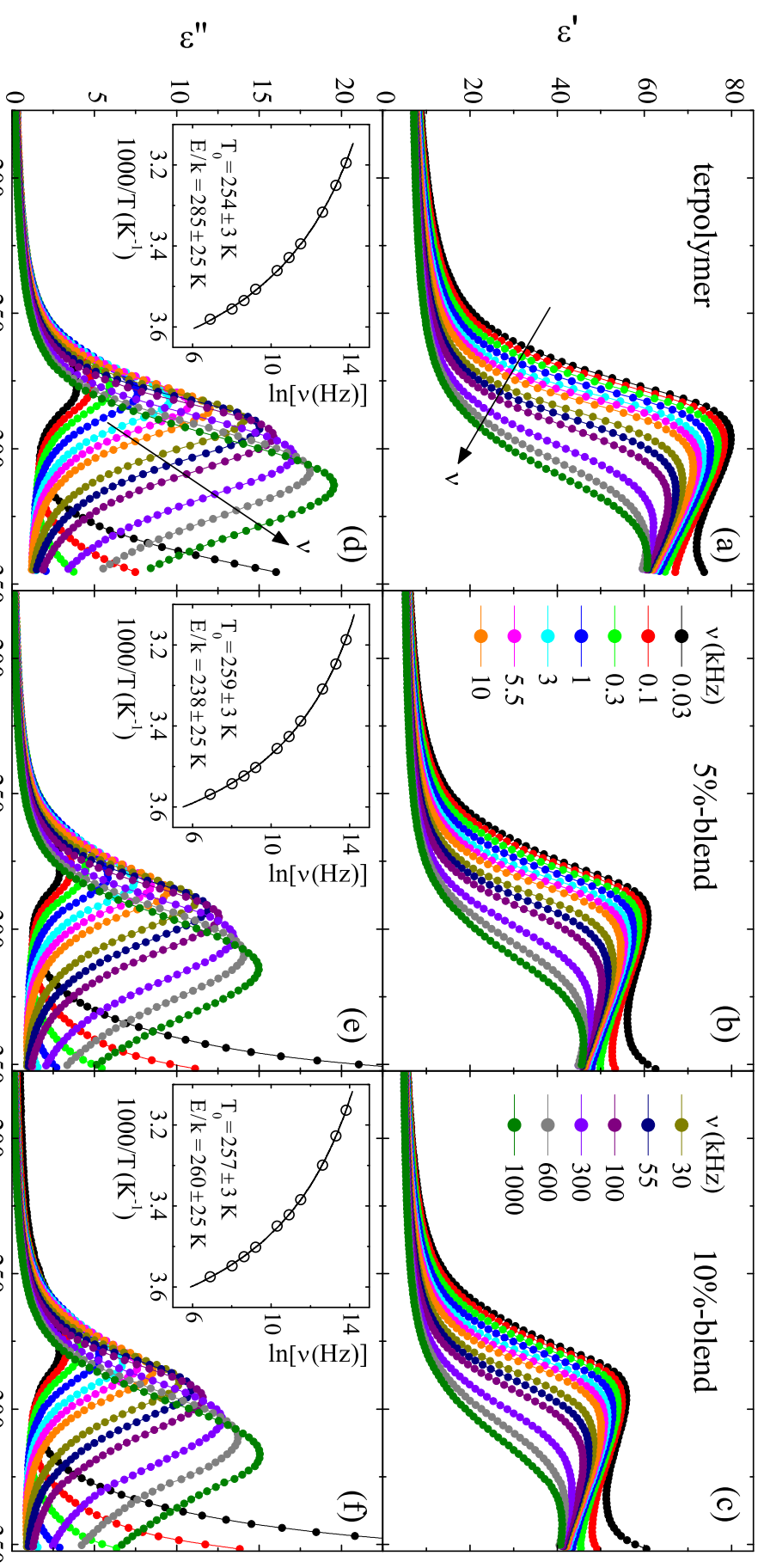

Figure 61: *Temperature-dependence of relaxor polymer films, developed on aluminium surface* The real, ε' (a–c), and the imaginary, ε'' (d–f), parts of the dielectric constant vs. temperature, detected at various frequencies in the terpolymer and blend films. Insets show the Vogel-Fulcher temperature dependence of the characteristic relaxation times.

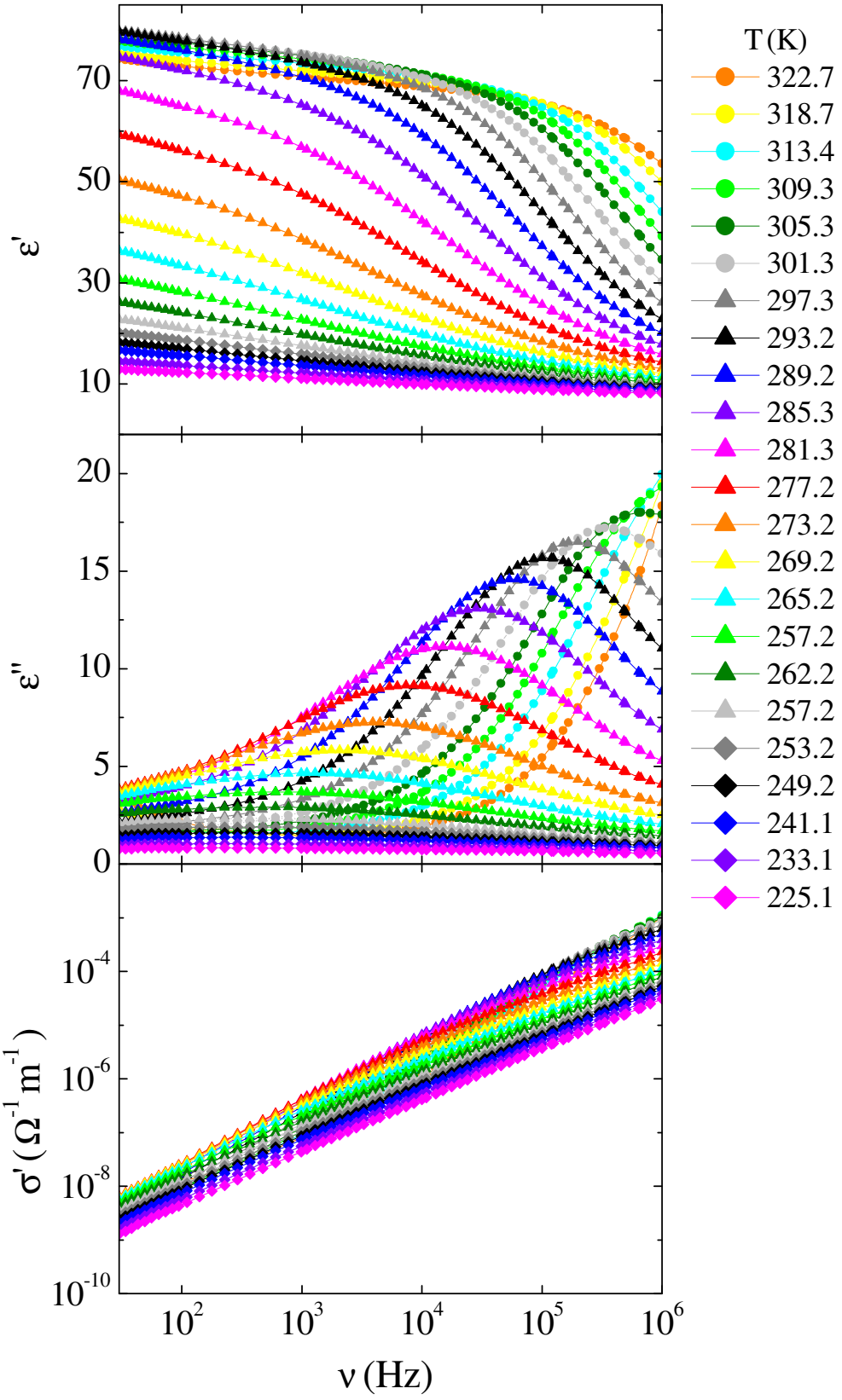

Figure 62: *Frequency-dependence of relaxor terpolymer film, developed on aluminium surface.* ε', ε'' and σ' vs. frequency, detected in the terpolymer film at various temperatures between 224 K and 323 K ($\Delta T = 4.5$ K).

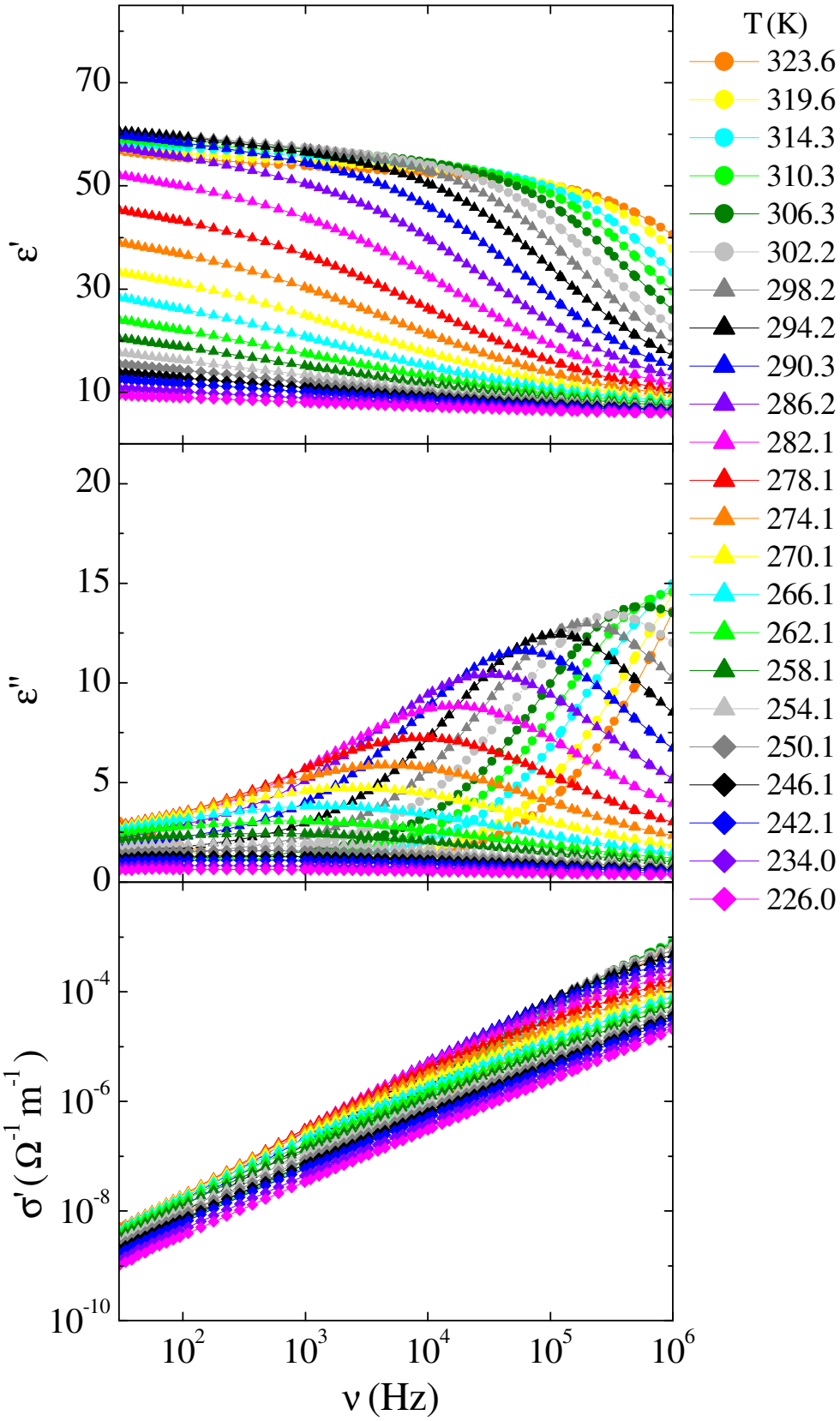

Figure 63: *Frequency-dependence of relaxor 5 % terpolymer-copolymer blend film, developed on aluminium surface.* ε', ε'' and σ' vs. frequency, detected in the blend film, consisting of the terpolymer with 5 % of the copolymer, developed on aluminium surface at various temperatures between 224 K and 323 K ($\Delta T = 4.5$ K).

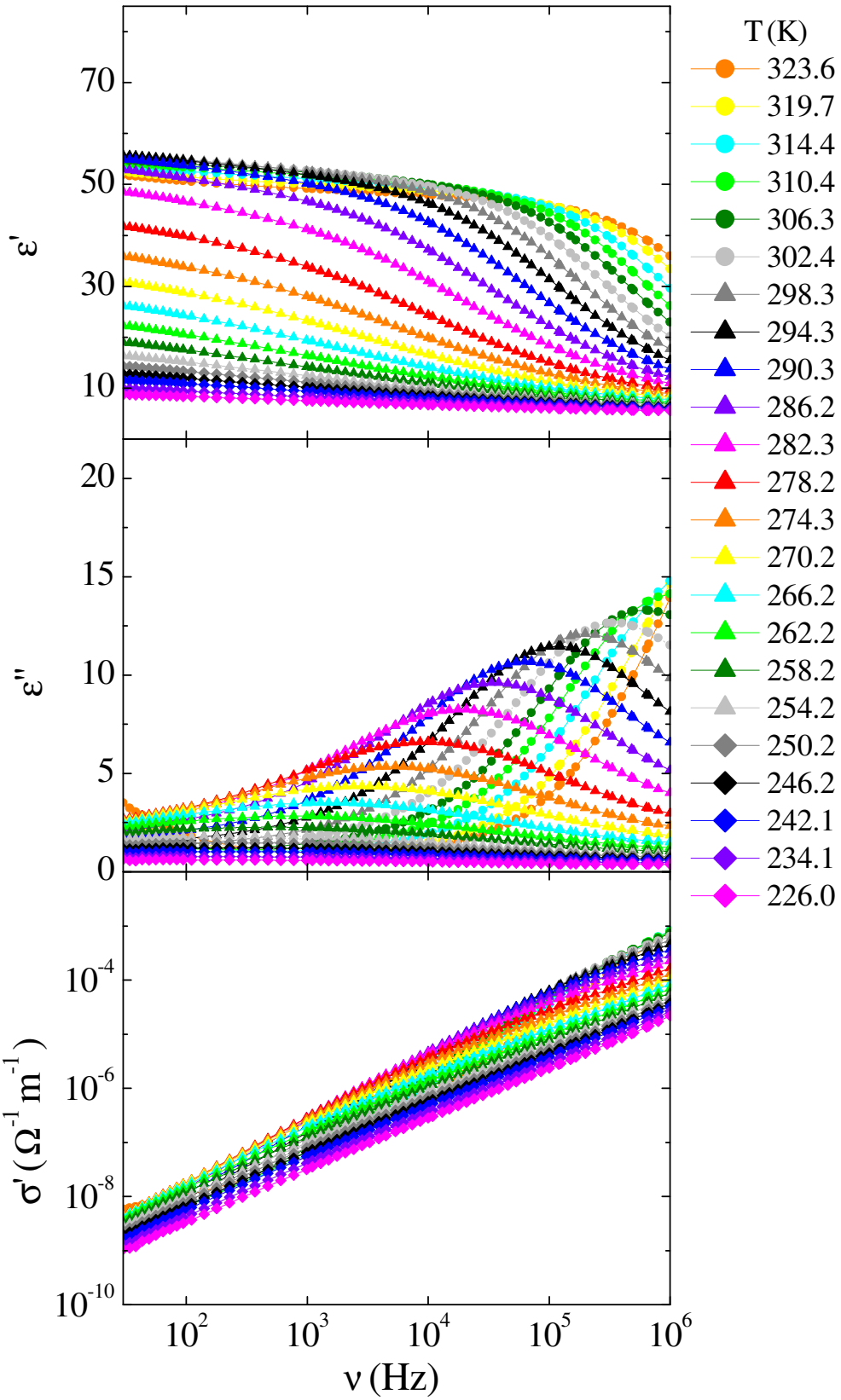

Figure 64: *Frequency-dependence of relaxor 10 % terpolymer-copolymer blend film, developed on aluminium surface.* ε', ε'' and σ' vs. frequency, detected in the blend film, consisting of the terpolymer with 10 % of the copolymer, developed on aluminium surface at various temperatures between 224 K and 323 K ($\Delta T = 4.5$ K).

in terpolymer/copolymer blends [6]. The differences between characteristic relaxation times obtained from T-scan and ν-scan in this case, are further extrapolated in section 6.3.

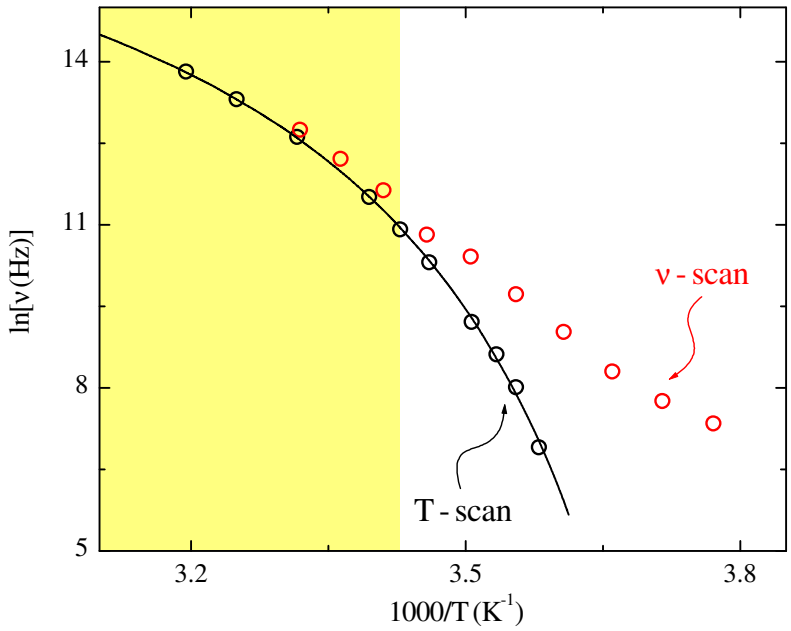

Figure 65: *Vogel-Fulcher plots of the characteristic relaxation times, obtained in P(VDF-TrFE-CFE) terpolymer, developed on aluminium surface.* The characteristic relaxation times determined from $\varepsilon^*(\nu)$ fit to Equation 35 (ν-scan) and those determined from $\varepsilon''(T)$ from Figure 61d (T-scan).

6.3 Influence of two superimposed dynamic contributions on the detected dielectric response of a relaxor system

Differences between characteristic relaxation times obtained from T-scan and ν-scan in Figure 65 may be explained by taking into account the structure of the studied system, which is composed of crystalline regions with spontaneous polarization embedded into an amorphous matrix [55]. As mentioned in section 5.1, a typical dielectric maximum observed in relaxor polymers is not only due to relaxor dynamics in the crystallites, but also comprises the contributions of glass-to-rubber transition in the amorphous matrix [3, 48]. This means that there are two similar dynamic processes taking place in the same temperature range, which complicates data interpretation and understanding, i.e., in analysis, we are obtaining characteristic relaxation times for the sum of the two dynamics.

In the temperature domain, a slight error in the value of temperature is made when obtaining data from $\varepsilon''(T)$ at discrete values of frequency, because in this case

$$\varepsilon^*(T, matrix) < \varepsilon^*(T, crys.), \tag{80}$$

which is engrafted into the fitting error to the Vogel-Fulcher ansatz (Equation 60) [6]. However, this is not the experimental case in the frequency domain, in which the superimposition of the two dynamics results in a much broader dispersive relaxor peak at lower temperatures, where

$$\varepsilon^*(\nu, matrix) \approx \varepsilon^*(\nu, crys.). \tag{81}$$

As both, glassy and relaxor, dynamics can be described using the Cole-Cole empiric expression, the frequency-dependent dielectric response of a relaxor polymer system was

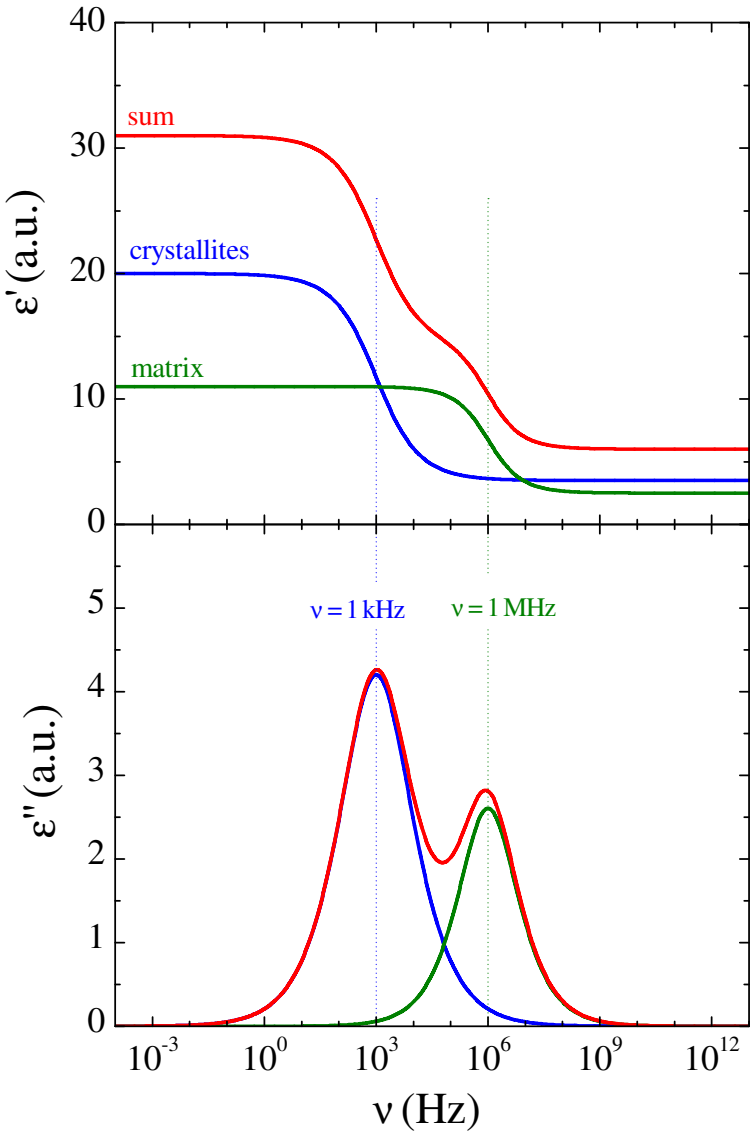

Figure 66: *Calculated dielectric response of a relaxor polymer: two dynamic processes.* Calculated dielectric response of a relaxor polymer system (red), in which two different dynamic processes that take place in separate temperature regions: the relaxor dynamics in the crystallites (blue) and the glassy dynamics in the amorphous matrix (green).

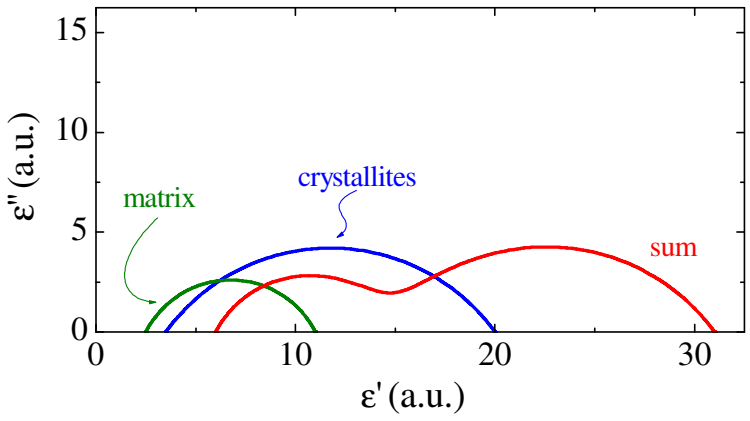

Figure 67: *Complex plain: two dynamic processes.* Calculated dielectric response of a relaxor polymer system from Figure 66, plotted in the complex ε', ε'' plane.

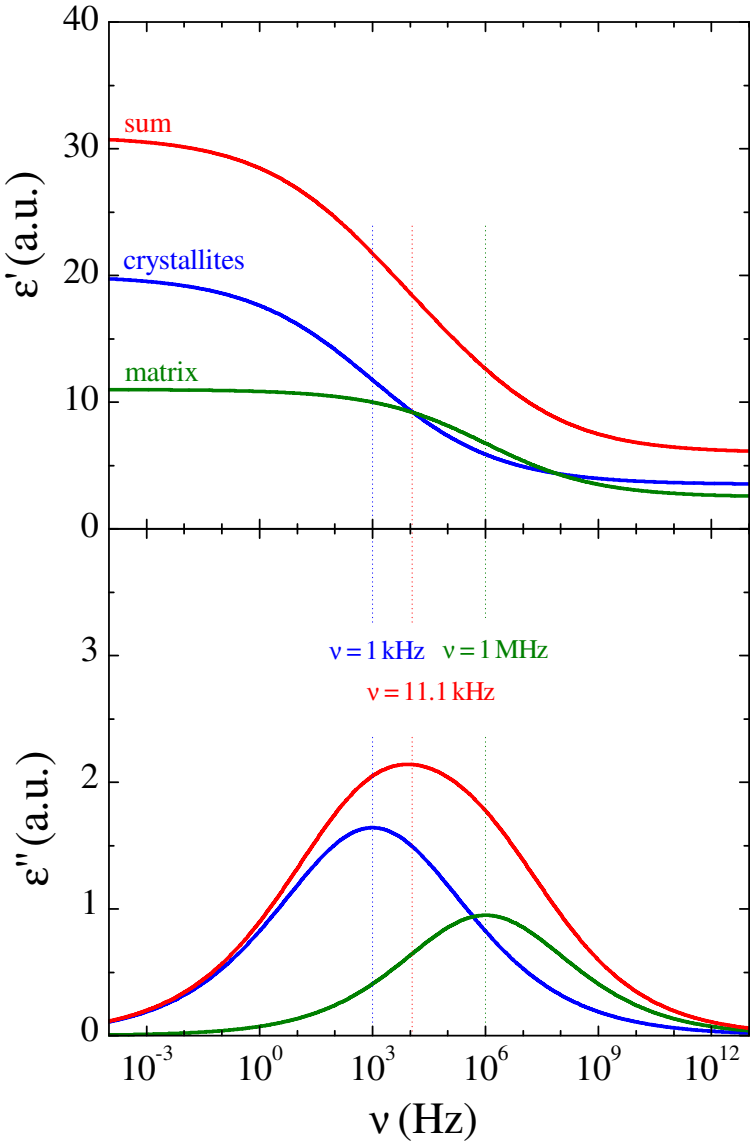

Figure 68: *Calculated dielectric response of a relaxor polymer: two superimposed dynamic processes.* Calculated dielectric response of a relaxor polymer (red). For both, the relaxor dynamics in the crystallites (blue) and the glassy dynamics in the amorphous matrix (green), a Cole-Cole ansatz with a broad distribution of relaxation times was used. The inset presents the data in the complex plane.

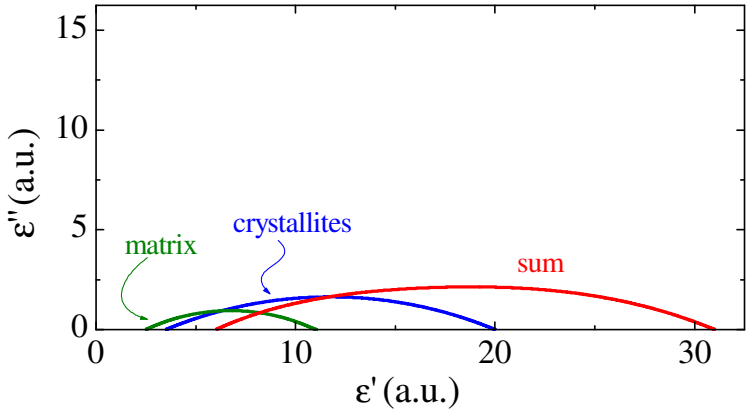

Figure 69: *Complex plain: two superimposed dynamic processes.* Calculated dielectric response of a relaxor polymer system from Figure 68, plotted in the complex ε', ε'' plane.

calculated using ansatz [6]:

$$\varepsilon^*_{sum} = \varepsilon_{\infty,crys.} + \frac{\Delta\varepsilon_{crys.}}{1 + (i\omega\tau_{crys.})^{1-h_{crys.}}} + \varepsilon_{\infty,matrix} + \frac{\Delta\varepsilon_{matrix}}{1 + (i\omega\tau_{matrix})^{1-h_{matrix}}}, \tag{82}$$

which in fact is a sum composed of two Cole-Cole expressions, representing relaxor dynamics in the crystallites and glassy dynamics in the amorphous matrix, and its characteristic relaxation frequency has been determined by fit to Equation 35. Figure 66 depicts the case, in which both dynamic processes can clearly be seen in the frequency-dependent dielectric response (denoted as sum). In this case, Cole-Cole fitting of $\varepsilon^*(\nu)$ gives (i) a small error in the obtained characteristic relaxation times data and (ii) a notable error in the obtained values of ε_s and ε_∞. The latter can clearly be seen in Figure 67, which shows the calculated data in the complex ε', ε'' plane. Figure 68 depicts the calculated data for the case, encountered in analysis of the dielectric response of terpolymer/copolymer blends (Figure 65). It can clearly be seen that the sum curve is broader, with the characteristic relaxation time for one order of magnitude higher in comparison to crystallites. Superimposition of the two dynamics also increases values of ε_s and ε_∞, as can be seen in the complex plane (see Figure 69).

To summarize the results presented in this subsection: The detected frequency-dependent dielectric response of relaxor polymer systems should not be fitted to a single Cole-Cole ansatz, as such a procedure provides incorrect values of the characteristic relaxation time. The obtained ε^* spectra have to be either

- fitted to the sum of two Cole-Cole expressions (Equation 82),

or, to omit errors in fitting the data with two similar (broad) distributions,

- the characteristic relaxation times should rather be determined from the $\varepsilon''(T)$ peaks [6].

7 Conclusions

This doctoral dissertation presented the results of investigations and separation of various contributions to the dielectric response of novel ceramic and polymeric materials, with a special emphasis on modelling the dielectric response of the investigated systems.

First, the temperature and frequency dependent dielectric response of core-shell structured ceramic material was modelled in terms of the equivalent circuit (the elements of which describe distinctive contributions of grains/bulk and grain boundaries) by assuming the Arrhenius law for temperature dependence of the bulk resistance. Modelling results reveal a dispersive dielectric behaviour, typically observed in core-shell structured materials, e.g., $CaCu_3Ti_4O_{12}$ (CCTO) thin film. Then, the results of the study of the influence of preparation conditions on the dielectric response of CCTO thin films were presented. In CCTO thin films, prepared by the chemical solution deposition method, the experimental results and analysis in terms of equivalent circuit reveal that each of the two constituents determines the dielectric behaviour of the CCTO thin film for different frequencies: insulating grain boundaries at lower and semiconducting grains at higher frequencies. The main influence on dielectric properties are the conditions under which the CCTO thin film was created, i.e., processes taking place upon heating and cooling of the samples: By proper post-annealing process a high dielectric constant of ~ 3000 was obtained in films with thickness below 600 nm. It was shown that ε' plateau values and the temperature of their drop (both quantities are successfully ascribed to the parameters of the artificial Debye relaxation arising from the equivalent circuit comprising contributions of grain boundaries and the bulk) strongly depend on the oxygen partial pressure in the atmosphere during the post-annealing process. The origin of such dielectric behaviour is attributed to (i) changes in geometry that are due to electrical heterogeneities in the microstructure, i.e., different distributions of Cu^+ and Cu^{2+} within grains and grain boundaries and (ii) differences in conductivity of both grains and grain boundaries and concomitantly their influences on ε' via Kramers-Kronig relations. Analysis in terms of the equivalent circuit and variable range hopping model reveal that 1D-hopping of localized charge carriers dominates the charge transport behaviour in CCTO thin films. In addition, it was shown that in the case of CCTO thin film, prepared on a nucleation layer, the dielectric response is determined by the microstructure consisting of large grains that extend throughout the whole thickness of the film. Such dielectric behaviour can be modelled with an equivalent circuit, composed of a set of parallel leaky capacitors, yielding a smooth temperature-dependent response.

Next, the results of measurements of the temperature and frequency-dependent linear and third-order nonlinear dielectric response of the dynamic processes in relaxor reduced poly(vinylidene fluoride-trifluoroethylene) [P(VDF-TrFE)] copolymer, synthesized via reductive dechlorination from the poly(vinylidene fluoride-chlorotrifluoroethylene) [P(VDF-CTFE)] copolymer, were shown. Analysis of the experimental data revealed that the relaxor dielectric dynamics in the reduced P(VDF-TrFE) copolymer is almost identical to that observed in classical relaxor systems and reminiscent of the dynamic behaviour observed in various spin glasses. Also, a clear indication was obtained that all polar dynamic processes terminate down to $\sim$ 100 K and that below this temperature only non-polar contributions govern the dielectric response of the reduced P(VDF-TrFE) copolymer. Furthermore,

the study of changes in dynamic processes due to a DC bias electric field in the reduced P(VDF-TrFE) copolymer revealed a strong electric field dependence of the Vogel-Fulcher temperature and the activation energy. Comparison of the results with those obtained in a classical inorganic relaxor, lanthanum-modified lead zirconate titanate ceramics, reveals that it is the nonlinear dielectric susceptibility that dominantly affects the dielectric dynamics of relaxors in DC bias electric fields. In addition, it was established that even low bias voltage effectively blocks the ac electrical conductivity of the studied copolymer, which can be afterwards restored to its initial value by applying a high enough AC voltage.

Finally, the results of structural, caloric, and dielectric properties of relaxor polymer blend films composed of poly(vinylidene fluoride-trifluoroethylene-chlorofluoroethylene) terpolymer and poly(vinylidene fluoride-chlorotrifluoroethylene) copolymer on aluminium foil were presented. Differential scanning calorimetry and X-ray diffraction results indicate that in this system, the copolymer additive disturbs the crystallizing process of the terpolymer. Measurements of temperature-dependent dielectric response revealed that upon increasing mol % of the copolymer, values of both, ε' and ε'', decrease in comparison to pure terpolymer, which is in concurrence with the interference effect (as values of the dielectric constant are lower in pure copolymer). Analysis of the temperature-dependent dielectric response has revealed that the addition of the copolymer does not influence the relaxor dynamics of the system: There are no notable differences within statistical error between Vogel-Fulcher temperatures and activation energies of terpolymer and blends with 5 or 10 mol % of copolymer. Furthermore, the analysis of the frequency-dependent dielectric response revealed that characteristic relaxation times obtained from $\varepsilon^*(\nu)$ do not follow Vogel-Fulcher law below room temperature, which indicates that, at lower temperatures, the dielectric response is not governed solely by relaxor dynamics. Therefore, the dielectric response of a relaxor polymer system was calculated for systems, in which two similar dynamic processes superimpose in the same temperature range, e.g., relaxor dynamics in the crystalline regions and glassy transition in the amorphous matrix in relaxor poly(vinylidene fluoride-trifluoroethylene-chlorofluoroethylene) terpolymers. It was thus shown that in such cases (superposition of two dynamic processes) the characteristic relaxation times should be determined from the $\varepsilon''(T)$ data and not by fitting frequency-dependent dielectric response to a single Cole-Cole expression, which provides incorrect values.

To summarize, this doctoral dissertation investigates in detail structural and, particularly, dielectric properties of

- core-shell structured $CaCu_3Ti_4O_{12}$ thin films prepared under various conditions,
- a new class of relaxor polymer, reduced P(VDF-TrFE) copolymer, and
- relaxor films of P(VDF-TrFE-CFE) terpolymer and its blends with P(VDF-CTFE) copolymer, developed on aluminium foil,

and thus presents the dielectric spectroscopy as a powerful tool for investigations of basic and applicatory-oriented properties of various organic and inorganic materials, which might result in their optimization or even in the synthesis of new materials for advanced applications.

More generally, with great power comes great dE/dt. [96]

8 Acknowledgements

With the following words, I would like to express my gratitude to all the people that have, directly or indirectly, contributed to the work presented in this doctoral dissertation.

Special thanks go to my supervisor, Asst. Prof. Dr. Vid Bobnar, who introduced me to the intriguing and, sometimes, rather mysterious world of dielectric constants and dielectric spectroscopy. I would like to thank him for his commitment, encouragement, enthusiasm and patience during my work and for stimulating me to participate at international conferences and introducing me as a member of international collaborations. It was a pleasure to work with Vid over the course of these three and a half years.

I also thank the members of our research group at the Jožef Stefan Institute, Prof. Dr. Zdravko Kutnjak, Dr. Brigita Rožič and Nikola Novak for teaching me many experimental tricks and stimulating me during our conversations. I also thank all other members of the group that is, alas, too numerous to list all names here. Thank you for all the insightful discussions, creating a positive atmosphere at the Institute and lending me a hand (or a keyboard), when I needed it.

I would like to thank the members of the Electronic Ceramics Department, Jožef Stefan Institute, and the group of Prof. Dr. Qun-Dong Shen at the Nanjing University in China, for preparing various samples and carrying out the preliminary material characterizations. I would also like to thank the members of the group of Prof. Dr. Horst Beige from the Martin Luther University in Halle, Germany, for their help in conducting the electromechanical measurements.

Finally, I would like to thank my family and friends for all they have done for me and for all the unlimited support and constant encouragement they have offered me during my PhD studies in the last three and a half years.

9 References

[1] Eršte, A.; Malič, B.; Kužnik, B.; Kosec, M.; Bobnar V. Equivalent circuit modelling of core-shell structured ceramic materials. In: *Nair, K. M.; Priya, S. (ed.) Advances and applications in electroceramics II: Ceramic transactions* **235**, 23–29 (Wiley, Hoboken, 2012).

[2] Eršte, A.; Malič, B.; Kužnik, B.; Kosec, M.; Bobnar V. Influence of preparation conditions on distinctive contributions to dielectric behavior of $CaCu_3Ti_4O_{12}$ thin films. *Journal of American Ceramic Society* **94**, 3900–3906 (2011).

[3] Eršte, A.; Filipič, C.; Levstik, A.; Bobnar, V.; Chen, X.-Z.; Jia, C.-L.; Shen, Q.-D. Contributions of distinctive dynamic processes to dielectric response of a relaxorlike reduced poly(vinylidene fluoride-trifluoroethylene) copolymer. *Physical Review B* **81**, 214103 (2010).

[4] Bobnar, V.; Eršte, A.; Chen, X.-Z.; Jia, C.-L.; Shen, Q.-D. Influence of dc bias electric field on Vogel-Fulcher dynamics in relaxor ferroelectrics. *Physical Review B* **83**, 132105 (2011).

[5] Pirc, R.; Blinc, R. Nonlinear magnetoelectric effect in magnetically disordered relaxor ferroelectrics. *Ferroelectrics* **400**, 387–394 (2010).

[6] Eršte, A.; Chen, X.-Z.; Cheng Z.-X.; Shen, Q.-D.; Bobnar, V. Structural and electrically-induced properties of relaxor poly(vinylidene fluoride)-based terpolymer/copolymer blends on aluminum foil. *Journal of Applied Physics* **112**, 053505 (2012).

[7] Blinc, R.; Žekš B. *Soft modes in ferroelectrics and antiferroelectrics* (North-Holland Publishing Company, Amsterdam, 1974).

[8] Kremer, F.; Schönhals, A. *Broadband dielectric spectroscopy* (Springer, Berlin, 2003).

[9] Hill, N. E.; Vaughan, W. E.; Price, A. H.; Davies, M. *Dielectric properties and molecular behaviour* (Van Nostrand Reinhold Company Ltd., London, 1969).

[10] Frölich, H. *Theory of dielectrics: dielectric constant and dielectric loss* (Clarendon Press, Oxford, 1958).

[11] Hass, D. D. *Dielectric sensing of ceramic particle suspensions* (Master's thesis, University of Virginia, 1996).

[12] Harrop, P. J. *Dielectrics* (Butterworths, London, 1972).

[13] Bronstein, I. N.; Semendjajew K. A.; Musiol G.; Mühlig H. *Matematični priročnik* (Tehniška založba Slovenije, Ljubljana, 1997).

[14] Sinclair, D. C.; Adams, T. B.; Morrison, F. D.; West, A. R. $CaCu_3Ti_4O_{12}$: One-step internal barrier layer capacitor. *Applied Physics Letters* **80**, 2153–2155 (2002).

[15] Lunkenheimer, P.; Khrons, S.; Riegg, S.; Ebbighaus, S. G.; Reller, A.; Loidl, A. Colossal dielectric constants in transition-metal oxides. *European Physical Journal Special Topics* **180**, 61–89 (2010).

[16] Lunkenheimer, P.; Fichtl, R.; Ebbinghaus, S. G.; Loidl, A. Nonintrinsic origin of the colossal dielectric constants in $CaCu_3Ti_4O_{12}$. *Physical Review B* **70**, 172102 (2004).

[17] Adams, T. B.; Sinclair, D. C.; West, A. R. Characterization of grain boundary impedances in fine- and coarse-grained $CaCu_3Ti_4O_{12}$ ceramics. *Physical Review B* **73**, 094124 (2006).

[18] Bobnar, V.; Lunkenheimer, P.; Paraskevopoulos, M.; Loidl, A. Separation of grain boundary effects and intrinsic properties in perovskite-like $Gd_{0.6}Y_{0.4}BaCo_2O_{5.5}$ using high-frequency dielectric spectroscopy. *Physical Review B* **65**, 184403 (2002).

[19] McNaught, A. D.; Wilkinson A. Compendium of chemical terminology, 2nd ed. (the "Gold Book") (Blackwell Scientific Publications, Oxford, 1997).

[20] Mott, N. F.; Davis, E. A. Theory of electrons in a non-crystaline medium. In: *Electronic Processes in Non-Crystalline Materials.* 32–37 (Clarendon Press, Oxford, 1979).

[21] Pirc, R.; Blinc, R. Vogel-Fulcher freezing in relaxor ferroelectrics. *Physical Review B* **76**, 020101 (2007).

[22] Honda, M. *The Impedance Measurement Handbook : A Guide to Measurement Technology and Techniques* (Agilent Technologies, USA, 2003).

[23] Takahura, C.; Hachioji, S. *HP 4284A Precision LCR Meter Operation Manual* (Yokogawa-Hewlet-Packard, LTD., Tokyo, 1998).

[24] Novocontrol Technologies. *Alpha and Beta Dielectric, Conductivity, Impedance and Gain Phase Analyzers (User's Manual)* (Novocontrol Technologies GmbH & Co. KG, Hundsangen, 2005).

[25] Bobnar, V. *Raziskave faznih prehodov v relaksorjih z dielektrično spektroskopijo – disertacija* (V. Bobnar, Ljubljana, 2000).

[26] Bobnar, V.; Lunkenheimer, P.; Hemberger, J.; Loidl, A.; Lichtenberg, F.; Mannhart, J. Dielectric properties and charge transport in the (Sr,La)$NbO_{3.5-x}$ system. *Physical Review B* **65**, 155115 (2002).

[27] Subramanian, M. A.; Li, D.; Duan, N.; Reisner, B. A.; Sleight, A. W. High dielectric constant in $ACu_3Ti_4O_{12}$ and $ACu_3Ti_3FeO_{12}$ phases. *Journal od Solid State Chemistry* **151**, 323–325 (2000).

[28] Ramirez, A. P.; Subramanian, M. A.; Gardel, M.; Blumberg, G.; Li, D.; Vogt, T.; Shapiro, S. M. Giant dielectric constant response in a copper-titanate. *Solid State Communications* **115**, 217–220 (2000).

[29] Homes, C. C.; Vogt, T.; Shapiro, S. M.; Wakimoto, S.; Ramirez, A. P. Optical response of high-dielectric-constant perovskite-related oxide. *Science* **293**, 673–676 (2001).

[30] Lunkenheimer, P.; Bobnar, V.; Pronin, A. V.; Ritus, A. I.; Volkov, A. A.; Loidl, A. Origin of apparent colossal dielectric constants. *Physical Review B* **66**, 052105 (2002).

[31] Momma, K.; Izumi, F. VESTA 3 for three-dimensionsional visualization of crystal, volumetric and morphology data. *Journal of Applied Crystallography* **44**, 1272–1276 (2011).

[32] Momma, K. VESTA: Visualization for Electronic and STructural Analysis. `http://jp-minerals.org/vesta/en/doc.html` (acessed: November 2012).

[33] Li, M.; Feteira, A.; Sinclair, D. C.; West, A. R. Influence of Mn doping on the semiconductor properties of $CaCu_3Ti_4O_{12}$ ceramics. *Applied Physics Letters* **88**, 232903 (2006).

[34] Fiorenza, P.; Nigro, R. L.; Bongiorno, C.; Raineri, V.; Ferarrelli, M. C.; Sinclair, D. C.; West A. R. Localised electrical characterisation of the giant permittivity effect in $CaCu_3Ti_4O_{12}$ ceramics. *Applied Physics Letters* **92**, 182907 (2008).

[35] Sebald, J.; Krohns, S.; Lunkenheimer, P.; Ebbinghaus, S. G.; Riegg, S.; Reller, A.; Loidl, A. Colossal dielectric constants: A common phenomenon in $CaCu_3Ti_4O_{12}$ related materials. *Solid State Communications* **150**, 857–860 (2010).

[36] Chung, S.-Y.; Kim, I.-L.; Kang, S.-J. L. Strong nonlinear current-voltage behaviour in perovskite-derivative calcium copper titanate. *Nature Materials* **3**, 774–778 (2004).

[37] Brizé, V.; Gruener, G.; Wolfman, J.; Fatyeyeva, K.; Tabellout, M.; Gervais, M.; Gervais, F. Grain size effects on the dielectric constant of $CaCu_3Ti_4O_{12}$ ceramics. *Materials Science and Engineering: B* **129**, 135–138 (2006).

[38] Deng, G.; Muralt, P. On origin and intrinsic electrical properties of the colossal dielectric constant state in $CaCu_3Ti_4O_{12}$. *IOP Conference Series: Materials Science and Engineering* **8**, 012016 (2009).

[39] Eršte, A.; Kužnik, B.; Malič, B.; Kosec, M.; Bobnar, V. Dielectric properties of $CaCu_3Ti_4O_{12}$ ceramic thin films. *Ferroelectrics* **419**, 14–19 (2011).

[40] PDF-ICDD, PCPDFW in Version 2.2, June 2001 (International Centre for Diffraction Data, Newtown Square, 2002).

[41] Li, W.; Schwartz, R. W. Maxwell-Wagner relaxations and their contributions to the high permittivity of calcium copper titanate ceramics. *Physical Review B* **75**, 012104 (2007).

[42] Jimenez, R.; Calzada, M. L.; Bretos, I.; Goes, J. C.; Sombra, A. S. B. Dielectric properties of sol-gel derived $CaCu_3Ti_4O_{12}$ thin films onto $Pt/TiO_2/Si(100)$ substrates. *Journal of European Ceramis Society* **27**, 3829–3833 (2007).

[43] Chang, L-C.; Lee, D.-Y.; Ho, C.-C.; Chiou, B.-S. Thickness-dependent microstructures and electrical properties of $CaCu_3Ti_4O_{12}$ films derived from sol-gel process. *Thin Solid Films* **516**, 454–459 (2007).

[44] Li, J.; Subramanian, M. A.; Rosenfeld, H. D.; Jones, C. Y.; Toby, B. H.; Sleight, A. W. Clues to the giant dielectric constant of $CaCu_3Ti_4O_{12}$ in the defect structure of "$SrCu_3Ti_4O_{12}$". *Chemistry of Materials* **16**, 5223–5225 (2004).

[45] Lovinger, A. J. Ferroelectric polymers. *Science* **220**, 1115–1121 (1983).

[46] Tashiro, K. Crystal Structure and Phase Transition of PVDF and Related Copolymer. In: *Nalwa, H. (ed.) Ferroelectric Polymers*. 63–181 (Marcel Dekker, New York, 1995).

[47] Zhang, Q. M.; Bharti, V.; Zhao, X. Giant electrostriction and relaxor ferroelectric behavior in electron-irradiated poly(vinylidene fluoride-trifluoroethylene) copolymer. *Science* **280**, 2101 (1998).

[48] Xia, F.; Cheng, Z.-Y.; Xu, H. S.; Li, H. F.; Zhang, Q. M.; Kavarnos, G. J.; Ting, R. Y.; Abdul-Sadek, G.; Belfield, K. D. High electromechanical responses in a poly(vinylidene-fluoride-trifluoroethylene-chlorofluoroethylene) terpolymer. *Advanced Materials* **14**, 1574–1577 (2002).

[49] Chu, B.; Zhou, X.; Ren, K.; Neese, B.; Lin, M.; Wang, Q.; Bauer, F.; Zhang, Q. M. A dielectric polymer with high electric energy density and fast discharge speed. *Science* **313**, 334–336 (2006).

[50] Neese, B.; Chu, B.; Lu, S.-G.; Wang, Y.; Furman, E.; Zhang, Q. M. Large electrocaloric effect in ferroelectric polymers near room temperature. *Science* **321**, 821–823 (2008).

[51] Samara, G. A. *Solid State Physics* (Academic Press, New York, 2001).

[52] Bobnar, V.; Kutnjak, Z.; Pirc, R.; Levstik, A. Electric-field-temperature phase diagram of the relaxor ferroelectric lanthanum-modified lead zirconate titanate. *Physical Review B* **60**, 6420 (1999).

[53] Sommer, R.; Yushin, N. K.; van der Klink, J. J. Polar metastability and an electric-field-induced phase transition in the disordered perovskite $Pb(Mg_{1/3}Nb_{2/3})O_3$. *Physical Review B* **48**, 13230–13237 (1993).

[54] Viehland, D.; Jang, S. J.; Cross, L. E.; Wuttig, M. Deviation from Curie-Weiss behavior in relaxor ferroelectrics. *Physical Review B* **46**, 8003–8006 (1992).

[55] Bobnar, V.; Vodopivec, B.; Levstik, A.; Kosec, M.; Hilczer, B.; Zhang, Q. M. Dielectric properties of relaxor-like vinylidene fluoride-trifluoroethylene-based electroactive polymers. *Macromolecules* **36**, 4436–4442 (2003).

[56] Structural changes and transitional behavior studied from both micro- and macroscale in the high-energy electron-irradiated poly(vinylidene fluoride-trifluoroethylene) copolymer. *Macromolecules* **35**, 664–672 (2002).

[57] Kutnjak, Z.; Filipič, C.; Pirc, R.; Levstik, A.; Farhi, R.: El Marssi, M. Slow dynamics and ergodicity breaking in a lanthanum-modified lead zirconate titanate relaxor system. *Physical Review B* **59**, 294–301 (1999).

[58] Kutnjak, Z.; Petzelt, J.; Blinc, R. The giant electromechanical response in ferroelectric relaxors as a critical phenomenon. *Nature* **441**, 956–959 (2006).

[59] Yan, F.; Bao, P.; Wang, Y. Phase transition in relaxor ferroelectrics studied by mechanical measurements. *Applied Physics Letters* **83**, 4384 (2003).

[60] Pirc, R.; Blinc, R.; Scott, J. F. Mesoscopic model of a system possessing both relaxor ferroelectric and relaxor ferromagnetic properties. *Physical Review B* **79**, 214114 (2009).

[61] Furukawa, T.; Tajitsu, Y.; Zhang, X.; Johnson, G. E. Dielectric relaxations in copolymers of vinylidene fluoride. *Ferroelectrics* **135**, 401–417 (1992).

[62] Furukawa, T. Ferroelectric properties of vinylidene fluoride copolymers. *Phase Transitions* **18**, 143 (1989).

[63] Bharti, V.; Xu, H. S.; Shanthi, G.; Zhang, Q. M. Polarization and structural properties of high-energy electron irradiated poly(vinylidene fluoride-trifluoroethylene) copolymer films. *Journal of Applied Physics* **87**, 452 (2000).

[64] Menegotto, J.; Ibos, L.; Bernes, A.; Demont, P.; Lacabanne, C. Dielectric relaxation spectra in ferroelectric P(VDF-TrFE) copolymers. *Ferroelectrics* **228**, 1–22 (1999).

[65] Guo, S. S.; Lau, S. T.; Chan, H. L. W.; Zhao, X.-Z.; Choy, C. L. Structural evolution and dielectric relaxation behavior of electron-irradiated poly(vinylidene fluoride-trifluoroethylene) 80/20 mol% copolymers. *Journal of Applied Physics* **94**, 5566 (2003).

[66] Bharti, V.; Zhang, Q. M. Dielectric study of the relaxor ferroelectric poly(vinylidene fluoride-trifluoroethylene) copolymer system. *Physical Review B* **63**, 184103 (2001).

[67] Bobnar, V.; Eršte, A.; Chen, X.-Z.; Shen, Q.-D. Glassy dielectric processes in reduced poly(vinylidene fluoride-trifluoroethylene) copolymer system. *Ferroelectrics* **419**, 59–65 (2011).

[68] Eršte, A.; Chen, X.-Z.; Jia, C.-L.; Shen, Q.-D.; Bobnar, V. Dielectric investigations of relaxor reduced poly(vinylidene fluoride-trifluoroethylene) copolymer in DC bias electric field. *Ferroelectrics* **427**, 157–162 (2012).

[69] Bobnar, V.; Li, X.; Casar, G.; Eršte, A.; Glinšek, S.; Qian, X.; Zhang, Q. M. Tailoring electrically induced properties by stretching relaxor polymer films. *Jornal of Applied Physics* **111**, 083515 (2012).

[70] Levstik, A.; Kutnjak, Z.; Filipič, C.; Pirc, R. Glassy freezing in relaxor ferroelectric lead magnesium niobate. *Physical Review B* **57**, 11204–11211 (1998).

[71] Bao, H.-M.; Jia, C.-L.; Wang, C.-C.; Shen, Q.-D.; Yang, C.-Z.; Zhang, Q. M. A type of poly(vinylidene fluoride-trifluoroethylene) copolymer exhibiting ferroelectric relaxor behavior at high temperature ($\sim$ 100 °C). *Applied Physics Letters* **92**, 042903 (2008).

[72] von Cieminski, J.; Schmidt, G.; Magatayev, V. K.; Glushkov, V. F.; Shwalov L. A. Electrostriction and phase transition in MASD. *Ferroelectrics Letters Section* **3**, 163–171 (1985).

[73] Colla, E. L.; Hong, S.; Taylor, D. V.; Tagantsev, A. K.; Setter, N.; No, K. Direct observation of region by region suppression of the switchable polarization (fatigue) in Pb(Zr,Ti)O_3 thin film capacitors with Pt electrodes. *Applied Physics Letters* **72**, 2763 (1998).

[74] Welter, C.; Faria, L. O.; Moreira, R. L. Relaxor ferroelectric behavior of γ-irradiated poly(vinylidene fluoride-trifluoroethylene) copolymers. *Physical Review B* **67**, 144103 (2003).

[75] Hilczer, B.; Smogor, H.; Pawlowski, T.; Goslar, J. Dielectric response and conformational disorder in polymer relaxors. *Ferroelectrics* **298**, 113 (2004).

[76] Stanley, H. E. *Introduction to Phase Transitions and Critical Phenomena* (Clarendon Press, Oxford, 1971).

[77] Hemberger, J.; Ries, H., Loidl, A.; Böhmer, R. Static freezing transition at a finite temperature in a quasi-one-dimensional deuteron glass. *Physical Review Letters* **76**, 2330–2333 (1996).

[78] Fischer, K. H.; Hertz, J. A. *Spin Glasses* (Cambridge University Press, Cambridge, 1991).

[79] Bobnar, V.; Kutnjak, Z.; Pirc, R.; Blinc, R.; Levstik, A. Crossover from glassy to inhomogeneous-ferroelectric nonlinear dielectric response in relaxor ferroelectrics. *Physical Review Letters* **84**, 5892 (2000).

[80] Bobnar, V.; Bernard, J.; Kosec, M. Relaxorlike dielectric properties and history-dependent effects in the lead-free $K_{0.5}Na_{0.5}NbO_3$–$SrTiO_3$ ceramic system. *Applied Physics Letters* **85**, 994 (2004).

[81] Glazounov, A. E.; Tagantsev, A. K. Phenomenological model of dynamic nonlinear response of relaxor ferroelectrics. *Physical Review Letters* **85**, 2192 (2000).

[82] Ko, J.-H.; Jiang, F.; Kojima, S.; Shaplygina, T. A.; Lushnikov, S. G. Linear and nonlinear dielectric susceptibilities of disordered lead scandium tantalate. *Journal of Physics: Condensed Matter* **13**, 5449 (2001).

[83] Tagantsev, A. K. Vogel-Fulcher relationship for the dielectric permittivity of relaxor ferroelectrics. *Physical Review Letters* **72**, 1100–1103 (1994).

[84] Bokov, A. A.; Maglione, M.; Ye, Z. G. Quasi-ferroelectric state in $Ba(Ti_{1-x}Zr_x)O_3$ relaxor: dielectric spectroscopy evidence. *Journal of Physics: Condensed Matter* **19**, 092001 (2007).

[85] Lines, M. E. Interfacial polarization effects in ionic conductors. *Physical Review B* **19**, 1189 (1979).

[86] Chen, X.; Kingon, A. I.; Auciello, O. AC conductivitty and dielectric properties of sol-gel PZT thin films for ferroelectric memory applications. In: *Proceedings of the 8th IEEE International Symposium on Applications of Ferroelectrics, Greenville, SC.* 229–232 (IEEE, Piscataway, 1992).

[87] Pirc, R.; Blinc, R.; Kutnjak, Z. Nonlinear dielectric response of relaxor ferroelectrics. *Physical Review B* **65**, 214101 (2002).

[88] Biallozor, S.; Kupniewska, A. Conducting polymers electrodeposited on active metals. *Synthetic Metals* **155**, 443–449 (2005).

[89] Eftekhari, A. Aluminum as a suitable substrate for the deposition of conducting polymers: application to polyaniline and enzyme-modified electrode. *Synthetic Metals* **125**, 295–300 (2001)

[90] Lu, S. G.; Rožič, B.; Zhang, Q. M.; Kutnjak, Z.; Pirc, R.; Lin, M.; Li, X.; Gorny, L. Comparison of directly and indirectly measured electrocaloric effect in relaxor ferroelectric polymers. *Applied Physics Letters* **97**, 202901 (2010).

[91] Klein R. J.; Xia F.; Zhang, Q. M.; Bauer, F. Influence of composition on relaxor ferroelectric and electromechanical properties of poly(vinylidene fluoride-trifluoroethylene-chlorofluoroethylene). *Journal of Applied Physics* **97**, 094105 (2005).

[92] Chu, B.; Neese, B.; Lin, M.; Lu, S.-G.; Zhang, Q. M. Enhancement of dielectric energy density in the poly(vinylidene fluoride)-based terpolymer/copolymer blends. *Applied Physics Letters* **93**, 152903 (2008).

[93] Zhang, S.; Neese. B.; Ren, K.; Chu, B.; Zhang, Q. M. Microstructure and electromechanical responses in semicrystalline ferroelectric relaxor polymer blends. *Journal of Applied Physics* **100**, 044113 (2006).

[94] Klein, R. J.; Runt, J.; Zhang, Q. M. Influence of crystallization conditions on the microstructure and electromechanical properties of poly(vinylidene fluoride-trifluoroethylene-chlorofluoroethylene) terpolymers. *Macromolecules* **36**, 7220–7226 (2003).

[95] Bao, H.-M.; Song, J.-F.; Zhang, J.; Shen, Q.-D.; Yang, C.-Z.; Zhang, Q. M. Phase transitions and ferroelectric relaxor behavior in P(VDF-TrFE-CFE) terpolymers. *Macromolecules* **40**, 2371–2379 (2007).

[96] Munroe, R. Ohm. `http://xkcd.com/643/` (acessed: November 2012).

Index of Figures

Index of Tables

Appendix A: List of publications related to this doctoral dissertation

[1] Eršte, A.; Filipič, C.; Levstik, A.; Bobnar, V.; Chen, X.-Z.; Jia, C.-L.; Shen, Q.-D. Contributions of distinctive dynamic processes to dielectric response of a relaxorlike reduced poly(vinylidene fluoride-trifluoroethylene) copolymer. *Physical Review B* **81**, 214103 (2010).

[2] Eršte, A.; Kužnik, B.; Malič, B.; Kosec, M.; Bobnar, V. Dielectric properties of $CaCu_3Ti_4O_{12}$ ceramic thin films. *Ferroelectrics* **419**, 14–19 (2011).

[3] Bobnar, V.; Eršte, A.; Chen, X.-Z.; Shen, Q.-D. Glassy dielectric processes in reduced poly(vinylidene fluoride-trifluoroethylene) copolymer system. *Ferroelectrics* **419**, 59–65 (2011).

[4] Eršte, A.; Malič, B.; Kužnik, B.; Kosec, M.; Bobnar V. Influence of preparation conditions on distinctive contributions to dielectric behavior of $CaCu_3Ti_4O_{12}$ thin films. *Journal of American Ceramic Society* **94**, 3900–3906 (2011).

[5] Bobnar, V.; Eršte, A.; Chen, X.-Z.; Jia, C.-L.; Shen, Q.-D. Influence of dc bias electric field on Vogel-Fulcher dynamics in relaxor ferroelectrics. *Physical Review B* **83**, 132105 (2011).

[6] Eršte, A.; Chen, X.-Z.; Jia, C.-L.; Shen, Q.-D.; Bobnar, V. Dielectric investigations of relaxor reduced poly(vinylidene fluoride-trifluoroethylene) copolymer in DC bias electric field. *Ferroelectrics* **427**, 157–162 (2012).

[7] Bobnar, V.; Li, X.; Casar, G.; Eršte, A.; Glinšek, S.; Qian, X.; Zhang, Q. M. Tailoring electrically induced properties by stretching relaxor polymer films. *Journal of Applied Physics* **111**, 083515 (2012).

[8] Eršte, A.; Chen, X.-Z.; Cheng Z.-X.; Shen, Q.-D.; Bobnar, V. Structural and electrically-induced properties of relaxor poly(vinylidene fluoride)-based terpolymer/copolymer blends on aluminum foil. *Journal of Applied Physics* **112**, 053505 (2012).

[9] Eršte, A.; Malič, B.; Kužnik, B.; Kosec, M.; Bobnar V. Equivalent circuit modelling of core-shell structured ceramic materials. In: *Nair, K. M.; Priya, S. (ed.) Advances and applications in electroceramics II: Ceramic transactions* **235**, 23–29 (Wiley, Hoboken, 2012).

Appendix B: Personal bibliography for the period 2009–2012

B.1 Articles and other component parts

B.1.1 Original scientific article

[1] Eršte, A.; Chen, X.-Z.; Jia, C.-L.; Shen, Q.-D.; Bobnar, V. Dielectric investigations of relaxor reduced poly(vinylidene fluoride-trifluoroethylene) copolymer in DC bias electric field. *Ferroelectrics* **427**, 157–162 (2012).

[2] Bobnar, V.; Li, X.; Casar, G.; Eršte, A.; Glinšek, S.; Qian, X.; Zhang, Q. M. Tailoring electrically induced properties by stretching relaxor polymer films. *Journal of Applied Physics* **111**, 083515 (2012).

[3] Eršte, A.; Chen, X.-Z.; Cheng Z.-X.; Shen, Q.-D.; Bobnar, V. Structural and electrically-induced properties of relaxor poly(vinylidene fluoride)-based terpolymer/copolymer blends on aluminum foil. *Journal of Applied Physics* **112**, 053505 (2012).

[4] Eršte, A.; Kužnik, B.; Malič, B.; Kosec, M.; Bobnar, V. Dielectric properties of $CaCu_3Ti_4O_{12}$ ceramic thin films. *Ferroelectrics* **419**, 14–19 (2011).

[5] Bobnar, V.; Eršte, A.; Chen, X.-Z.; Shen, Q.-D. Glassy dielectric processes in reduced poly(vinylidene fluoride-trifluoroethylene) copolymer system. *Ferroelectrics* **419**, 59–65 (2011).

[6] Bobnar, V.; Eršte, A.; Gradišar, U.; Filipič, C.; Levstik, A.; Kutnjak, Z. High-temperature dielectric response of ferroelectric relaxors. *IEEE transactions on ultrasonics, ferroelectrics and frequency control* **58**, 2270–2275 (2011).

[7] Eršte, A.; Malič, B.; Kužnik, B.; Kosec, M.; Bobnar V. Influence of preparation conditions on distinctive contributions to dielectric behavior of $CaCu_3Ti_4O_{12}$ thin films. *Journal of American Ceramic Society* **94**, 3900–3906 (2011).

[8] Bobnar, V.; Eršte, A.; Chen, X.-Z.; Jia, C.-L.; Shen, Q.-D. Influence of dc bias electric field on Vogel-Fulcher dynamics in relaxor ferroelectrics. *Physical Review B* **83**, 132105 (2011).

[9] Eršte, A.; Filipič, C.; Levstik, A.; Bobnar, V.; Chen, X.-Z.; Jia, C.-L.; Shen, Q.-D. Contributions of distinctive dynamic processes to dielectric response of a relaxorlike reduced poly(vinylidene fluoride-trifluoroethylene) copolymer. *Physical Review B* **81**, 214103 (2010).

B.1.2 Published scientific conference contribution

[1] Eršte, A.; Malič, B.; Kužnik, B.; Kosec, M.; Bobnar V. Equivalent circuit modelling of core-shell structured ceramic materials. In: *Nair, K. M.; Priya, S. (ed.) Advances and*

applications in electroceramics II: Ceramic transactions **235**, 23–29 (Wiley, Hoboken, 2012).

[2] Casar, G.; Eršte, A.; Glinšek, S.; Li, X.; Qian, X.; Zhang, Q. M.; Bobnar, V. Tailoring electrically induced properties by stretching relaxor. In: *Petelin, D.; Tavčar, A.; Kaluža, B. (ed.) Zbornik, 4. študentska konferenca Mednarodne podiplomske šole Jožefa Stefana.* 210–215 (Mednarodna podiplomska šola Jožefa Stefana, Ljubljana, 2012).

[3] Eršte, A.; Bobnar, V.; Chen, X.-Z.; Jia, C.-L.; Shen, Q.-D. Terpolymer/copolymer blends on aluminum surface: structural, caloric and dielectric properties. In: *Petelin, D.; Tavčar, A.; Kaluža, B. (ed.) Zbornik, 4. študentska konferenca Mednarodne podiplomske šole Jožefa Stefana.* 216–221 (Mednarodna podiplomska šola Jožefa Stefana, Ljubljana, 2012).

[4] Eršte, A.; Bobnar, V.; Chen, X.-Z.; Jia, C.-L.; Shen, Q.-D. Dielectric investigations of a new class of relaxor polymer. In: *Petelin, D.; Tavčar, A.; Rožič, B.; Pogorelc, B. (ed.) Zbornik prispevkov, 3. študentska konferenca Mednarodne podiplomske šole Jožefa Stefana.* 148–153 (Mednarodna podiplomska šola Jožefa Stefana, Ljubljana, 2011).

B.1.3 Published scientific conference contribution abstract (invited lecture)

[1] Bobnar, V.; Eršte, A.; Chen, X.-Z.; Li, X.; Casar, G.; Glinšek, S.; Qian, X.; Shen, Q.-D.; Zhang, Q. M. Structural and dielectric investigations of advanced relaxor polymer systems. In: *Uskoković, D. (ed.) Programme and the book of abstracts, Fourteenth Annual Conference YUCOMAT 2012.* 29 (Materials Research Society of Serbia, Belgrade, 2012).

B.1.4 Published scientific conference contribution abstract

[1] Eršte, A.; Bobnar, V.; Kosec, M.; Kužnik, M.; Malič, B. Equivalent circuit modelling of dielectric response of core-shell structured ceramic materials. In: *Program and abstracts, 10th CMCee, International Symposium on Ceramic Materials and Components for Energy and Environmental Applications.* 87–88 (Fraunhofer Institute for Ceramic Technologies and System, Dresden, 2012).

[2] Casar, G.; Li, X.; Eršte, A.; Glinšek, S.; Qian, X.; Zhang, Q. M.; Bobnar, V. Influence of stretching on dielectric, electromechanical and electrocaloric response of P(VDF-TrFE-CFE) terpolymer. In: *Uskoković, D. (ed.) Programme and the book of abstracts, Fourteenth Annual Conference YUCOMAT 2012.* 72 (Materials Research Society of Serbia, Belgrade, 2012).

[3] Casar, G.; Li, X.; Eršte, A.; Glinšek, S.; Qian, X.; Zhang, Q. M.; Bobnar, V. Vpliv raztegovanja na dielektrični, elektromehanski in elektrokaloričnі odziv P(VDF-TrFE-CFE) terpolimera. In: *Humar, M.; Škarabot, M. (ed.) Zbornik povzetkov, 8. konferenca fizikov v osnovnih raziskavah.* 45 (DMFA-založništvo, Ljubljana, 2012).

[4] Eršte, A.; Bobnar, V. Strukturne in dielektrične lastnosti relaksorskih polimernih mešanic na aluminijevi podlagi. In: *Humar, M.; Škarabot, M. (ed.) Zbornik povzetkov, 8. konferenca fizikov v osnovnih raziskavah.* 47 (DMFA-založništvo, Ljubljana, 2012).

[5] Eršte, A.; Bobnar, V.; Chen, X.-Z.; Jia, C.-L.; Shen, Q.-D. Dielectric investigations of relaxor reduced poly(vinylidene fluoride-trifluoroethylene) copolymer. In: *EMF 2011, 12th European Meeting on Ferroelectricity* (EMF 2011, Bordeaux, 2011).

[6] Eršte, A.; Malič, B.; Kužnik, B.; Kosec, M.; Bobnar, V. Influence of preparation conditions on distinctive contributions to dielectric behavior of $CaCu_3Ti_4O_{12}$ thin films. In: *Final program and exhibit directory, MS&T'11, Materials Science & Technology Conference & Exhibition* (The Minerals, Metals & Materials Society, Denver, 2011).

[7] Eršte, A.; Chen, X.-Z.; Jia, C.-L.; Shen, Q.-D.; Bobnar, V. Dielectric investigations of a new class relaxor polymer. In: *ISAF-PFM'11, The 20th IEEE International Symposium on Applications of Ferroelectrics,* [*and*] *International Symposium on Piezoresponse Force Microscopy & Nanoscale phenomena in Polar Materials* (ISAF-PFM'11, Vancouver, 2011).

[8] Eršte, A.; Kužnik, B.; Malič, B.; Kosec, M.; Bobnar, V. Dielectric properties of $CaCu_3Ti_4O_{12}$ thin films. In: *Abstracts and CD proceedings, Electroceramics XII* (Norwegian University of Science and Technology, Trondheim, 2010).

[9] Malič, B.; Kužnik, B.; Glinšek, S.; Benčan, A.; Kosec, M.; Eršte, A.; Bobnar, V. Influence of microstructure on dielectric properties of solution-derived $CaCu_3Ti_4O_{12}$ thin films. In: *Abstracts and CD proceedings, Electroceramics XII* (Norwegian University of Science and Technology, Trondheim, 2010).

[10] Malič, B.; Kužnik, B.; Glinšek, S.; Benčan, A.; Tchernychova, E.; Kosec, M.; Eršte, A.; Bobnar, V. Tailoring of dielectric properties of solution-derived $CaCu_3Ti4O_{12}$thin films by processing. In: *Book of abstracts, 6th International Conference on Microwave Materials and their Applications.* 78 (Faculty of Electronics and Information, Warsaw, 2010).

[11] Eršte, A.; Kužnik, A.; Malič, B.; Kosec, M.; Bobnar, V. Dielectric properties of $CaCu_3Ti_4O_{12}$ ceramic thin films. In: *ISAF ECAPD 2010, 19th International Symposium on the Applications of Ferroelectrics, 10th European Conference on the Applications of Polar Dielectrics.* 46 (ISAF ECAPD 2010, Edinburgh, 2010).

[12] Eršte, A.; Filipič, C.; Levstik, A.; Bobnar, V. Relaksorski dielektrični dinamični procesi v reduciranem poli(viniliden florid-trifloretilen) kopolimernem sistemu. In: *Humar, M.; Škarabot, M. (ed.) Zbornik povzetkov, 7. konferenca fizikov v osnovnih raziskavah.* 40 (DMFA-založništvo, Ljubljana, 2010).

[13] Eršte, A.; Malič, B.; Kužnik, B.; Kosec, M.; Bobnar, V. Vpliv pogojev priprave na posamične prispevke k dielektričnemu odzivu $CaCu_3Ti_4O_{12}$ tankih plasti. In: *Humar, M.; Škarabot, M. (ed.) Zbornik povzetkov, 7. konferenca fizikov v osnovnih raziskavah.* 46 (DMFA-založništvo, Ljubljana, 2010).

[14] Eršte, A.; Kužnik, B.; Malič, B.; Kosec, M.; Bobnar, V. Influence of processing conditins on dielectric properties of $CaCu_3Ti_4O_{12}$. In: *Kaluža, B; Eleršič, K.; Pogorelc, B.; Šetina, B.; Vahčič, M. (ed.) Zbornik prispevkov, 2. študentska konferenca Mednarodne podiplomske šole Jožefa Stefana.* 48 (Mednarodna podiplomska šola Jožefa Stefana, Ljubljana, 2010).

B.2 Monographs and other completed works

B.2.1 Undergraduate thesis

[1] Eršte, A. *Demonstracijski prikaz univerzalne resonančne škatle: diplomsko delo* (A. Eršte, Ljubljana, 2009).

B.3 Performed works (events)

B.3.1 Invited lecture at foreign university

[1] Eršte, A. *Svetilke znanosti: vabljeno predavanje: spoznajte mlade raziskovalce in njihovo delo* (Hiša eksperimentov, Ljubljana, 2012).

[2] Eršte, A. *Zvok v škatli: vabljeno predavanje* (Društvo matematikov, fizikov in astronomov Slovenije, Ljubljana, 2011).

[3] Eršte, A. *Investigations of distinctive dielectric contributions in advanced polymeric and inorganic systems: invited talk*, (Martin Luther Unicersity, Halle-Wittenberg, 2010).